UNIVERSITAT DE BARCELONA

Aberrant TIMP-1 regulation in tumor-associated fibroblasts by the TGF-β1/SMAD3 pathway in lung cancer: implications in tumor progression and resistance to antifibrotic therapies

Paula Duch Gili

Aquesta tesi doctoral està subjecta a la llicència ***Reconeixement- NoComercial – SenseObraDerivada 4.0. Espanya de Creative Commons***.

Esta tesis doctoral está sujeta a la licencia ***Reconocimiento - NoComercial – SinObraDerivada 4.0. España de Creative Commons.***

This doctoral thesis is licensed under the ***Creative Commons Attribution-NonCommercial-NoDerivs 4.0. Spain License.***

UNIVERSITAT DE BARCELONA

PhD Thesis

Doctoral Programme in Biomedicine

Aberrant TIMP-1 regulation in tumor-associated fibroblasts by the TGF-β1/SMAD3 pathway in lung cancer: implications in tumor progression and resistance to antifibrotic therapies

Paula Duch Gili

This PhD Thesis has been performed under the direction of Dr. Jordi Alcaraz Casademunt, in the Unit of Biophysics and Bioengineering at the Department of Biomedicine in the School of Medicine.

Dr. Jordi Alcaraz Casademunt

Jordi Alcaraz

Paula Duch Gili

Barcelona, 2022

AGRAÏMENTS

En aquesta aventura que ha sigut la tesi, hi ha hagut moments de tot però sobretot em quedo amb les persones que n'heu format part i m'heu acompanyat. D'alguna manera un trosset de tesi us correspon i ara us intentaré fer saber lo important que heu sigut per a mi.

Jordi, primer que res t'he d'agrair haver-me donat l'oportunitat de fer la tesi. Gràcies per haver-me deixat aprendre però també equivocar-me. M'has donat l'espai per estavellar-me i alhora la confiança per poder sortir-me'n. També t'agraeixo haver-me donat consell tant científic com personal quan ha sigut necessari. Estic molt contenta d'haver après i compartit ciència amb tu i amb l'equip que has creat.

També als professors de la Unitat de Biofísica i Bioenginyeria, Daniel, Ramon, Isaac, Domènec i Roser.

Noemí, la teva xispa i punt de vista traslacional són la clau dels nostres *labmeetings*. Moltes gràcies per sempre estar disposada a enfocar els nostres projectes més enllà del laboratori.

Als meus companys de laboratori que sou fantàstics moltes gràcies pels cafès, converses de centrífuga i dinars de tupper. Els primers en marxar, Ignasi i Jair, us trobem molt a faltar. Ignasi, al meu calaix sempre hi haurà menjar per quan el necessitis. Jair, ahora ya nadie pone motes, espero poder-te visitar pronto. Esther, trabajadora incansable. Empezamos esta aventura más o menos a la vez y con todos nuestros altibajos en el camino estoy muy contenta de haber podido contar contigo, siempre dispuesta a ayudar y a hacer de cualquier cosa una conversación interesante. Héctor, que siempre llegas con una sonrisa y no sabes decir que no a un café o cualquier plan que surja, lástima que no hayamos podido aprovechar tanto nuestros últimos años de tesis. Agnès, al final no t'hem ensenyat del pipeteo, quan vulguis et fem un seminari on de recompensa tinguis molta orxata. Álvaro, hemos compartido menos tiempo pero te has sabido ganar el corazón de todos con tu sonrisa y tus ganas de aprender. Eliiii! Que vas arribar com un huracà i així has marxat també. Amb tu tots els problemes tenen solució i si no la tenen doncs ho arreglem fent una birra, oi? Moltes gràcies per la teva energia i força!

A la gran família del grup del Jordi que vau començar sent companys de feina i ara sou amics, mil gràcies, sense vosaltres aquesta tesi no hagués sigut possible! Marta, Rafa y Nata siento que me habéis visto crecer, gracias por haberme enseñado a tunear los protocolos para que todo salga bien pero que no se hagan las tantas en el lab. Marta, estic molt contenta d'haver-te conegut amb la teva perspectiva i capacitat de girar l'enfoc, he après molt al teu costat, crec que de la vida més que de la ciència. Recordaré mil converses a cultius o quan ja teníem el cervell fregit a l'ordinador. Rafa! Mira lo diferentes que somos y todo el cariño que nos hemos terminado cogiendo. Muchas gracias por todos los consejos, las risas gratuitas en cualquier momento y el portuguès más loco. Nata, llegaste y tintaste el laboratorio de tu energía, ganas de vivir la vida y pasión por la ciencia. Me enseñaste a volar cuando más lo necesitaba. Siempre dispuesta a hacer un *break* para aclarar la mente o el espíritu. Creo que de las 5 veces en mi vida que me ha pillado la lluvia, 4 estaba contigo. Y es que contigo todo puede ser una aventura y me encanta! Marselina, otra trabajadora incansable, un placer trabajar contigo, creo que nunca me llegaré a imaginar la de tiempo que nos ahorras. Espero que disfrutes mucho de tu nueva etapa. Elba, ets sempre una alenada d'aire fresc, un plaer compartir ciència i riures amb tu. Ale, el polluelo que empieza a volar, creo que llegaste siendo más *viejoven* de lo que eres ahora, así que espero que se te siga llenando el espíritu de juventud. Mireya que aunque no formes parte del grupo oficialmente, no hay nada más oficial en nuestro laboratorio que el café contigo, con tu optimismo y alegría que siempre vienen con dosis de realidad. Muchas gracias por haberme enseñado a pasar la depresión post-vacacional pensando en las siguientes vacaciones.

Al 710 us dec la motivació per fer la tesi. Des del primer moment em vau fer sentir com una més i em vau transmetre la vostra passió per la ciència, les vostres ganes d'aprendre cada dia i la il·lusió d'un nou experiment. Anna, Nacho, Gemma i Sabri al vostre costat sento que tot és possible, mil gràcies per les vostres ganes de viure i disfrutar! Sou genials!

Bioquímiques sóc molt feliç d'haver-vos conegut i que formeu part de la meua vida. Adri que per més lluny que marxis és com si no haguessis marxat mai, una conversa amb tu és sempre un plaer, espero que mos veiguem pronte! Marina per mil moments amb tu, des de converses profundes a les més xorres, des de cantar a ple pulmó en una furgo fins al Cruïlla, sempre un plaer abraçar la vida tal i com ve al teu costat. Marta que sempre tens un joc de taula per ensenyar-nos o alguna excursió/viatge en ment, sempre entusiasta i disposada a unir-te a qualsevol plan, feliç de pensar en la nostra següent aventura juntes. Carlota que sempre tens ganes de passar ni que sigui un ratet juntes per més farta que estiguis de ser tu la que vens a BCN, espero poder-te ensenyar els raconets més bonics del terreno. Laura, sempre lluny però sempre a prop, per mil viatges i seguir fent volar coloms juntes.

Als Xoto's que sou los amics de tota la vida, família vaiga, moltes gràcies per ser-hi. Sou la meua xarxa de suport i saber que esteu incondicionalment m'ha ajudat en los moments més difícils. Aleix en la teua passió i entusiasme, Anca en la teua alegria i ganes d'aprendre, Blanca en la teua manera d'escoltar, Blas en la teua ironia i sarcasme, Clara en la teua energia, vitalitat i força, Eduard en la teua xalera, Feli en les teues ganes d'ajudar i compartir i en les teues caigudes tan mítiques, Jordi en la teua tranquil·litat i ganes de festa, Laura en la teua perspicàcia i la teua rissa , Marta B. en la teua presència reconfortant, Marta R. en la teua manera d'estar tot i els quilòmetres, Robert en la teua manera de ser un amic/germà, i Tania en la teua dolçor i il·lusió feu que sempre tingue ganes d'estar en vatros. Sou los més xaladors i vull seguir fent més records en tots vatros!

Anna i Laia moltes gràcies per haver fet de germanes grans.

Lourdes moltes gràcies per ser-hi sempre, tot i els quilòmetres. Anna i Myriam moltes gràcies per haver sigut els meus referents des de ben petita. Elisa moltes gràcies per fer feliç a mun pare.

David, sóc molt feliç de compartir la vida en tu. Moltes gràcies per les infinites converses i reflexions, gràcies per fer de qualsevol raconet un record especial.

Als meus pares moltes gràcies per haver-me donat tot l'amor del mon. Papa gràcies per sempre tenir un llibre per recomanar-me però sobretot moltes gràcies per la teua manera tan particular de viure la vida plena de llibertat, entusiasme i una curiosa barreja de serenor i disbauxa. Mama, gràcies per ensenyar-me a ser forta sense deixar de ser sensible, et trobo molt a faltar.

TABLE OF CONTENTS

ABBREVIATIONS xi

ABSTRACT xiii

RESUM xiv

INTRODUCTION 1

1. GENERAL CLINICAL ASPECTS OF LUNG CANCER 3

2. TUMOR MICROENVIRONMENT IN LUNG CANCER 4

3. TUMOR-ASSOCIATED FIBROBLASTS 7

3.1. Activation of fibroblasts 8

3.2. TAFs in tumor progression 9

4. PULMONARY TAFs 10

4.1. Hystotype-specific phenotype of lung TAFs 11

5. NINTEDANIB 13

5.1. Nintedanib in lung cancer 14

5.2. Nintedanib targeting fibroblast activation 14

6. TISSUE INHIBITOR OF METALLOPROTEINASES-1 15

6.1. TIMP-1 in lung cancer 18

6.2. TIMP-1 signaling 19

OBJECTIVES 21

MATERIALS AND METHODS 25

1. CELL CULTURE AND GENETIC MANIPULATIONS 27

1.1. Isolation of primary lung fibroblasts 27

1.2. Immortalization of primary fibroblasts 28

1.3. Culture of fibroblasts 28

1.4. Viral transduction of immortalized fibroblasts 29

1.5. Culture of cancer cell lines 29

1.6. Cell transfections 30

1.7. Conditioned medium harvesting 30

1.8. Recombinant TIMP-1 production 31

2. CELLULAR AND MOLECULAR PROCEDURES 31

2.1. hTERT immunofluorescence 31

2.2. Senescence-associated beta-galactosidase activity 31

2.3. Population Doubling Level 32

2.4. Flow cytometry analysis of CD63 32

2.3. Enzyme-linked immunosorbent assay (ELISA) of TIMP-1 32

2.4. TGF-β activity assay 33

2.5. RNA extraction, reverse transcription and quantitative RT-PCR 33
2.6. Protein extraction and western blot 34
3. CELL-BASED FUNCTIONAL ASSAYS 34
3.1. Cell density assay.. 34
3.2. Invasion assay... 35
4. GENERATION OF TUMOR XENOGRAFT MODELS 35
5. HISTOLOGIC ANALYSIS.. 36
5.1. Patient samples: TIMP-1 and CD63 36
5.2. Tumor xenograft: cytokeratins AE1/AE3... 37
6. GENE EXPRESSION ANALYSIS USING PUBLIC DATABASES.. 37
6.1. *TIMP1* and *CD63* expression in lung tissue 37
6.2. *TIMP1* expression in cell lines 37
7. STATISTICAL ANALYSIS 38
RESULTS... 39
1. CHARACTERIZATION OF TIMP-1 AND CD63 EXPRESSION IN NSCLC.................................. 41
1.1. Lung ADC-TAFs show an excessive secretion of TIMP-1 42
1.2. CD63 expression is downregulated in SCC 44
1.3. The expression of the natural CD63 competitor for TIMP-1 binding, *MMP9*, is upregulated in SCC 45
2. THE TGF-β1/SMAD3 FIBROTIC PATHWAY REGULATES THE EXPRESSION AND SECRETION OF TIMP-1 IN LUNG TAFs 46
2.1. TGF-β1/SMAD3 pathway remains active in immortalized fibroblasts 46
2.2. TGF-β1 promotes the expression and secretion of TIMP-1 in lung TAFs.................... 48
2.3. *SMAD3* expression is necessary for the induction of TIMP-1 expression and secretion with TGF-β1 49
2.4. *SMAD3* overexpression is sufficient to promote the expression and secretion of TIMP-1 with TGF-β1 51
3. PRO-TUMORIGENIC CROSSTALK BETWEEN TIMP-1 FROM TAFs AND CD63 IN CANCER CELLS IN LUNG ADC 52
3.1. Inhibition of TIMP-1 in ADC-TAFs diminishes the pro-tumoral activity of their secretome.. 53
3.2. CD63 in ADC cells is necessary for a tumor-promoting crosstalk with the stromal secretome.. 56
3.3. TIMP-1 in TAFs and CD63 in cancer cells are both necessary effector proteins of a tumor-promoting paracrine interaction in lung ADC.. 58
3.4. Recombinant TIMP-1 is sufficient to promote growth and invasion of ADC cells in a CD63-dependent manner... 59
3.5. TIMP-1/CD63/pAkt axis in lung ADC 62

4. TIMP-1 SECRETED FROM LUNG ADC-TAFS ENHANCES INVASIVE GROWTH *IN VIVO* 64

5. LACK OF TIMP-1 MEDIATES RESISTANCE TO NINTEDANIB *IN VITRO* AND *IN VIVO* 67

5.1. Nintedanib abrogates the pro-tumorigenic crosstalk between TIMP-1 from TAFs and CD63^{high} cells 67

5.2. Nintedanib markedly reduces TIMP-1 secretion in ADC-TAFs but not in SCC-TAFS 68

5.3. Nintedanib treatment inhibits pAkt stimulation with TAFs secretome only in CD63^{high} ADC cells 70

5.4. SCC models show resistance to nintedanib *in vivo* 70

5.5. Knocking-down TIMP-1 secretion in ADC-TAFs abrogates the anti-tumor function of nintedanib *in vitro* and *in vivo* 72

DISCUSSION 75

1. HISTOLOGIC SUBTYPE DEPENDENT EXPRESSION OF STROMAL TIMP-1 AND TUMORAL CD63 IN NSCLC 77

2. TIMP-1 IS AN ESSENTIAL SECRETED FACTOR IN THE ABERRANT CROSSTALK BETWEEN TAFs AND CD63^{high} CANCER CELLS IN LUNG ADC 79

3. LIMITED TIMP-1 IN SCC-TAFs ELICITS RESISTANCE TO NINTEDANIB 81

4. IMPLICATION OF THE TIMP-1/CD63 AXIS IN OTHER PULMONARY DISEASES 83

5. EMERGING MODEL: TGF-β1/SMAD3 pathway drives a tumor-promoting TAF-carcinoma crosstalk in ADC through TIMP-1/CD63 that is inhibited by nintedanib 84

CONCLUSIONS 85

SCIENTIFIC ACTIVITY 89

PUBLICATIONS 91

ANNEX 93

A1. Viral transduction of immortalized fibroblasts 95

A2. Transient transfection of fibroblasts and cancer cells using siRNA 98

A3. Flow cytometry of CD63 (membrane protein) 100

A4. TGF-β activity assay 102

A5. Tumor xenograft model of lung fibroblasts co-injected with cancer cells 104

A6. List of ADC and SCC cell lines used in this study and expression values of key genes obtained in the Sanger database 107

BIBLIOGRAPHY 109

ABBREVIATIONS

ADC	Adenocarcinoma
BCA	Bicinchoninic acid
BMP	Bone morphogenic proteins
BSA	Bovine serum albumin
cDNA	Complementary Desoxyribonucleic Acid
CFs	Control fibroblasts
CM	Conditioned medium
COL1A1	Collagen type 1 α-1 chain
COL3A1	Collagen type 3 α-1 chain
DAPI	4′,6-diamidino-2-phenylindole
ECM	Extracellular matrix
ELISA	Enzyme-linked immunosorbent assay
ERK	Extracellular signal-regulated kinases
FAK	Focal adhesion kinase
FAP	Fibroblast Activation Protein
FBS	Fetal bovine serum
FGFR	Fibroblast growth factor receptor
GNB	Galunisertib
HRP	Horseradish peroxidase
hTERT	Human telomerase enzyme
IPF	Idiopathic pulmonary fibrosis
ITS	Insulin-transferrin-selenium-A
MMPs	Matrix Metalloproteinases
mRNA	Messenger Ribonucleic Acid
NSCLC	Non-small cell lung cancer
NTD	Nintedanib
P4HA2	Prolyl 4-hydroxylase subunit α-2
PDAC	Pancreatic ductal adenocarcinoma
PDGFR	Platelet-derived growth factor receptor
PD-1	Programmed death 1

PD-L1	Programmed death-ligand 1 (PD-L1)
PI3K/Akt	Phosphoinositide 3-kinase/Akt pathway
PFA	Paraformaldehyde
rhTIMP-1	Recombinant human tissue inhibitor of metalloproteinases-1
RNA	Ribonucleic Acid
RNA-seq	RNA-sequencing
RT	Room temperature
RT-PCR	Real time-Polymerase chain reaction
SA-βgal	Senescence-associated beta-galactosidase
SB	SB431542
SCC	Squamous cell carcinoma
shCTRL	shRNA control
siCTRL	siRNA control
SMAD3	Mothers against decapentaplegic homolog 3
TAFs	Tumor-associated fibroblasts
TβRI	TGF-β receptor type I
TβRII	TGF-β receptor type II
TCGA	The Cancer Genome Atlas
TIMP-1	Tissue inhibitor of metalloproteinases-1
TGF-β	Transforming Growth Factor β
TMAs	Tissue microarrays
TME	Tumor microenvironment
VEFGR	Vascular endothelial growth factor receptor
WT	Wild-type
α-SMA	α-Smooth Muscle Actin

ABSTRACT

Increased expression of TIMP-1 is associated with poor prognosis in virtually all cancer types, including lung cancer. However, how TIMP-1 is regulated in lung cancer and how it drives tumor progression is poorly defined. In the first part of this thesis, we analyze the expression of TIMP-1 and its cell surface receptor CD63 in two major lung cancer subtypes: lung adenocarcinoma (ADC) and squamous cell carcinoma (SCC). We report that TIMP-1 is aberrantly overproduced in tumor-associated fibroblasts (TAFs) in ADC compared to SCC-TAFs, and identify the selective hyperactivity of the pro-fibrotic TGF-β1/SMAD3 pathway in ADC-TAFs as a major mechanism driving the excessive secretion of TIMP-1 in ADC-TAFs. In contrast, CD63 was markedly downregulated in SCC cells compared to ADC cells. In the second part of this thesis, we define the tumor-promoting effects of the heterotypic crosstalk, specific for ADC patients, between TIMP-1 secreted by TAFs and CD63 in cancer cells. Functional assays revealed that TIMP-1 within the pro-tumoral secretome of TGF-β1-activated ADC-TAFs is necessary and sufficient to promote the growth and invasion of ADC cells in culture. Concomitantly, tumor cell expression of CD63 was required for the tumor-promoting effects of TIMP-1. Consistently, *in vivo* analyses revealed that ADC cells co-injected with fibroblasts with reduced TIMP-1 expression into immunocompromised mice exhibited a lower tumor volume together with a less invasive growth pattern compared to tumors bearing parental fibroblasts. Finally, we studied the relationship of TIMP-1/CD63 crosstalk with the resistance mechanism of SCC patients to nintedanib, which is an antifibrotic drug that has been selectively approved for the treatment of ADC patients. Of note, nintedanib strongly inhibited TIMP-1 secretion in TAFs. Moreover, we observed that TIMP-1 deficient TAFs are resistant to the nintedanib inhibition of their pro-tumoral traits, both *in vitro* and *in vivo*, compared to parental TAFs. This work identifies the first tumor-promoting TAF-carcinoma crosstalk that is selective for lung ADC, provides new insights on the pathologic role of stromal TIMP-1 in lung cancer, identifies a novel resistance mechanism to nintedanib in SCC, and points to the TIMP-1/CD63 interaction as a novel therapeutic target.

RESUM

L'expressió elevada de TIMP-1 està associada a un mal pronòstic en gairebé tots els tipus de càncer, inclòs el càncer de pulmó. No obstant, es desconeix com es regula l'expressió de TIMP-1 en càncer de pulmó ni mitjançant quins mecanismes promou la progressió tumoral. En la primera part d'aquesta tesi, s'han analitzat els nivells de TIMP-1 i CD63, el seu receptor de membrana, en els dos subtipus majoritaris de càncer de pulmó: l'adenocarcinoma (ADC) i el carcinoma escatós (CE). Hem trobat que en els fibroblasts associats al tumor (TAFs de l'anglès) del subtipus ADC hi ha una secreció aberrant de TIMP-1 en comparació amb els TAFs de CE. Aquesta excessiva secreció de TIMP-1 en ADC es deu a la hiperactivació selectiva de la via del TGF-β1/SMAD3 en aquest subtipus de TAFs. D'altra banda, els nivells de CD63 són més baixos en les cèl·lules canceroses de CE que en les d'ADC. En la segona part d'aquesta tesi, hem descrit els efectes pro-tumorals d'un mecanisme de comunicació creuada entre el TIMP-1 secretat pels TAFs i el CD63 de les cèl·lules canceroses que és específic per als pacients amb ADC. El TIMP-1 secretat pels TAFs d'ADC és necessari i suficient per promoure el creixement i la invasió en les cèl·lules de càncer. Simultàniament, l'expressió de CD63 en les cèl·lules tumorals es necessària per observar aquests efectes pro-tumorals del TIMP-1. De manera consistent, *in vivo* hem observat que la inhibició de la secreció del TIMP-1 redueix tant el volum tumoral com el creixement invasiu en ratolins co-injectats amb cèl·lules canceroses i TAFs. Finalment, hem estudiat la relació d'aquesta comunicació creuada amb la resistència al nintedanib trobada en pacients amb CE, el qual és un fàrmac antifibròtic aprovat selectivament en pacients amb ADC. Hem observat que en els TAFs en els quals s'ha inhibit genèticament la secreció de TIMP-1, hi ha una menor resposta a nintedanib. Aquest treball identifica per primer cop un mecanisme de comunicació creuada entre TAFs i cèl·lules canceroses que és específic per pacients amb ADC, aporta nous coneixements sobre el rol patològic del TIMP-1 en càncer de pulmó, descriu un nou mecanisme de resistència al nintedanib en CE i apunta la interacció TIMP-1/CD63 com a nova diana terapèutica.

INTRODUCTION

1. GENERAL CLINICAL ASPECTS OF LUNG CANCER

Lung cancer is an aggressive heterogeneous disease with multiple histologic subtypes and molecular phenotypes. According to the World Health Organization, in 2020, lung cancer was the second most common form of cancer and the leading cause of cancer mortality in men and women worldwide, representing 18% of cancer deaths [1]. After diagnosis, the overall 5-year survival rate is 18%. This poor prognosis is partly caused by the fact that most lung cancer patients are asymptomatic while the disease develops and are consequently diagnosed with locally advanced or widely metastatic tumors [2].

According to histopathologic characteristics, more than 85% of lung cancer patients are diagnosed with non-small cell lung cancer (NSCLC). NSCLC is further classified into adenocarcinoma (ADC; ~ 50%), squamous cell carcinoma (SCC; ~ 40%), and other less frequent subtypes (~ 10%) [3].

In NSCLC, treatment intervention is decided according to histology and stage, which is based on the TNM system [4]. This system associates groups of patients with similar prognosis based on the tumor size (T), lymph node metastasis (N) and metastatic disease (M).

Treatment options for lung cancer include surgical resection, chemotherapy, radiotherapy, targeted therapies, and immunotherapy (**Table 1**). Surgical resection is the most effective therapy for early stages. However, patients at stages I and II only represent ~5-20% of NSCLC, and tumor resection is only feasible in a fraction of these patients [2]. The standard therapy for locally advanced NSCLC (stage III) is combined cytotoxic chemotherapy with thoracic radiation [5]. However, these treatments have limited response, commonly relapsing with aggressive metastasis [6]. For these patients diagnosed with advanced NSCLC (stage IV), several therapeutic strategies exist, depending on the histologic, molecular, and immunologic characteristics of the tumor.

A promising step in lung cancer treatment was the identification of driver mutations that are sensitive to tyrosine kinase inhibitors or monoclonal antibodies. Of note, the potentially targetable mutations in ADC are not prevalent in SCC [3]. Even though targeted therapies have improved survival rates in metastatic patients (stage IV), tumors treated with targeted therapies commonly relapse, and disease progression eventually occurs [7]. Furthermore, patients harboring targetable mutations are only 15-20% [8]. Moreover, research focused on cancer cell-intrinsic properties has not improved the overall survival rates for NSCLC, and chemotherapy remains the standard first-line treatment for patients at advanced stage who do not fit an approved molecular targeted therapy [9].

On the other hand, therapeutic approaches modulating the immune system of lung cancer patients have been the most recent improvement in the treatment of metastatic NSCLC. The axis mediated by programmed death 1 (PD-1) protein binding to programmed death-ligand 1 (PD-L1) is a major mediator of immune evasion. Pembrolizumab, a humanized antibody against PD-1 protein [10], is the standard of care for lung tumors expressing ≥ 50% of PD-L1 [5]. The 30% of lung tumors have an increased activity of PD-L1, and those have shown notable clinical responses to immunotherapy [11].

STAGE	INCIDENCE	TREATMENT	5-YEAR SRUVIVAL
I	15-20%	Surgery	70-90%
II	5-10%	Surgery	50-60%
III	30-35%	Combined chemotherapy and radiotherapy	13-36%
IV	35-40%	Chemotherapy, immunotherapy, targeted therapies	0-10%

Table 1. Summary of incidence (%), treatment and 5-year survival (%) of NSCLC patients according to staging. *Adapted from the Thoracic Oncology course of the University of Michigan* offered by Coursera (https://es.coursera.org/learn/thoracic-oncology).

To summarize, surgical resection is the only treatment with curative intent, whereas the disease becomes chronic with the other therapeutic strategies at their best. Therefore, despite advances in treatment options for subsets of patients, the overall cure and survival rates remain poor. Therefore, there is an urgent need to improve the outcome of lung cancer patients.

2. TUMOR MICROENVIRONMENT IN LUNG CANCER

Tumor progression has been recognized as the product of an evolving interaction between different cell types and the surrounding supporting tissue. This new ecosystem within the host organ is known as the tumor microenvironment (TME), which consists of fibroblasts, vascular cells, immune cells, and a dense extracellular matrix (ECM) (**Figure 1**) [12]. The cancer cells harboring oncogenic mutations are embedded in this TME, which varies considerably from tumor to tumor. The TME not only contributes to the progression of lung carcinomas but determines treatment outcomes [13]. Hence, in addition to elucidating the molecular alterations of cancer cells, it is necessary to characterize the complex TME biology to understand and treat lung cancer.

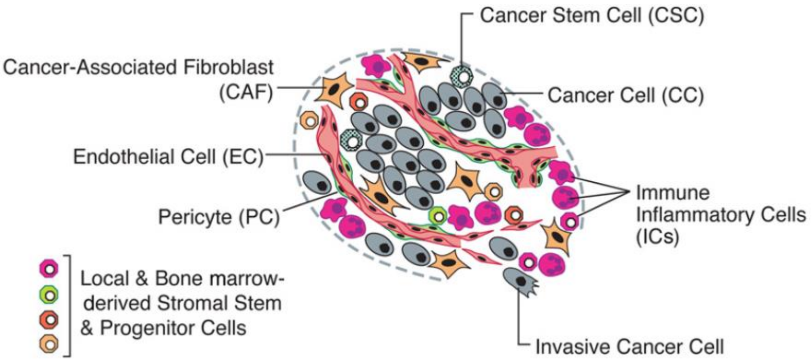
Cancer Stem Cell (CSC)
Cancer-Associated Fibroblast (CAF)
Cancer Cell (CC)
Endothelial Cell (EC)
Pericyte (PC)
Immune Inflammatory Cells (ICs)
Local & Bone marrow-derived Stromal Stem & Progenitor Cells
Invasive Cancer Cell

Figure 1. Picture showing the complex cellular composition of the tumor microenvironment. In tumors, cancers cells (CC) are surrounded by cancer stem cells, cancer-associated fibroblasts, endothelial cells, perycites, immune inflammatory cells, and a variety of bone marrow-derived cells. *Adapted from Hanahan and Weinberg 2011*.

In normal physiologic conditions, the stroma of the lung is essential for maintaining the airway epithelium integrity and homeostasis (**Figure 2**). Of note, both the epithelial and the stromal compartments are characteristic for each location of the lung (**Figure 2**). However, in tumors, cancer cells alter normal tissue homeostasis through an aberrant signaling with the adjacent stroma to ultimately form a permissive and supportive microenvironment. Changes in the stroma commonly accompanying tumor progression include loss of the integrity of the basement membrane, several immune responses, formation of new blood vessels (angiogenesis), activation of stromal fibroblasts, and subsequent remodeling of the ECM [14]. The cooperation of the supportive stroma with cancer cells drives tumorigenesis, ultimately resulting in a fatal disease [15].

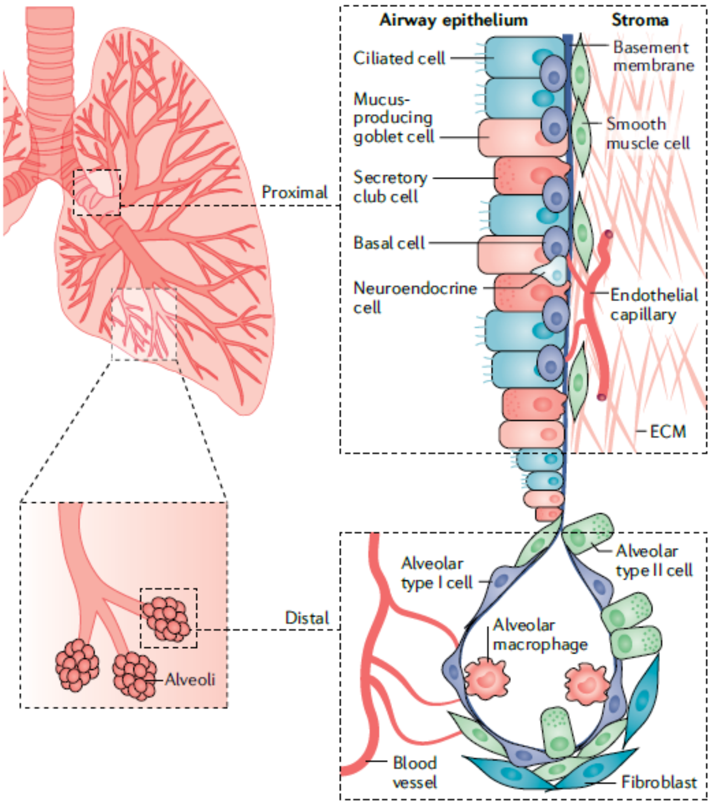
Airway epithelium
Stroma
Ciliated cell
Mucus-producing goblet cell
Secretory club cell
Basal cell
Neuroendocrine cell
Basement membrane
Smooth muscle cell
Endothelial capillary
ECM
Proximal
Distal
Alveoli
Alveolar type I cell
Alveolar type II cell
Alveolar macrophage
Blood vessel
Fibroblast

Figure 2. Schematic representation of the lung architecture and cellular composition of the airway epithelium and stroma in normal conditions. The proximal epithelium contains ciliated, globet, basal, and neuroendocrine cells surrounded by an organized ECM containing endothelial and smooth muscle cells. The basement membrane, separating the airway epithelium from the stroma, organizes the structure of the epithelium. In the distal lung, the alveolar epithelium is constituted by alveolar type I and type II cells surrounded by fibroblasts, muscle cells, and capillaries. The alveolar space contains alveolar macrophages. *From Altorki et al, 2019*.

Although ADC and SCC are malignant epithelial tumors, both tumor subtypes frequently have a desmoplastic stroma, which accounts for the expansion of an overabundant stroma around an invasive tumor [16]. Regarding their origin, ADC typically derives from alveolar type II cells and arises in more distal airways, whereas SCC frequently derives from basal cells, appears in more proximal airways, and is more strongly associated with smoking and chronic inflammation than ADCs [3]. Remarkably, increasing data shows that the genetic alterations of cancer cells, which markedly influence the phenotype of stromal cells, are distinct in ADC and SCC tumors [3]. Likewise, based on the different origin, anatomic location, and smoking association, it is conceivable that ADC and SCC tumors may have subtype-specific stromal aberrations. In line with this hypothesis, in a recent study of the TME transcriptome of lung tumors using single-cell RNA-sequencing (RNA-seq), Lambrechts et al. pictured the complexity and heterogeneity of lung TME, identifying 7 subtypes of TAFs (some of them enriched in a particular histologic subtype) and up to 45 other subtypes of stromal cells within lung tumors [17].

In further agreement with this idea, drugs targeting the TME have shown beneficial effects in NSCLC in a histologic subtype-dependent manner. Exclusively in non-SCC patients, bevacizumab, an antiangiogenic monoclonal antibody against the vascular endothelial growth factor (VEGF), in combination with chemotherapy, increased their overall survival [18]. In addition, the triple angiokinase inhibitor, nintedanib, combined with cytotoxic docetaxel, significantly extended the median overall survival in ADC patients [19]. However, neither the mode of action of nintedanib in ADC nor its resistance mechanism in SCC have been elucidated. These clinical characteristics support a histologic subtype-dependent TME phenotype in lung cancer. However, the histotype specificity of stromal desmoplastic features remains poorly defined in NSCLC.

3. TUMOR-ASSOCIATED FIBROBLASTS

Although the normal stroma of the lung contains non-activated fibroblasts, the stroma of ADC and SCC patients is highly fibrotic and contains abundant activated fibroblasts exhibiting a myofibroblast-like phenotype (**Figure 3**) [20, 21]. Fibroblasts within tumors are called tumor-associated fibroblasts (TAFs) or cancer-associated fibroblasts (CAFs).

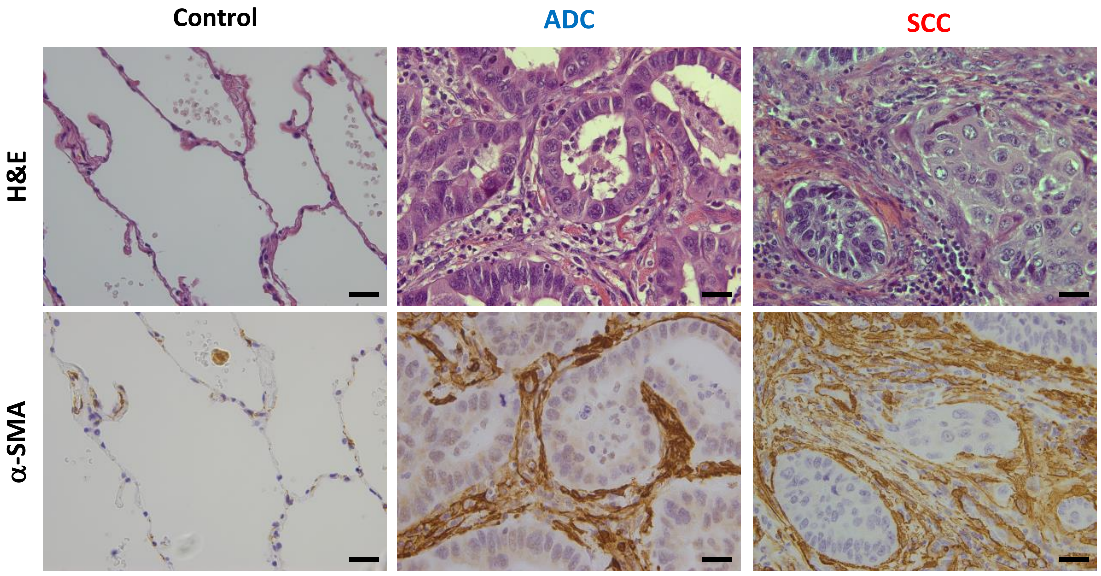

Figure 3. Illustrative images of normal lungs and highly desmoplastic ADC and SCC tumors. Hematoxylin & eosin (H&E, top) and α-SMA (bottom) staining of histologic samples from primary control (left), ADC (middle), and SCC (right column) pulmonary tissue obtained with a x40 objective. *Adapted from Puig et al, 2015.*

Fibroblasts in a normal tissue synthesize the ECM, regulate ECM turnover by secreting ECM-degrading proteases such as matrix metalloproteinases (MMPs), and maintain tissue homeostasis through direct or indirect interaction with epithelial cells. Normal fibroblasts are spindle-shaped cells responsible for healing the wound after tissue injury. Upon injury, fibroblasts become activated, exhibiting a higher deposition of ECM and acquiring contractile properties to ultimately close the wound (**Figure 4**). Under physiologic conditions, fibroblast activation is a tightly controlled process; after tissue repair, fibroblast phenotype is restored or undergo apoptosis [22]. Similar to wound repair, TAFs within the tumor are activated and frequently identified by a higher secretory activity concomitantly with the expression of fibroblast activation protein (FAP), vimentin, contractile proteins such as α-smooth muscle actin (α-SMA), and ECM components such as fibrillar collagens [16]. However, unlike fibroblasts healing a wound, TAFs show a chronically activated phenotype, which has granted the interpretation of tumors as “wounds that never heal” [23].

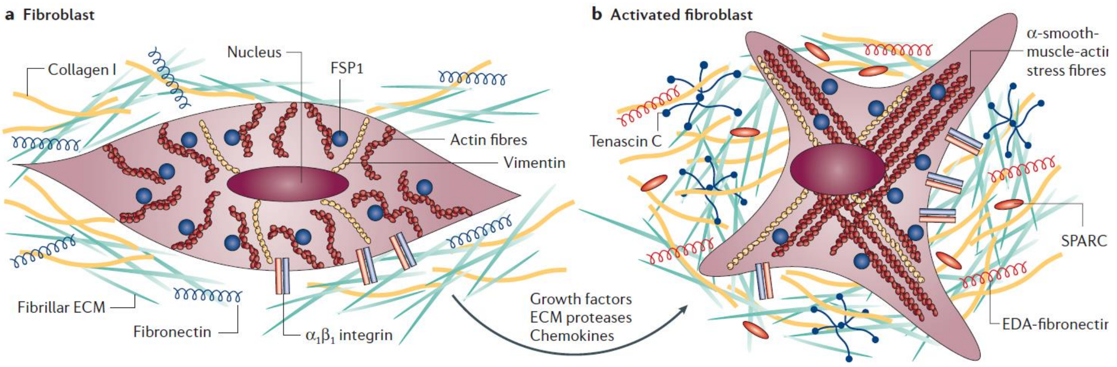
a Fibroblast
Collagen I
Nucleus
FSP1
Actin fibres
Vimentin
Fibrillar ECM
Fibronectin
$\alpha_1\beta_1$ integrin
Growth factors
ECM proteases
Chemokines
b Activated fibroblast
α-smooth-
muscle-acti
stress fibres
Tenascin C
SPARC
EDA-fibronecti

Figure 4. Phenotypic and morphologic characteristics of normal and activated fibroblasts. a, Normal fibroblasts **b**, Activated fibroblasts expressing contractile proteins such as α-SMA. Numerous growth factors but especially Transforming Growth Factor β mediate the activation of fibroblasts. *From Kalluri and Zeisberg 2006.*

3.1. Activation of fibroblasts

Fibroblasts are strongly activated by Transforming Growth Factor β (TGF-β), a pleiotropic cytokine frequently upregulated in NSCLC [24] that has a central role in running a complete pro-fibrotic program [14, 25]. In tumors, TGF-β is largely expressed by cancer cells and immune cells; additionally, fully activated fibroblasts sustain their active status by autocrine production of this cytokine [26].

The large TGF-β family of cytokines includes TGF-β and the bone morphogenic proteins (BMP) among others [27]. Three TGF-β isoforms have been identified in mammals: TGF-β1, TGF-β2, and TGF-β3 [28]. TGF-β signals are transduced to the nucleus through mothers against decapentaplegic-2/3 (SMAD2/3) transcription factors to coordinately induce α-SMA and collagens expression in TAFs. Active TGF-β binds to a complex receptor composed of transmembrane receptor serine/threonine kinases, the type I

(TβRI/ALK 5) and type II (TβRII) receptors. Subsequently, receptor type II phosphorylates the kinase domain of the receptor type I, propagating the signal transduction through SMAD2/3 phosphorylation (**Figure 5**) [29]. Phosphorylated SMADs form assembled complexes with SMAD4 that translocate to the nucleus to directly control gene expression. In addition to the receptor-regulated SMADs (R-SMADs: 1, 2, 3, 5 and 8) and the Co-mediator SMAD4, the inhibitory SMADs (SMADs 6 and 7) negatively regulate TGF-β signaling by competing with R-SMADs for receptor or Co-SMAD interaction. SMAD2 and SMAD3 respond to signaling by the TGF-β subfamily, whereas SMADs 1, 5, and 8 primarily respond to cytokines of the BMP subfamily.

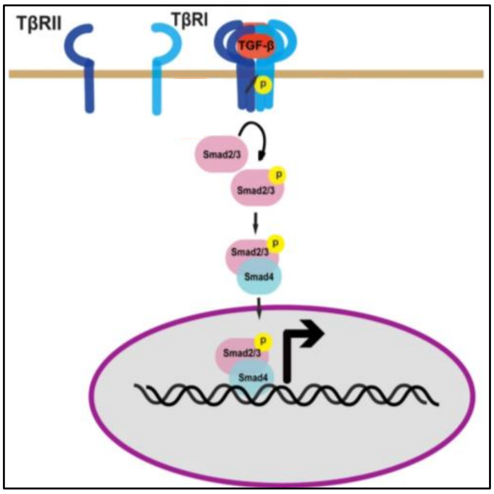

Figure 5. TGF-β signaling through SMAD2/3. Active pSMAD2/3 after TGF-β binding to TβRI and TβRII form a complex with SMAD4 that translocates to the nucleus and controls gene transcription. *Adapted from Huang et al, 2012*.

3.2. TAFs in tumor progression

Several studies have evaluated the association of TAF-related factors with patient outcome to shed light on their role in the progression of certain cancers. Moreover, studying the prognostic value of TAF-derived factors is also interesting to predict their suitability for being targeted in anticancer therapies [30].

Navab and colleagues demonstrated that an expression signature derived from lung TAFs associated genes had prognostic impact in NSCLC [31]. Similarly, in breast cancer, the presence of TAFs in the stroma correlated with poor prognosis [32]. Likewise, the global set of genes that showed a positive association with colorectal cancer recurrence was significantly upregulated in TAFs [33].

In line with these findings supporting that TAFs promote tumor progression, two decades ago, Olumi and colleagues indicated that TAFs from prostate tumors stimulated tumor progression in a mice model when co-injected with nontumorigenic prostate epithelial cells, whereas co-injection with normal prostatic fibroblasts did not give rise to neoplasia [34]. Likewise, breast cancer cells co-injected with TAFs formed larger tumors than those co-injected with healthy fibroblasts [12, 35]. Yet, how normal fibroblasts prevent tumorigenesis remains unknown.

Remarkably, even though the malignant transformation of cancer cells implies acquiring the capability to sustain proliferative signaling and to invade [13], the secretome of TAFs increases these proliferating and invading capacities *in vitro* [36, 37]. Moreover, TAFs remodel the ECM around the primary tumor, facilitating and guiding the invasion of cancer cells [38]. To sum up, the interaction between cancer cells and TAFs, either through cell-cell contact or paracrine signaling, is essential for invasive growth and is associated with poor clinical prognosis [39].

In contrast with these pro-tumorigenic functions of TAFs, Ozdemir et al. illustrated the complexity of TAFs function in pancreatic ductal adenocarcinoma (PDAC) using transgenic mice with depleted α-SMA$^+$ fibroblasts, which resulted in highly invasive tumors [40]. Similarly, the deletion of a signaling factor that promotes stromal desmoplasia in PDAC led to more aggressive tumors with reduced stromal content in a mice model [41].

Therefore, determining the role of TAFs in tumor progression and metastasis is challenging. It has become apparent that this challenge lies in the phenotypical heterogeneity of TAFs [17] and the consequent lack of appropriate markers for identifying tumor-promoting TAFs. Since TAFs can have both protumorigenic and antitumorigenic activities, non-specific targeting or deletion of TAFs may not improve tumor management. Alternatively, to effectively compromise the tumor-promoting activity of lung TAFs, understanding the molecular and phenotypical differences between normal and tumor fibroblasts together with defining the functions of TAF subtypes is imperative.

4. PULMONARY TAFs

Paracrine signaling through secreted factors from TAFs is a relevant mechanism modulating the behavior of cancer cells and the other cellular components of the TME. Accordingly, lung TAFs show an altered pattern of paracrine and autocrine effectors that have been described to induce angiogenesis [42], tumor growth and invasion [43, 44], and resistance to therapies [45, 46]. Blocking the specific proteins involved in the pathologic cancer cell-TAF communication is an attractive therapeutic option [47]. However, since lung TAFs populations have emerged as molecularly heterogeneous [17], there is a subtle line between favorable and detrimental anti-TAF treatments. The successful prevention of the paracrine signaling of TAFs in NSCLC requires identifying the relationship between TAFs populations and these TAF-secreted factors that drive tumorigenesis.

The first step for defining tumor-promoting TAFs in lung cancer was the analysis of gene-expression differences between normal and tumoral pulmonary fibroblasts [31]. Notably, some of the genes that appeared differentially expressed in this study are regulated by the TGF-β signaling pathway. However, the molecular mechanisms regulating the aberrant phenotype of lung TAFs remained unknown.

On the other hand, lung TAFs cultured in the absence of cancer cells maintain their tumor-promoting traits [37, 48], indicating that TAFs acquire epigenetic alterations that sustain their chronic activation.

Accordingly, epigenetic modifications of fibroblasts have emerged as a crucial mechanism driving the irreversible activation of TAFs in cancer [49-52]. The best-studied epigenetic modification is DNA methylation, in which a methyl group (CH3) is added to the CpG islands within the genomic DNA by DNA methyltransferases. An aberrant DNA methylation leads to either hypermethylated or hypomethylated DNA. The hypermethylation of gene promoters represses gene transcription, whereas the loss of the methyl group in a CpG island that is normally methylated can lead to gene transcription activation [53]. Comparing the genome-wide DNA methylation status between control fibroblasts (CFs) and paired TAFs from surgical patients with early stage NSCLC, our group observed a global DNA hypomethylation concomitantly with a selective impact on *SMAD3* and other key transcription factors of the TGF-β pathway in TAFs [54]. Nonetheless, how the epigenetic reprogramming of lung TAFs influences either TAF heterogeneity or its tumor-promoting phenotype is poorly understood.

4.1. Hystotype-specific phenotype of lung TAFs

Chang and colleagues brought to the field the idea that fibroblast phenotype can be specific for each anatomic location. They conducted gene expression analyses of fibroblasts derived from different organs and revealed that fibroblasts display characteristic transcriptional patterns for each tissue of origin [55]. Since fibroblasts phenotypes are highly context-dependent and clinical evidence indicates that ADC and

SCC tumors may have distinct TME aberrations [18, 19], it is conceivable that TAFs from each histologic subtype exhibit specific phenotypes.

In line with this idea, previous investigations of our group have sought to determine the nature of the responses to TGF-β1 of lung TAFs isolated from ADC and SCC patients to ultimately identify selective antifibrotic therapies against the pathologic stroma-carcinoma interactions for each subtype [56]. In agreement with previous work showing that epigenetic reprogramming drives the aberrant phenotype of TAFs, it was found that the promoter of the TGF-β pathway transcription factor, *SMAD3,* was strongly hypermethylated in SCC-TAFs with respect to paired CFs. The epigenetic repression of *SMAD3* in SCC-TAFs elicited a lower expression of α-SMA and collagens compared to ADC-TAFs, which overexpressed these fibrotic factors regulated by the TGF-β1/SMAD3 pathway in comparison to paired CFs. Therefore, our group unveiled that ADC-TAFs are more fibrotic than SCC-TAFs and that this different phenotype is partly due to the epigenetic repression of TGF-β1/SMAD3 pathway in lung SCC-TAFs. Consistently, SMAD3 staining and tumor fibrosis, as determined by collagen staining, are higher in ADC than in SCC patients [56, 57]. Accordingly, it is reasonable to expect that antifibrotic therapies targeting the TGF-β1/SAMD3 signaling pathway could be more effective in ADC-TAFs than SCC-TAFs (**Figure 6**).

Furthermore, this previous work also established a causal link between smoking and the larger *SMAD3* epigenetic repression of SCC-TAFs (**Figure 6**) [56]. Indeed, smoking is more strongly associated with SCC than ADC patients and induces diverse epigenetic alterations.

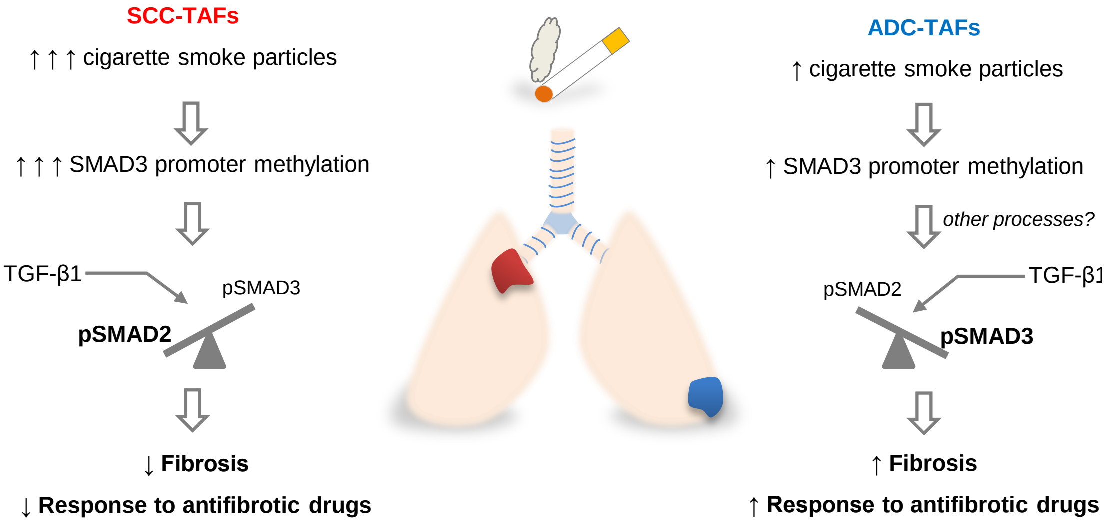
SCC-TAFs
↑↑↑ cigarette smoke particles
↑↑↑ SMAD3 promoter methylation
TGF-β1
pSMAD3
pSMAD2
↓ Fibrosis
↓ Response to antifibrotic drugs
ADC-TAFs
↑ cigarette smoke particles
↑ SMAD3 promoter methylation
other processes?
pSMAD2
TGF-β1
pSMAD3
↑ Fibrosis
↑ Response to antifibrotic drugs

Figure 6. Proposed model for the role of *SMAD3* promoter methylation to the response to antifibrotic drugs in lung TAFs. The downregulation of SMAD3 through promoter methylation drives a lower fibrotic phenotype in SCC-TAFs (left), while the hyperactivation of TGF-β1/SMAD3 pathway in ADC-TAFs (right) drives to a more fibrotic phenotype. *Adapted from Ikemori et al, 2020*.

On the other hand, whether the phenotypical differences between ADC-TAFs and SCC-TAFs found in this previous work [56] may elicit specific paracrine signaling in each TAF subtype remains poorly defined. The aberrant hyperactivation of the TGF-β1/SMAD3 pathway in ADC-TAFs was associated with the secretion of pro-tumoral factors, although the precise identity of these factors was not determined. Likewise, in SCC-TAFs, the mechanisms driving a pro-tumorigenic phenotype and the specific pro-tumoral molecules within their secretome remain largely undefined.

5. NINTEDANIB

Nintedanib (BIBF 1120) is a multityrosine kinase inhibitor simultaneously blocking the pathways mediated by the vascular endothelial growth factor receptor (VEGFR) family, the fibroblast growth factor receptor (FGFR) family, the platelet-derived growth factor receptor (PDGFR) family, as well as Src and Flt-3 kinases [58]. These three families have well-known roles in tumor angiogenesis and cancer progression, as illustrated by the formation of new blood vessels by VEGF signaling through VEGFR [59, 60]. On the other hand, tumors acquire resistance to anticancer therapies blocking VEGF and may reactivate tumor angiogenesis through FGF signaling [61]. Alternatively, PDGF in synergy with FGF has been described to promote tumor angiogenesis [62]. Accordingly, this triple angiokinase inhibitor was initially tested in the clinic for its potential in completely inhibiting tumor angiogenesis. Moreover, nintedanib has also reported an impairment of fibrosis.

Indeed, even though nintedanib was originally developed for oncology, it has also been approved as an antifibrotic drug for Idiopathic Pulmonary Fibrosis (IPF) treatment. IPF is characterized by the loss of the pulmonary architecture in which the alveolar epithelium is replaced by abundant activated fibroblasts and excessive ECM deposition [63]. Hence, IPF patients have a reduced reserve volume of the lungs concomitantly with a declined forced vital capacity [64]. Nintedanib slowed the decrease of the forced vital capacity, consequently improving the quality of life of IPF patients and slowing the progression of this chronic and fatal lung disease [65].

Although nintedanib is increasingly acknowledged as a potent antifibrotic drug, the mechanism underlying its attenuation of fibrosis has not been fully elucidated. Several investigations thus far have shown that nintedanib inhibits TGF-β1-induced expression of α-SMA, collagens, and the early activation of SMAD3 in lung fibroblasts [66, 67], revealing that nintedanib interferes with the TGF-β/SMAD3 signaling pathway in lung fibroblasts.

5.1. Nintedanib in lung cancer

The first-line treatment for NSCLC patients with advanced or metastatic tumors without targetable mutations is chemotherapy or immunotherapy, depending on the PD-L1 levels. Unfortunately, the disease often progresses in many patients, subsequently needing second-line therapy [5]. Non-squamous patients relapsing after first-line chemotherapy receive cytotoxic docetaxel in combination with nintedanib as second-line therapy owing to the clinical benefits observed in the LUME-Lung 1 clinical trial in this patient group [19].

In the LUME-Lung 1 clinical trial (testing the clinical efficacy of nintedanib + docetaxel *versus* docetaxel alone), 658 patients with lung ADC and 555 with lung SCC were included, and it was observed that nintedanib significantly improved the efficacy of docetaxel only in ADC but not in patients with SCC histology (**Figure 7**) [19]. However, the biological processes underlying this nintedanib-dependent increased overall survival selectively in ADC were not identified. To date, tumor xenografts and *in vitro* experiments have shown that nintedanib has a poor effect on reducing the proliferative activity of cancer cells; instead, it is widely accepted that nintedanib diminishes tumor growth by targeting the TME [58, 68].

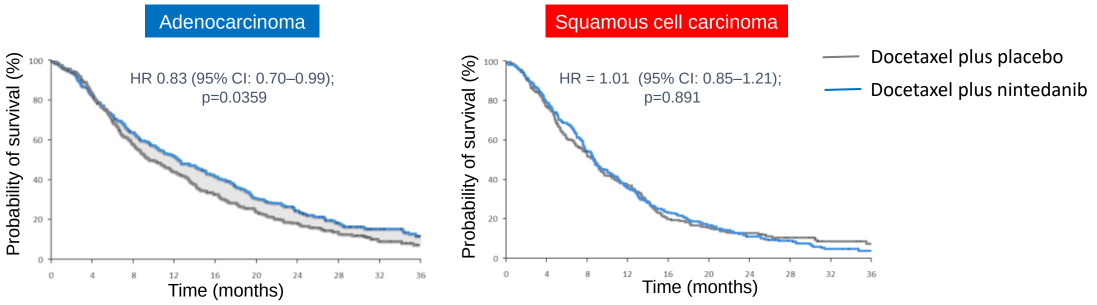

Figure 7. Kaplan-Meier survival curves stratifying NSCLC patients for treatment. Patients with adenocarcinoma (left) and squamous cell carcinoma (right) receiving docetaxel plus placebo (grey line) or docetaxel plus nintedanib (blue line). HR= hazard ratio. *Adapted from Reck et al, 2014*.

5.2. Nintedanib targeting fibroblast activation

Aiming to determine the potential antifibrotic mechanism underlying the selective efficacy of nintedanib in lung ADC patients, and in line with previous studies [66, 67], our group observed that nintedanib hindered TGF-β1-activation of lung TAFs [37]. Remarkably, SCC-TAFs in culture showed a poorer response to nintedanib than ADC-

TAFs [37]. Furthermore, this reduced response to nintedanib was associated with the stronger hypermethylation of the *SMAD3* promoter of SCC-TAFs [56].

In addition to inhibiting TAFs activation, it has been reported that nintedanib hindered the production of several tumor-promoting factors in TAFs from intrahepatic cholangiocarcinoma, such as interleukin-6 and interleukin-8, impairing the pro-tumoral activity of their secretome [69].

In line with this study, we demonstrated that nintedanib abrogates the pro-tumoral activity of the secretome in ADC-TAFs but not in SCC-TAFs [37]. These results unveiled that the paracrine signaling of TAFs in NSCLC is subtype-specific. However, the growth factors and cytokines from ADC-TAFs and SCC-TAFs that control the behavior of ADC and SCC cancer cells and are differentially targeted by nintedanib have not been determined yet.

On the other hand, since TAFs have been implicated in several resistance mechanisms to anticancer therapies [70, 71], it is conceivable that SCC-TAFs may mediate the resistance to nintedanib found in SCC. However, the molecular mechanism underlying the resistance of SCC-TAFs to nintedanib and its contribution to the therapeutic resistance observed in SCC patients have been only partially addressed [56]. Fully comprehending the molecular aberrations driving the weak response of SCC-TAFs to nintedanib can lead to the development of therapies effectively targeting the stroma of lung SCC. Moreover, defining the stromal secreted factors underlying the selective response of ADC patients to nintedanib may facilitate the identification of predictive biomarkers.

6. TISSUE INHIBITOR OF METALLOPROTEINASES-1

The tissue inhibitor of metalloproteinases-1 (TIMP-1) appeared as one of the molecular targets of nintedanib [72]. TIMP-1 is one of the four members of the TIMP family of secreted proteins (TIMP-1,-2,-3, and -4), which have ubiquitous expression and are generally synthesized by the tissue stroma [73, 74]. The role of TIMP-1 in cancer progression has been historically controversial since there is evidence supporting both a favorable and a detrimental influence.

Initially, TIMP-1 was considered to inhibit cancer progression for being a natural broad-spectrum inhibitor of MMPs [75], which may facilitate cancer dissemination through proteolytic degradation of the ECM; moreover, there is evidence that TIMP-1 overexpression can have inhibitory/negative effects on the invasive capacity of cancer cells *in vitro* [76]. However, early studies showed that a wide range of cells, including normal epithelial or carcinoma cells, needed TIMP-1 in the serum to proliferate [77]; alternatively, secreted TIMP-1 inhibited apoptosis of tumor cells [78, 79]. Furthermore, increased tissue levels of TIMP-1 are associated with aggressive cancers and poor outcome in nearly all cancer types [73, 80-83], including lung cancer [84-86], thereby favoring a tumor-promoting function.

The paradox of the diverse and often opposing functions of TIMP-1 has been partially addressed by identifying its structure in two functionally independent and physically distinct domains [87]. The N-terminal domain binds to and inhibits MMPs, whereas the C-terminal domain exhibits cytokine-like functions by interacting with the cell surface receptor CD63 to initiate intracellular signaling cascades [79] (**Figure 8**). Accordingly, TIMP-1 is now recognized as a multi-functional protein harboring a large interactome.

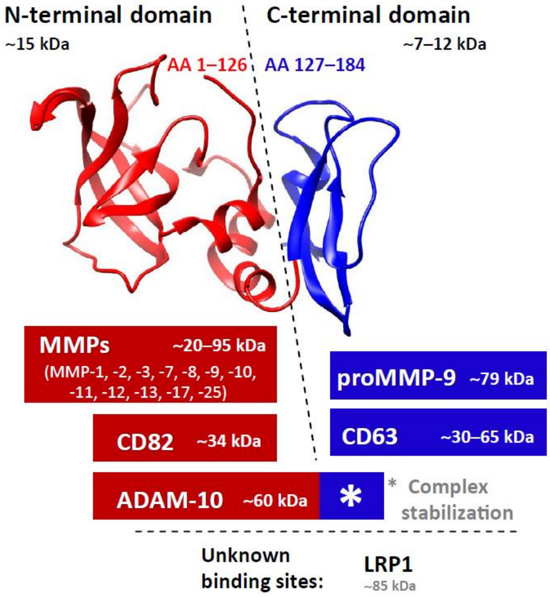
N-terminal domain
~15 kDa
AA 1–126
C-terminal domain
~7–12 kDa
AA 127–184
MMPs ~20–95 kDa
(MMP-1, -2, -3, -7, -8, -9, -10, -11, -12, -13, -17, -25)
CD82 ~34 kDa
ADAM-10 ~60 kDa
proMMP-9 ~79 kDa
CD63 ~30–65 kDa
*
* Complex stabilization
Unknown binding sites:
LRP1
~85 kDa

Figure 8. Two-domain structure of TIMP-1. Proteins that interact with TIMP-1 through its N-terminal (left) or C-terminal (right) domain. *From Grunwald et al, 2019*.

Illustrating TIMP-1 complexity, Guedez and colleagues observed that TIMP-1 overexpression in Burkitt's lymphoma cells had different activities throughout lymphomas progression *in vivo* with an initial tumor promoting phase, followed by tumor regression and necrosis due to angiogenesis inhibition by TIMP-1 [88]. In agreement with this study, it is becoming apparent that TIMP-1 not only alters cancer cells behavior but modulates the host tissue response [89]. Therefore, TIMP-1 is emerging as a protein released within the tumor with different effects in each cell type as tumor progresses.

Furthermore, recent reviews have pointed that the biological role of this complex protein, both in health and disease, may depend on free TIMP-1 availability, which is determined by the composition of proteases in the extracellular space [89, 90] (**Figure 9**). Hence, TIMP-1 has the potential to affect tissue pathology by separated but co-existing mechanisms whose individual activities depend on the cellular and molecular context. Since TIMP-1 functions are strongly context-dependent, its role in cancer progression has to be studied for each TME.

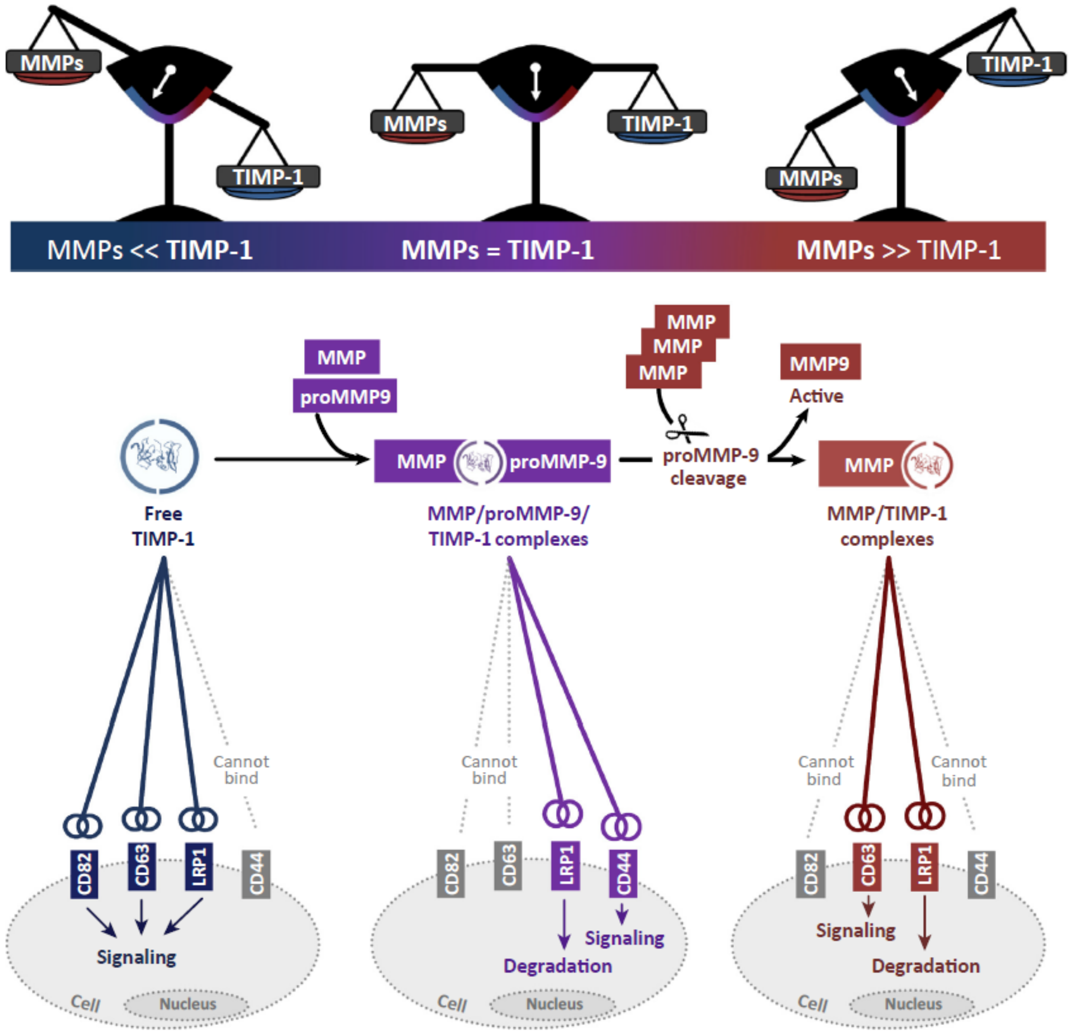
MMPs
TIMP-1
MMPs
TIMP-1
TIMP-1
MMPs
MMPs << TIMP-1
MMPs = TIMP-1
MMPs >> TIMP-1
MMP
proMMP9
MMP
MMP
MMP
MMP9
Active
Free
TIMP-1
MMP
proMMP-9
proMMP-9
cleavage
MMP
MMP/proMMP-9/
TIMP-1 complexes
MMP/TIMP-1
complexes
Cannot
bind
CD82
CD63
LRP1
CD44
Signaling
Cell
Nucleus
Cannot
bind
CD82
CD63
LRP1
CD44
Signaling
Degradation
Cell
Nucleus
Cannot
bind
Cannot
bind
CD82
CD63
LRP1
CD44
Signaling
Degradation
Cell
Nucleus

Figure 9. Proposed model of TIMP-1 regulation by MMPs composition. There are three possible proteolytic states of the TIMP-1/MMP system in a tissue that impact on signaling capacities of TIMP-1: excess of TIMP-1 (left), balanced TIMP-1:MMP levels (middle), and excess of MMPs (right). *From Grunwald et al, 2019*.

On the other hand, the cellular source of TIMP-1 in tumors is also controversial. Illustrating this, studies in PDAC have considered TIMP-1 as a stroma-associated pro-tumoral factor [91, 92]. Conversely, most studies attempting to determine the role of TIMP-1 in cancer progression assume that elevated TIMP-1 levels in tumors are the consequence of its overexpression by cancer cells and have therefore exclusively manipulated TIMP-1 on cancer cells. Not addressing the cellular source of TIMP-1 in each TME may probably limit our understanding of a protein displaying a broad range of context-dependent functions.

6.1. TIMP-1 in lung cancer

Recent studies have reported that TIMP-1 is the only TIMP member that is both markedly overexpressed and associated with poor prognosis in lung cancer (**Figure 10**) [73]. However, how TIMP-1 is regulated in lung cancer and how it drives tumor progression is poorly understood.

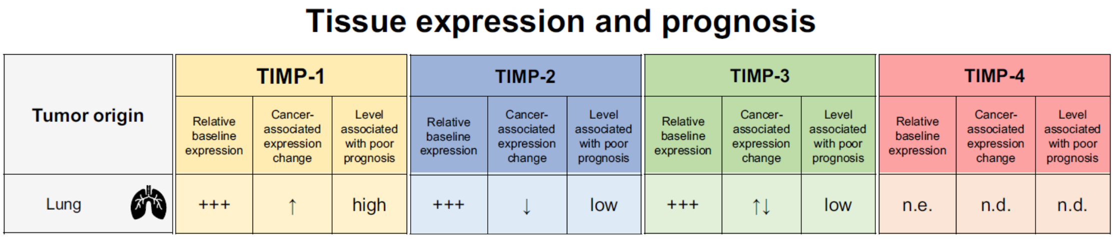

Tissue expression and prognosis

Tumor origin	TIMP-1			TIMP-2			TIMP-3			TIMP-4		
	Relative baseline expression	Cancer-associated expression change	Level associated with poor prognosis	Relative baseline expression	Cancer-associated expression change	Level associated with poor prognosis	Relative baseline expression	Cancer-associated expression change	Level associated with poor prognosis	Relative baseline expression	Cancer-associated expression change	Level associated with poor prognosis
Lung	+++	↑	high	+++	↓	low	+++	↑↓	low	n.e.	n.d.	n.d.

Figure 10. Comparison of TIMPs levels in healthy and lung cancer tissue. Relative baseline expression corresponds to RNA expression on healthy tissue based on HTA dataset (https://www.proteinatlas.org). 100-300 TPM = +++, n.e. = not expressed. Cancer-associated TIMP expression changes (up arrow: increase, down arrow: decrease of expression) compared with healthy tissues. Correlation of poor prognosis with increased (high) or decreased (low) TIMPs expression in lung cancer tissue (n.d.: no data available). *Adapted from Eckfeld et al, 2019*.

Since one of the main functions of fibroblasts is to remodel the ECM by coordinately synthesizing ECM proteins and secreting MMPs, it is reasonable to expect that one of the major sources of TIMP-1 in tumors may be TAFs. However, previous studies have reported TIMP-1 expression in TAFs and cancer cells in patients with lung cancer [93, 94], and it remains to be established which cell type is underlying the increased expression of TIMP-1 in lung cancer.

In line with the idea that lung TAFs may be involved in the elevated expression of TIMP-1 in lung tumors, several studies reported that TGF-β1, which is frequently upregulated in NSCLC [24], promotes *TIMP1* expression in fibroblasts [95, 96].

Likewise, the role of TIMP-1 secreted by TAFs in lung cancer remains largely unknown. Yet, several studies investigating the role of stromal TIMP-1 in other cancer types support that TIMP-1 secreted by lung TAFs may have pro-tumoral activity. The TIMP-1 secreted by pancreatic TAFs induced migration of pancreatic cells, although it was not established whether it worked through an MMP-inhibitory or cytokine-like mechanism [91]. Likewise, in hepatocellular carcinoma, stromal TIMP-1 promoted proliferation, motility, and survival of hepatic cancer cells through CD63 interaction [95].

On the other hand, it is worth noting that TIMP-1, a protein associated with poor prognosis in nearly all cancer types, is targeted by nintedanib [72]. Further supporting that stromal TIMP-1 may be relevant for lung cancer progression, nintedanib inhibited the expression of *TIMP1* in TGF-β-activated mouse fibroblasts and primary human hepatic stellate cells [96]. However, it remains undetermined whether nintedanib targets TIMP-1 in lung TAFs and the potential therapeutic effect of this inhibition. Furthermore, it remains unexplored whether TIMP-1 may underlie the paracrine signaling through secreted factors from TAFs that appeared specific for each histologic subtype in NSCLC [37].

6.2. TIMP-1 signaling

First studies attempting to discriminate between MMP-inhibitory dependent or independent functions of TIMP-1 chemically or genetically abrogated its N-terminal domain, hindering thus the MMP-inhibitory activity, and observed that TIMP-1 retained the ability to suppress apoptosis on different cell types [78, 97]. However, which processes were underlying such effects remained poorly understood. The discovery that the C-terminal domain of TIMP-1 interacts with the extracellular loop of the tetraspanin CD63 was a crucial step towards identifying TIMP-1 protease-independent pathways [79, 98].

Since then, growing evidence has confirmed that the TIMP-1/CD63 axis promotes cancer cell growth, invasion, and even metastasis through activation of extracellular signal-regulated kinases (ERK), focal adhesion kinase (FAK), and phosphoinositide 3-kinase/Akt (Pi3K/Akt) signaling pathways in leukemic, hepatocellular, and lung tumor cells [95, 99-101]. Even though it is widely accepted that oncogenic functions of TIMP-1 are mainly rendered by its cytokine-like activity [102], it is less clear how these functions are regulated within tumors. Along with CD63, proMMP-9 binds to TIMP-1 through the C-terminal domain (**Figure 9**) [103]. Hence it is likely that proMMP-9 influences the TIMP-1/CD63 axis.

In summary, although it is clear that TIMP-1 is overexpressed in patients with lung cancer [104, 105], major questions remain unanswered, including what is the principal source of elevated TIMP-1 (stromal or tumoral), what are the tumor-promoting effects of TIMP-1 in NSCLC, whether it interacts with CD63 in lung cancer cells, and whether TIMP-1 is also targeted by nintedanib.

These are the main questions that this thesis intended to address.

OBJECTIVES

GENERAL OBJECTIVE

To study the crosstalk between stromal TIMP-1 and CD63 in cancer cells and their role in the selective effects of nintedanib in lung ADC patients.

Specific Objectives

1. To characterize the expression pattern of TIMP-1 and CD63 in ADC and SCC.
2. To evaluate the role of the TGF-β1/SMAD3 signaling pathway in the regulation of the expression and secretion of TIMP-1 in lung fibroblasts and TAFs.
3. To examine whether there is a heterotypic crosstalk between lung TAFs and cancer cells through TIMP-1 and CD63 selectively in ADC.
4. To determine the role of TIMP-1 from ADC-TAFs in tumor progression *in vivo*.
5. To assess the role of stromal TIMP-1 in the differential responses to nintedanib between ADC and SCC.

MATERIALS AND METHODS

1. CELL CULTURE AND GENETIC MANIPULATIONS

1.1. Isolation of primary lung fibroblasts

Human lung fibroblasts were previously obtained by outgrowth of tissue explants [106] from a cohort of 20 NSCLC surgical patients (8 ADC; 12 SCC) [20]. All protocols were approved by the Ethics Committee of *Hospital Clínic de Barcelona* and the *Universitat de Barcelona*, and all patients gave their written informed consent. Patient selection criteria were male, Caucasian, ≥ 55 years old, current smoker, chemo-naïve, and early-stage (I/II/III) (**Table 2**) according to the grading system of the 7th lung cancer stage grouping, reported by the International Association for the Study of Lung Cancer [107]. For each patient, samples from both tumor and paired tumor-free lung parenchyma were collected in sterile conditions under the surgeon's guidance. Tumor-free lung tissue was collected from the resected pulmonary lobe, at least 5 cm away from the tumor mass. Each tissue sample was cut in pieces measuring ~1 mm^3, which were then seeded on 6-well plates, maintained in fibroblast culture medium (described in **section 1.3.**) and kept at 37^{o}C with 5% CO^2 in a humidified atmosphere. Once fibroblasts migrated over ~90% of the surface as a monolayer, cells were trypsinized, expanded on new flasks, frozen, and preserved in liquid nitrogen for long-term storage. Tumor-associated fibroblasts (TAFs) were obtained from tumor regions and paired control fibroblasts (CFs) from tumor-free areas. All primary cultures were tested for the presence of mycoplasma contamination by PCR techniques. Fibroblasts were characterized by the expression of vimentin and the lack of cytokeratins (epithelial marker), using immunofluorescence techniques (data not shown) [20].

PATIENT REFERENCE	AGE (y.o.)	HISTOLOGIC SUBTYPE	pT	pN	STAGE
P2	82	SCC	T3	N2	IIIA
P4	73	SCC	T2b	N1*	IIB
P5	69	SCC	T2b	N2	IIIA
P6	65	SCC	T1a	N0	IA
P7	61	ADC	T1b	N0	IA
P10	76	ADC	T1a	N0	IA
P12	70	ADC	T3	N0	IIB
P13	59	ADC	T2b	N2	IIIA
P15	73	ADC	T1a	N0	IA
P16	64	SCC	T2a	N1*	-
P18	83	SCC	T2a	N0	IB
P20	78	SCC	T1b	N0	IA
P22	76	SCC	T2a	N1	IIA
P27	71	ADC	T1a	N0	IA
P28	80	ADC	T1a	N0	IA
P31	62	SCC	T3	N0	IIB

P33	72	SCC	T2a	N0	IB
P34	76	SCC	T2b	N0	IIA
P35	60	SCC	T2a	N1	IIA
P37	58	ADC	T1b	N0	IA

Table 2. Summary of patients' clinical data. N*: direct hilar ganglionar infiltration by the tumor.

1.2. Immortalization of primary fibroblasts

Human lung fibroblasts from randomly selected patients were infected with a retroviral vector expressing the human telomerase enzyme (hTERT) and a hygromycin resistance gene (pBABE Hygro) [56]. First, PT67 cells (ATCC) were transfected with the retroviral vector (#1773, AddGene), and their supernatant containing retroviruses was filtered in 0.45 µm pore membranes (GVS filter technology). Secondly, this supernatant was used to transduce fibroblasts in the presence of 8 µg/mL of polybrene (Sigma). After infection, immortalized fibroblasts were selected with Hygromycin-B (Invitrogen), expanded, frozen, and preserved in liquid nitrogen for long-term storage.

1.3. Culture of fibroblasts

Primary and immortalized fibroblasts (CFs and TAFs) were fast thawed and maintained in high glucose DMEM culture medium (Gibco) supplemented with 10% fetal bovine serum (FBS) (Gibco) and 1% Antibiotic-Antimycotic (Gibco). Primary fibroblasts were used up to passage 7 to prevent replicative senescence and maintain their phenotypic characteristics [108].

The experiments with fibroblasts were performed on a fibroblast culture medium containing serum-free high glucose DMEM supplemented with 1% insulin-transferrin-selenium-A (ITS, Gibco) and 1% Antibiotic-Antimycotic [37]. Fibroblasts were activated with 2.5 ng/mL recombinant human TGF-β1 (R&D systems) in 0.1% collagen (Sigma)-coated culture plates for 3 days. Unless otherwise indicated, all fibroblasts were treated with TGF-β1 to regain the activated phenotype observed in histologic samples from patients [20, 109], which is partially lost in culture [54]. In some experiments, fibroblasts were activated with TGF-β1 and treated with the drugs summarized in **Table 3**.

TREATMENT	CONCENTRATION	COMPANY
SB431542	0 – 5 µM	(Millipore)
Galunisertib	0 – 5 µM	(Lilly, provided by Kyla Driscoll)
Nintedanib	2 µM	(Boehringer Ingelheim, provided by Frank Hilberg)

Table 3. Fibroblasts' treatments used in this study.

1.4. Viral transduction of immortalized fibroblasts

To generate fibroblasts stably knocked down for SMAD3, we used a lentiviral shRNA vector TRCN 0000330128 (shSMAD3) targeting SMAD3 (pLKO.1-puro MISSION collection, Sigma) [56]. A non-mammalian targeting shRNA vector SHC002 (shCTRL) that does not recognize any human gene was used as a negative control. First, HEK 293T cells (ATCC) at 70% confluence were transfected with shSMAD3 or shCTRL plasmids using the CalPhos Mammalian Transfection kit (TakaraBio) following the manufacturer's protocol. hTERT immortalized fibroblasts were transduced with the medium containing lentivirus in the presence of 8 µg/mL of polybrene (Sigma). Transduced cells were selected with 2 µg/mL puromycin (Sigma) for 72 h and 1 µg/ml thereafter.

To generate CFs stably overexpressing SMAD3, we used retroviral vectors expressing SMAD3 (#12638, Addgene) (rv-SMAD3) [110] or GFP (#65436, Addgene) (rv-GFP, which was used as infection control) [111]. Phoenix-AMPHO cells (ATCC) at 70% confluence were transfected with rv-SMAD3 or rv-GFP plasmids using the CalPhos Mammalian Transfection kit. Medium containing retroviruses for protein expression was filtered and used for hTERT immortalized fibroblast infection with polybrene (8 µg/mL). Transduced cells were selected using puromycin antibiotic.

All steps for the viral transduction were optimized and the resulting standardized protocol is detailed in **Annex section A1**.

1.5. Culture of cancer cell lines

Cancer cell lines were maintained in an RPMI culture medium (Gibco) supplemented with 10% FBS, 1% Antibiotic-Antimycotic, and 1mM L-Glutamine (Gibco) [37]. A panel of cell lines derived from lung ADC patients (H1437, H23, H522, H1975, H441, H2126, H1792, PC9, II-18, HCC4006 and HCC827) (ATCC) was used for TIMP-1 analysis by ELISA. In addition, to examine the tumor-promoting effects of ADC-TAFs, H1437 and H23 were used, which do not harbor mutations in driver genes sensitive to targeted therapies [112] to mimic critical genetic aspects of lung ADC patients that may be treated with nintedanib in the clinic [113].

The experiments with cancer cells were performed on an epithelial culture medium containing serum-free RPMI supplemented with 1% ITS, 1% Antibiotic-Antimycotic, and 1mM L-Glutamine.

1.6. Cell transfections

TIMP-1 was transiently knocked down in ADC-TAFs by siRNA [114]. For this purpose, fibroblasts were seeded in complete medium overnight to reach a 30-50% confluence the next day. The following day, fibroblasts had their medium replaced with high glucose DMEM without serum and antibiotics. Lipofectamine RNAiMAX (Invitrogen) and Silencer Pre-Designed siRNA constructs (control siRNA #4390843, siRNA TIMP-1#α ID: 12759, and siRNA TIMP-1#β ID: 118687, Thermo Fisher) were separately pre-diluted in OPTI-MEM (Thermo Fisher). Lipofectamine RNAiMAX and siRNAs were mixed and incubated at room temperature (RT) for 5 minutes and added to fibroblasts at 30 nM final concentration for 6 hours. Then, FBS and antibiotics were added, and cells were kept in the incubator for 48 hours for TIMP-1 knockdown. Then the culture medium was washed, and the conditioned medium of the transfected fibroblasts was obtained (as described in **section 1.7.**).

Similarly, CD63 was transiently knocked down in ADC cells by siRNA. H1437 and H23 cells at 50-80% confluence were transfected with 30 nM of Silencer Select pre-designed siRNA constructs (control siRNA #4390843, siRNA CD63#A ID: 10318, and siRNA CD63#B ID: 145984, Thermo Fisher) and Lipofectamine RNAiMAX for 6 hours. Then, FBS and antibiotics were added, and cells were kept in the incubator for 24 hours for CD63 knockdown. Transfected cells were used for cell density and invasion assays (as described in **section 3**).

All steps for cell transfections were optimized and the resulting standardized protocol is detailed in **Annex section A2**.

1.7. Conditioned medium harvesting

For cell density and invasion assays (**section 3**), we stimulated ADC cells with the conditioned medium (CM) derived from activated fibroblasts [37]. First, primary or transfected fibroblasts were activated with 2.5 ng/mL TGF-β1 and treated or not with the drugs specified in **Table 3** for 3 days in the serum-free fibroblast culture medium and subsequently kept in serum-free medium for 2 days in the absence of exogenous TGF-β1 or any treatment. The corresponding CM was collected, centrifuged, and stored at -80°C until use. In addition, we counted the number of cells/mL for TIMP-1 ELISA normalization. For this purpose, once the CM was collected, fibroblasts were trypsinized, resuspended as a single cell suspension, and counted with the Neubauer Chamber. The same protocol was applied to collect CM of ADC cell lines using serum-free epithelial culture medium.

1.8. Recombinant TIMP-1 production

For cell density and invasion assays (**section 3**), we stimulated ADC cells with recombinant human TIMP-1 (rhTIMP-1). Mature secreted full-length rhTIMP-1 was obtained by expressing the pTT/TIMP-1 construct transfected into HEK 293E cells [115], and purifying it with SP-Sepharose chromatography as described [116]. The production and purification were done in the laboratory of Dr. Radisky (Mayo Clinic, Jacksonville, FL) who kindly provided us the soluble rh-TIMP-1.

2. CELLULAR AND MOLECULAR PROCEDURES

2.1. hTERT immunofluorescence

To assess hTERT expression in the nuclei of immortalized fibroblasts by immunofluorescence [117], cells were cultured on chamber slides (BD Falcon). Unless otherwise indicated, all steps were carried out at RT. Slides were washed with cold PBS, and cells were fixed with cold PBS containing 4% paraformaldehyde (PFA) (Sigma) for 15 minutes. Cells were then permeabilized with PBS containing 0.5% Triton X-100 (Sigma) for 30 minutes and blocked with 5% bovine serum albumin (BSA) diluted in PBS for 1 hour. Slides were incubated for 1 hour at 37ºC with a primary antibody against TERT (1:200) (sc-393013, Santa Cruz). Next, slides were washed with PBS and incubated with a suitable fluorescent secondary antibody (#A-11029, Invitrogen) for 1 hour at 37ºC. Nuclei were counterstained with DAPI 1:10.000 (4′,6-diamidino-2-phenylindole, Sigma), and slides were mounted with Prolong Gold Antifade Reagent (Invitrogen). Images were obtained with a x20 objective (Eclipse TE2000 microscope, Nikon), and image analysis was performed using the Image J software [118].

2.2. Senescence-associated beta-galactosidase activity

Cultured fibroblasts were fixed with PBS containing 4% PFA for 5 minutes at RT and incubated with senescence-associated beta-galactosidase (SA-βgal) staining solution containing 0.2 M citric acid/sodium phosphate buffer (pH 6.0), 100 mM potassium ferricyanide, 100 mM potassium ferrocyanide, 5 M NaCl, 2 M $MgCl_2$, and 20 mg/mL of X-gal solution (5-Bromo-4-chloro-3-indolyl β-D-galactopyranoside) (Sigma) at 37ºC for ~12h. 9 randomized images were obtained from each biological duplicate with a x10 objective in a phase-contrast microscope (Zeiss Axiovert S100) provided with a UI-1240SE color camera (IDS). The percentage of SA-βgal+ (blue) cells was assessed for each image and averaged for each experimental condition [119].

2.3. Population Doubling Level

We assessed the gained population doubling level in primary and immortalized fibroblasts during 77 days. To compute the population doubling level, fibroblasts were first trypsinized, resuspended as a single cell suspension, and counted with the Neubauer Chamber. Then, equal amounts of primary and immortalized fibroblasts were reseeded and considered to be Population Doubling Level = 0. Next, we calculated the population doubling at each passage by using the formula: $Population\ Doubling\ Level = \frac{\log\left({}^{Nh}/_{Ns}\right)}{log2}$; where N_h = the number of harvested cells, N_s = the number of seeded cells. The population doubling level calculated at each passage was summed to the population doubling level calculated in the previous passage to obtain the gained population doubling level [120]. For each cell type, we plotted the gained Population Doubling Level at every passage against time.

2.4. Flow cytometry analysis of CD63

To detect CD63 on the cell surface of NSCLC cell lines (H1437, H23, H522, and H520), either transfected with siRNA or non-transfected, named wild-type (WT) throughout the text, cells were trypsinized, and the cell suspension was incubated with 10 µg/mL anti-CD63 monoclonal antibody (ab8219, Abcam) for 30 minutes at 4^{o}C. Subsequently, cells were tagged with Alexa fluor 488 secondary antibody (A-11029, Invitrogen) for 30 minutes at 4^{o}C and fixed with 2% PFA in PBS for 15 minutes. Control cells without staining were used to determine the autofluorescence levels, and cells stained only with the secondary antibody were used to ensure the specificity of the anti-CD63 antibody. Stained cells were analyzed with a FACS Canto II cytometer (BD Biosciences), and data were processed using the FlowJo software (BD Biosciences) [121].

All steps for flow cytometry analysis were optimized and the resulting standardized protocol is detailed in **Annex section A3**.

2.3. Enzyme-linked immunosorbent assay (ELISA) of TIMP-1

Commercial DuoSet Human ELISA kit (R&D Systems) was used to measure secreted TIMP-1 protein within the CM as pg/mL following the manufacturer´s instructions [122]. The pg of TIMP-1/mL were normalized by the number of cells/mL for each condition to assess final TIMP-1 as pg/cell.

2.4. TGF-β activity assay

The activity of bioactive TGF-β was monitored using the TGF-β-inducible $p(CAGA)_{12}$ luciferase-reporter [56]. First, HEK 293T cells were co-transfected with the Firefly luciferase TGF-β reporter plasmid (pCAGA-Luc12X, provided by Elena Sancho IRB) [123] and the *Renilla* luciferase reporter plasmid (pRL-TK, Promega, used as an internal control). The following day, HEK 293T cells were stimulated with the CM of TAFs for 6h. Then, Firefly and *Renilla* luciferases activity were measured using the Dual-Luciferase® Reporter Assay System (Promega) following the manufacturer´s instructions. Final TGF-β activity was determined by normalizing the Firefly luciferase activity with *Renilla* luciferase activity.

All steps for TGF-β bioactivity determination were optimized and the resulting standardized protocol is detailed in **Annex section A4**.

2.5. RNA extraction, reverse transcription and quantitative RT-PCR

Total RNA from fibroblasts or cancer cells was extracted with RNeasy Mini Kit (Quiagen) according to manufacturer's instructions, and quantified using a NanoDrop® Spectrophotometer. Then, equal amounts of RNA of each sample were reverse transcripted into cDNA using the High-Capacity cDNA Reverse Transcription kit (Applied Biosystems) following manufacturer's indications. For *TIMP1*, *CD63*, *COL1A1* and *COL3A1* mRNA expression analysis [114], quantitative real-time PCR (RT-PCR) reactions were performed in technical duplicates with 10 ng of each cDNA sample with the StepOnePlus Real-Time PCR System (Applied Biosystems) using specific TaqMan® probes (Applied Biosystems) for each gene (see **Table 4**) and the TaqMan® Gene Expression Master Mix (Applied Biosystems). RNA polymerase II (*POLR2A*) was used as a reference housekeeping gene. To evaluate the expression of *SMAD3* [56], quantitative RT-PCR analysis was performed using specific primers for *SMAD3* (forward 5' ATC CCA CCA GGA TGC AAC 3', reverse 5' TCA ACT GGT AGA CAG CCT CA 3') and *ACTB* (forward 5' CAA GGC CAA CCG CGA GAA GAT 3', reverse 5' CCA GAG GCG TAC AGG GAT AGC AC 3') and SYBR Green Master Mix (Thermo Fisher Scientific). *ACTB* was used as a reference housekeeping gene. Relative gene expression with respect to the corresponding reference housekeeping gene was assessed as $2^{-\Delta Ct}$ [124].

GENE SYMBOL	Taqman® Cat#
TIMP1	Hs00171558_m1
CD63	Hs01041238_g1
COL1A1	Hs00164004_m1
COL3A1	Hs00943809_m1
POLR2A	Hs00172187_m1

Table 4. TaqMan® probes used in the quantitative RT-PCR analysis in this study.

2.6. Protein extraction and western blot

For total protein extraction, cultured fibroblasts or cancer cells were washed twice with cold PBS and scraped off the dish with lysis buffer (Tris 50mM (pH 7.4), NaCl 150mM, SDS 0.1%, Triton X-100 1% (Sigma) and Nonidet P-40 1% (Igepal)) supplemented with phosphatase inhibitor (Phostop, Roche) and protease inhibitor cocktail (Protease Inhibitor Cocktail Set I, Merck; Pefabloc, Roche). Protein concentration of the lysate was quantified with the Bicinchoninic acid (BCA) assay (Thermo Scientific). Afterwards, equal amounts of total protein were electrophoretically separated on a 10% Mini- PROTEAN TGX precast gel (Bio-Rad), transferred to a polyvinylidene difluoride membrane (GE Healthcare), blocked with 5% non-fat milk for 1 hour at RT, and then incubated with the primary antibody overnight at 4^{o}C. Primary antibodies are listed in **Table 5**. Protein bands were labeled with Horseradish peroxidase (HRP)-conjugated secondary antibodies (Millipore) and visualized by chemiluminescence in a digital imaging system (Chemidoc Imaging Systems, Bio-Rad). Band intensities were analyzed with ImageJ and normalized to the corresponding loading control.

ANTIBODY	Cat#	COMPANY	SPECIE OF ORIGIN	DILUTION
pSMAD3	#07-1389	Millipore	Rabbit	1:1000
αSMA	#A5228	Sigma	Mouse	1:3000
P4HA2	#13759-I-AP	Proteintech	Rabbit	1:3000
β-Actin-Peroxidase	#A3854	Sigma	Mouse	1:100000
α-Tubulin	#2144S	Cell signaling	Rabbit	1:2000
pAKT	#4060S	Cell signaling	Rabbit	1:2000
AKT	#9272S	Cell signaling	Rabbit	1:1000

Table 5. Antibodies used in the Western Blot analysis in this study.

3. CELL-BASED FUNCTIONAL ASSAYS

3.1. Cell density assay

For cancer cell density assessment, H1437 and H23 cells were stimulated with a 1:1 mixture of serum-free epithelial culture medium and either CM or serum-free fibroblast culture medium (referred to as basal medium) supplemented with 0.25% FBS (to facilitate cell attachment) for 3 days [37]. In some experiments, 160 ng/mL of rhTIMP-1 were added to the basal medium. Cells were then fixed with PBS containing 4% PFA, and their nuclei counterstained with Hoechst 33342 (Molecular Probes). Fluorescent nuclei were imaged in 7 randomized images for each experimental duplicate with a x10 objective (Eclipse TE2000 microscope) and counted with ImageJ. Cell density was measured as the average nuclear density/image. Results of each image were averaged for each CM and subsequently normalized to the value obtained with the basal medium.

3.2. Invasion assay

To assess cancer cell invasion, the Matrigel Transwell invasion assay was used [37]. First, Matrigel (Corning) was diluted in serum-free epithelial culture medium (1:5), and transwell filters (24 Transwell plate, 8 µm filter pore size, Merck Millipore) were coated with 50 µL of diluted Matrigel and incubated for 2 hours at 37ºC. Cancer cells were immediately seeded on the Matrigel-coated filter-inserts in serum-free epithelial culture medium, and the CM or basal medium (see **section 3.1.**) added to the lower Transwell compartment. In some experiments, 160 ng/mL of rhTIMP-1 were added to the basal medium. After 48 hours, cancer cells that invaded the Matrigel layer through the other side of the Transwell porous membrane were fixed with 100% methanol for 15 minutes and stained with 0.5% crystal violet (Sigma) for 30 minutes at RT. Invading cells were visualized by a phase-contrast microscope provided with a color camera and a ×5 objective. Cell invasion was computed as the average crystal violet positive area/image and normalized to that obtained with basal medium.

4. GENERATION OF TUMOR XENOGRAFT MODELS

The tumorigenicity of lung cancer cells mixed with lung fibroblasts was examined in 6- to 8-week-old male NOD/SCID mice (Janvier Labs). Animals were kept under specific pathogen-free conditions at constant ambient temperature (22ºC – 24ºC) and humidity (30% – 50%) in the animal facility laboratory of the School of Medicine (University of Barcelona). All procedures were approved by the Animal Care and Ethics Committee of the University of Barcelona.

For the establishment of ADC based tumor xengorafts, H1437 cells (1×10^6) were mixed with either pre-activated siCTRL or siTIMP-1 ADC-TAF^{hTERT} (#37) (1×10^6) within 100 µL solution of Matrigel mixed with type I collagen (IAC-50, Koken) (1:1) and co-injected subcutaneously in the dorsal flank of NOD/SCID mice (n = 4-8 mice/condition). For the establishment of SCC based tumor xenografts, H520 cells (1×10^6) were mixed with pre-activated SCC-TAF^{hTERT} (#20) (1×10^6) within 100 µL solution of Matrigel mixed with type I collagen (IAC-50, Koken) (1:1) and co-injected subcutaneously in the dorsal flank of 8 NOD/SCID mice. All fibroblasts were pre-activated with 2.5 ng/mL TGF-β1 for 3 days before co-injection. Once tumors reached volumes of 50 mm^3, mice were randomized into groups including four mice per group, and oral treatment with nintedanib (50mg/kg) or PBS was administered. Animals were treated daily during 11 days. Tumor growth was assessed twice weekly using calipers, and tumor volume was calculated as $0.5\times\text{width}^2\times\text{length}$ [114]. After 21 days, animals were euthanized, and tumor xenografts were collected for histologic analysis [56].

All steps of tumor xenograft models co-injecting lung fibroblasts were optimized and the resulting standardized protocol is detailed in **Annex section A5**.

5. HISTOLOGIC ANALYSIS

5.1. Patient samples: TIMP-1 and CD63

Tissue Microarray (TMAs) images of 12 NSCLC patients (6 ADC; 6 SCC) stained for TIMP-1 (HPA053417 antibody) and CD63 (HPA010088 antibody) were downloaded from the Human Protein Atlas database (Version 19.0) (http://www.proteinatlas.org) for image analysis [125]. Two images from each patient were quantified.

TIMP-1 staining in stromal fibroblasts was scored blind by two independent observers under the guidance of an expert pathologist (J. Ramírez, MD, PhD) [20]. Fibroblasts in the tumor section were identified by their spindle-shaped nuclei in Hematoxylin staining [126]. For each image, 2 observers counted the number of TIMP-1 positive and negative fibroblasts independently (coefficient of correlation $r^2 = 0.8$), and the percentage of TIMP-1 positive fibroblasts/image was averaged for each patient to render the final percentage in ADC and SCC.

CD63 positive stained area/image quantification was assessed with Image J [56]. First, images were color deconvoluted to separate the CD63 color channel from the other colors. Next, images were binarized to finally calculate the CD63 positive area fraction with respect to the total area of the TMA. When necessary, necrotic areas were subtracted manually. Results of each image were averaged for each patient and subsequently for all patients within the same subtype.

5.2. Tumor xenograft: cytokeratins AE1/AE3

Primary tumor xenografts obtained from *in vivo* studies were stained for pan-cytokeratin (AE1/AE3 anti pan-keratin antibody cocktail, Diagnostic Biosystems) [127]. Image analysis was carried out under the guidance of an expert pathologist (J. Ramírez, MD, PhD). Invasion of cytokeratin-positive cancer cells within tumor xenografts into adjacent mouse host tissue was scored semiquantitatively by examining tumor budding [128], which is defined as the presence of isolated small tumor nests in the stroma of the invasive tumor edge. For this purpose, ~10 images of the tumor edge in AE1/AE3 staining samples were randomly acquired with a bright-field microscope (BX43) coupled to a digital camera (DP72) using a ×20 objective (Olympus). Invasive features (i.e. tumor nests) at the tumor edge were counted blind for each image by two independent observers, and scored into 3 categories: 0 (negative), 1 (< 7 tumor nests, with a clear pseudocapsule), and 2 (≥ 7 tumor nests, usually without a clear pseudocapsule). The pseudocapsule corresponds to the reactive stromal host tissue that tends to encapsulate the tumor [129]. For each sample, the frequency of each score n_i (where i corresponds to score 0, 1 or 2) was computed as ni/N (where N is the total number of images) and averaged across the two observers to render the final score frequencies. A good agreement on invasion scores was found for each category and observer (coefficient of correlation $r^2 = 0.9$).

6. GENE EXPRESSION ANALYSIS USING PUBLIC DATABASES

6.1. *TIMP1* and *CD63* expression in lung tissue

TIMP1 and *CD63* mRNA were analyzed using The Cancer Genome Atlas (TCGA) database (https://cancergenome.nih.gov/) [56]. The whole-tumor Level 3 RNA-seq expression data for tumor (n=517 ADC, n=501 SCC) and normal tissues (n=59 ADC, n=51 SCC) was normalized using the RNASeq by Expectation Maximization (RSEM) and analyzed using the *limma* package [130] in R (version 3.5.3; http://www.R-project.org/).

6.2. *TIMP1* expression in cell lines

TIMP1 mRNA expression was analyzed in a panel of cell lines (43 ADC, 12 SCC) [114] using the publicly available gene expression microarray dataset from the Sanger Cell Line Project (GSE68950) with the CellExpress system [131] using R software. Cell lines and corresponding *TIMP1* levels are listed **Annex section A6**.

7. STATISTICAL ANALYSIS

Two-group comparisons were performed with two-tailed Student *t*-test unless otherwise indicated (GraphPad Prism v5.0.). Time-dependent tumor volume or TIMP-1 secretion data were analyzed with two-way ANOVA (Sigmaplot). Statistical significance was assumed at $p < 0.05$. All data shown are mean ± s.e.m.

RESULTS

1. CHARACTERIZATION OF TIMP-1 AND CD63 EXPRESSION IN NSCLC

To address the objective 1 of this thesis, we first determined the expression pattern of *TIMP1* and *CD63* in the two main NSCLC histologic subtypes using the TCGA RNA-seq database. We observed that in whole tumor samples, mRNA levels of *TIMP1* and *CD63* were significantly higher in ADC patients compared to SCC (**Figure 11A-B**). Moreover, compared with patient-matched control tissue, the expression of *TIMP1* was increased in ADC (**Figure 11C-D**), whereas *CD63* levels were decreased in SCC (**Figure 11E-F**). These results reveal an aberrant expression pattern of *TIMP1* and *CD63* in NSCLC in which *TIMP1* is overexpressed in ADC tissue, and *CD63* is downregulated in SCC tumors.

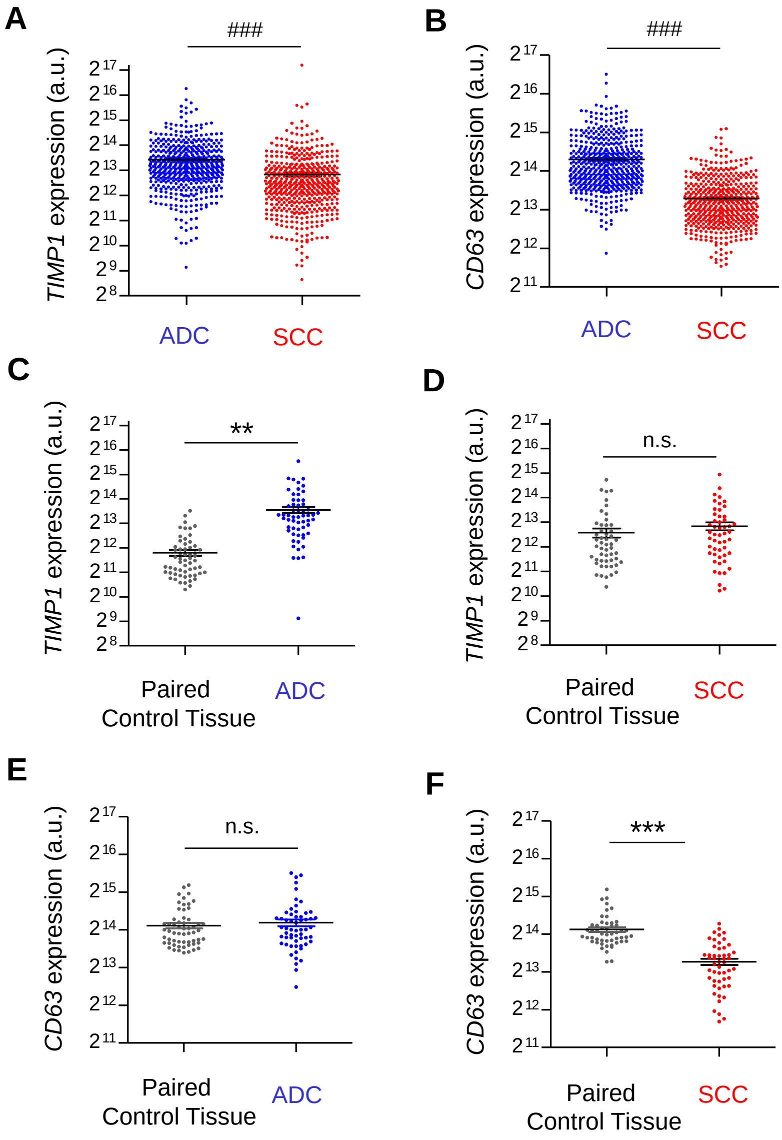

Figure 11. Expression of *TIMP1* and *CD63* in lung ADC and SCC tissue. A-F RNA-seq data of *TIMP1* and *CD63* mRNA in tumoral tissue (A, B) (515 ADC, 501 SCC), in ADC and paired control tissue (C, E) (58 ADC), and in SCC and paired control tissue (D, F) (51 SCC). Error bars represent mean ± s.e.m. ###, $p < 0.005$ comparing ADC with SCC. **, $p < 0.01$; ***, $p < 0.005$ comparing with respective to control tissue. n.s.: non-significant. Statistical comparisons were done using Mann Whitney test.

1.1. Lung ADC-TAFs show an excessive secretion of TIMP-1

Previous studies have detected TIMP-1 in both stromal and cancer cells in lung tumors [93]. To determine which cell type may contribute to *TIMP1* overexpression in lung ADC, we compared TIMP-1 mRNA and secreted protein between lung cancer cells and TAFs. All TAFs were activated with TGF-β1 for 3 days to mimic their ubiquitous activated/myofibroblast-like phenotype observed in patient samples [20, 109] and are referred to as activated TAFs throughout the text. In a randomly selected panel of cultured ADC and SCC cell lines from the Sanger RNA-Seq database (43 ADC, 12 SCC), differences in *TIMP1* mRNA levels were not observed (**Figure 12A**). In contrast, the expression of *TIMP1*, as determined by qRT-PCR, was significantly higher in activated ADC-TAFs than in SCC-TAFs (8 ADC, 9 SCC) (**Figure 12B**). Next, we analyzed the secreted TIMP-1 protein by ELISA in activated TAFs (7 ADC, 9 SCC) and a panel of TGF-β1-stimulated ADC cell lines (n = 11). The content of TIMP-1 in the secretome was significantly higher in either ADC-TAFs or SCC-TAFs compared to ADC cell lines (**Figure 12C**). Remarkably, the production of soluble TIMP-1 was larger in ADC-TAFs than in SCC-TAFs (**Figure 12C**). Moreover, ADC-TAFs showed an aberrant overproduction of TIMP-1 compared to their patient-matched control fibroblasts (**Figure 12D**). Conversely, SCC-TAFs showed a similar secretion of TIMP-1 than their patient-matched control fibroblasts (**Figure 12D**). These results indicate that TIMP-1 is expressed by both stromal and cancer cells but is selectively overexpressed in ADC-TAFs.

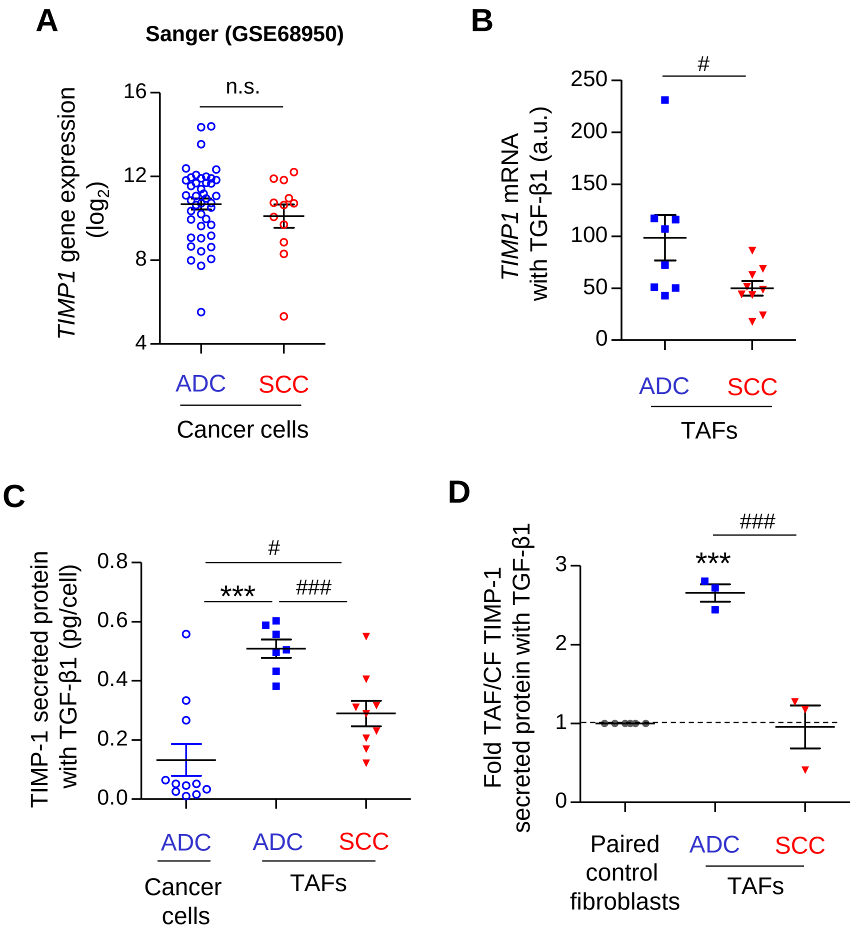

Figure 12. Expression of *TIMP1* in lung ADC cancer cells and lung TAFs. A, RNA-seq data of *TIMP1* mRNA expression in a panel of lung cancer cell lines (43 ADC, 12 SCC). **B**, *TIMP1* mRNA expression of TAFs (8 ADC, 9 SCC) activated with 2.5 ng/mL TGF-β1 for 3 days (here and thereafter unless otherwise indicated). **C**, ELISA quantification of TIMP-1 protein (pg of TIMP-1/number of cells) secreted by cancer cells (11 ADC) and TAFs (7 ADC, 9 SCC) activated with 2.5 ng/mL TGF-β1 for 3 days and subsequently maintained in serum-free medium for 2 days. **D**, Fold (TAF/CF) secretion of TIMP-1 of ADC (n = 3; TAFs and CFs) and SCC (n = 3; TAFs and CFs) fibroblasts cultured as in (C). Error bars indicate mean ± s.e.m. #, $p < 0.05$; ###, $p < 0.005$ comparing ADC with SCC. ***, $p < 0.005$ comparing ADC-TAFs with either ADC cancer cells or CFs. n.s.: non-significant. All comparisons were done using Student *t*-test.

The histologic subtype specificity for *TIMP1* overexpression found in ADC was confirmed analyzing TIMP-1 staining in TMAs from the Human Protein Atlas. In agreement with our *in vitro* observations, we found an increased tendency in the percentage of TIMP-1 positive fibroblasts in ADC than in SCC that attained marginal significance (**Figure 13A-B**).

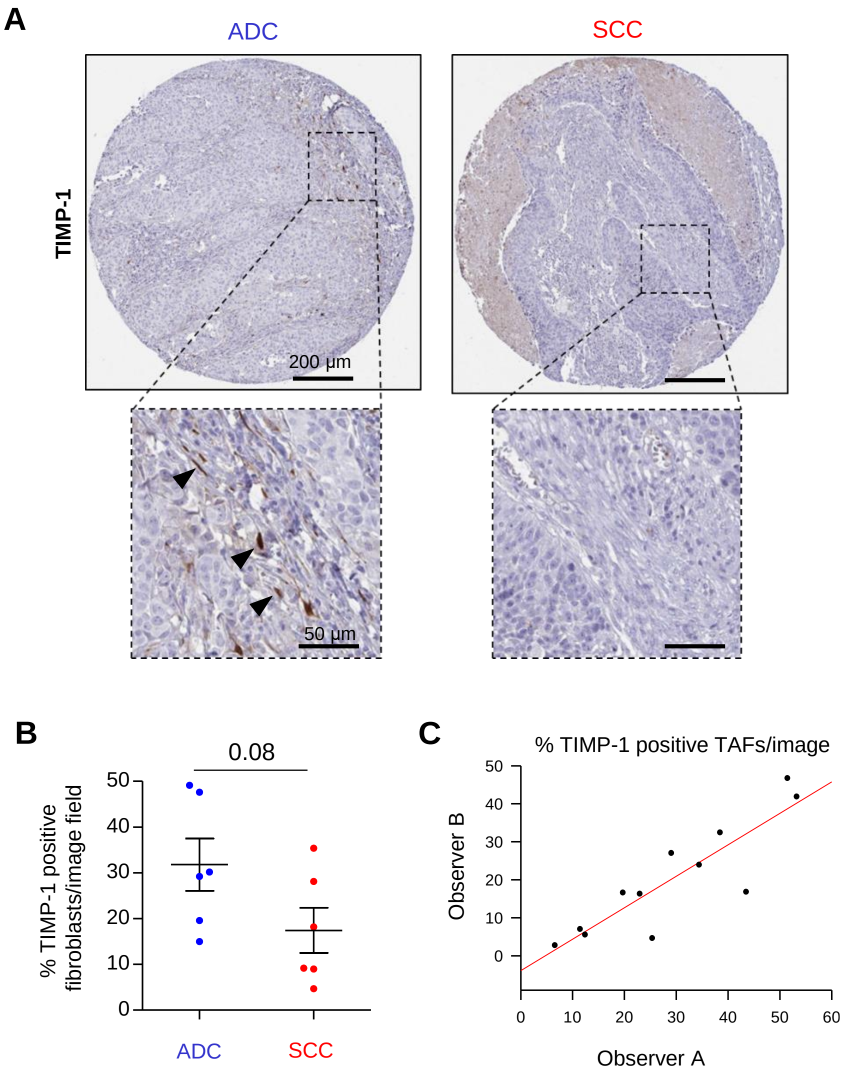
A
ADC
SCC
TIMP-1
200 µm
50 µm
B
0.08
% TIMP-1 positive fibroblasts/image field
50
40
30
20
10
0
ADC
SCC
C
% TIMP-1 positive TAFs/image
Observer B
Observer A
0
10
20
30
40
50
60

Figure 13. TIMP-1 staining in lung ADC and SCC tissue A, Representative histologic images of ADC and SCC patient samples within TMAs from the Human Protein Atlas database stained for TIMP-1. Black arrowheads point at TIMP-1 positive fibroblasts. **B**, Percentage of TIMP-1 positive TAFs in TMAs (6 ADC, 6 SCC). **C**, Correlation between two independent observers in TIMP-1 positive fibroblasts staining quantification. % of positive fibroblasts: $p < 0.001$, R squared: 0.767. Error bars indicate mean ± s.e.m. All comparisons were done using Student *t*-test.

1.2. CD63 expression is downregulated in SCC

To independently validate our observed differences between ADC and SCC, further, we analyzed CD63 staining in TMAs from the Human Protein Atlas. In agreement with our previous results, CD63 staining was scarce in SCC compared to ADC samples and mainly restricted to cancer cells (**Figure 14A-B**).

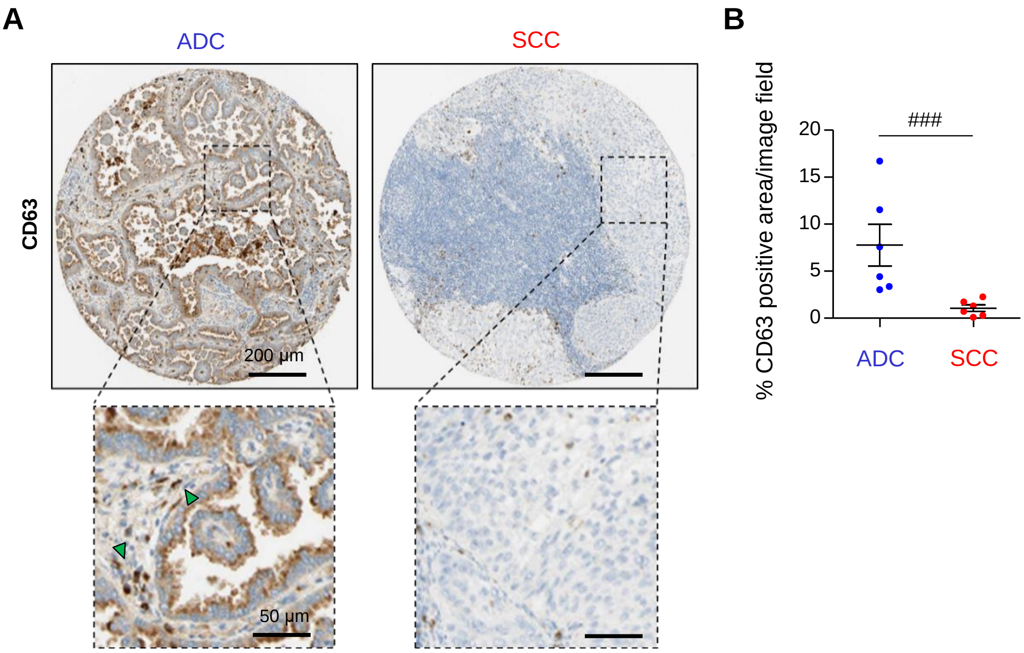

Figure 14. Histo-type specific expression of CD63. A, Representative histologic images of ADC and SCC patient samples within TMAs from the Human Protein Atlas database stained for CD63. **B**, Quantification of the percentage of CD63-positive area/image field for each patient in TMAs (6 ADC, 6 SCC). Green arrowheads point at CD63 positive cancer cells. Error bars indicate mean ± s.e.m. ###, $p <$ 0.005 comparing ADC with SCC. All comparisons were done using Student *t*-test.

1.3. The expression of the natural CD63 competitor for TIMP-1 binding, *MMP9*, is upregulated in SCC

ProMMP-9 is a natural competitor of CD63 for TIMP-1 binding (**Figure 8**) [89, 103] and therefore may influence the potential interaction between TIMP-1 and CD63. The differential expression of *MMP9* was evaluated using the TCGA database. Interestingly, significantly higher *MMP9* mRNA levels were found in SCC compared to ADC tissue (**Figure 15**), indicating that ADC tumors may potentially exhibit more free TIMP-1 that can interact with CD63 expressing cancer cells.

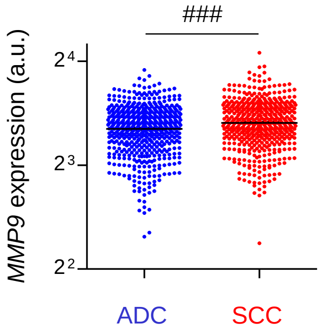

Figure 15. Expression of *MMP9* in ADC and SCC tissue. RNA-seq data of *MMP9* mRNA in tumoral tissue (517 ADC, 501 SCC). Error bars indicate mean ± s.e.m. ###, $p < 0.005$ comparing ADC with SCC. Statistical comparisons were done using Mann Whitney test.

2. THE TGF-β1/SMAD3 FIBROTIC PATHWAY REGULATES THE EXPRESSION AND SECRETION OF TIMP-1 IN LUNG TAFs

2.1. TGF-β1/SMAD3 pathway remains active in immortalized fibroblasts

It has been described that primary fibroblasts in culture undergo a finite number of cell divisions [120]. When fibroblasts reach the maximum population doubling level in culture, cells enter into a cell growth-arrest state called replicative senescence [132]. In our experience, primary fibroblasts can be used up to passage 7 to prevent this cell growth arrest. It is known that this limited growth is due in part to the gradual loss of DNA at the telomeres [133]. To avoid this limitation in further experiments of this thesis, we immortalized randomly selected fibroblasts from our patient cohort (3 ADC, 2 SCC, and 3 CFs) with retrovirus expressing the human telomerase enzyme (hTERT), which restores telomeric DNA *de novo* [134]. hTERT expression in the nuclei of a pulmonary control fibroblast from a randomly selected patient (CF^{hTERT} (#5), where the number identifies the selected patient throughout the text) was confirmed by immunofluorescence staining as shown in **Figure 16**.

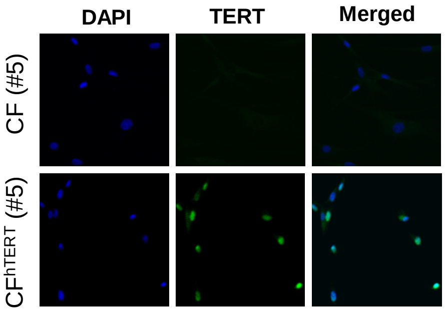

Figure 16. Immunofluorescence of hTERT. Selected regions from representative immunofluorescence images of DAPI (left), TERT (middle) and their corresponding co-localization (right) of primary CF (#5) and CF^{hTERT} (#5). Images obtained with a ×20 objective.

Next, we confirmed that the resulting immortalized fibroblasts did not enter to replicative senescence by assessing the population doubling level during 77 days. The population doubling level is defined as the total number of times that fibroblast growth is doubled. Primary CF (#5) failed to continue doubling beyond day 50 while CF^{hTERT} (#5) kept its doubling ratio within the experimental time window (77 days) (**Figure 17A**). Moreover, a hallmark of senescent cells is the expression of the senescence-associated acidic β-galactosidase enzyme (SA-βgal) [135]. At day 54 SA-βgal activity was detected as blue staining in primary fibroblasts but not in hTERT-immortalized fibroblasts (**Figure 17B-C**), further supporting that CF^{hTERT} do not enter replicative senescence.

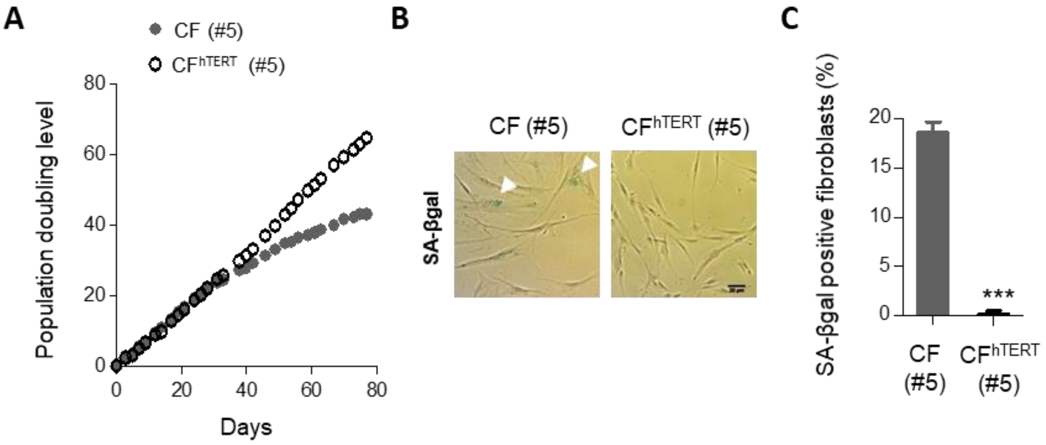

Figure 17. Fibroblast immortalization confirmation at long term maintenance in culture. A, Population doubling level of primary CF (#5) and CF^{hTERT} (#5) assessed during 77 days. At each passage, the gained population doubling level of each cell type was calculated and plotted against time. **B,** Representative images of SA-βgal staining of primary CF (#5) and CF^{hTERT} (#5) at day 54. White arrowheads point at SA-βgal+ fibroblasts (blue staining). **C,** Percentage of SA-βgal+ fibroblasts shown in **B**. Error bars indicate mean ± s.e.m. ***, $p < 0.005$ comparing primary CF (#5) with CF^{hTERT} (#5). All comparisons were done using Student *t*-test.

To guarantee that hTERT immortalization did not modify the ability of pulmonary TAFs and CFs to respond to TGF-β1 [37, 56], we studied the response to TGF-β1 of immortalized fibroblasts. As expected, the immortalization of CF^{hTERT} (#5) did not alter the TGF-β1/SMAD3 activation pathway (**Figure 18A-B**) neither the expression of the standard fibrosis markers, αSMA (**Figure 18C-D**), and *COL1A1* (**Figure 18E**).

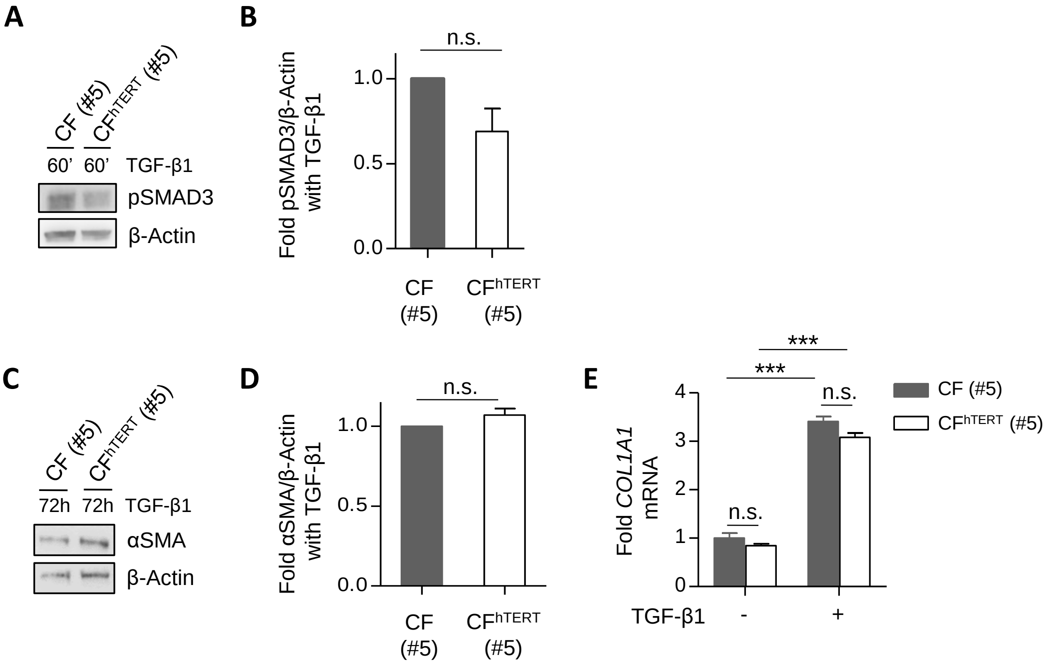

Figure 18. Fibrosis markers study upon fibroblast immortalization. A, Representative Western blot for pSMAD3 and β-Actin of primary CF (#5) and CF^{hTERT} (#5) stimulated with 2.5 ng/mL TGF-β1 for 60 min. **B**, Densitometry analysis of pSMAD3 expression normalized to β-actin. **C**, Representative Western Blot for αSMA and β-Actin of primary CF (#5) and CF^{hTERT} (#5) cultured as in Figure 12B. **D**, Densitometry analysis of α-SMA expression normalized to β-actin. **E**, Fold *COL1A1* mRNA expression of fibroblasts cultured as in (C). Error bars indicate mean ± s.e.m. ***, $p < 0.005$ comparing primary CF (#5) or CF^{hTERT} (#5) with their respective untreated condition. n.s.: non-significant. All comparisons were done using Student *t*-test.

Finally, since TIMP-1 is the main pro-tumoral stromal factor studied in this thesis, its secreted levels were also evaluated by ELISA upon immortalization. TIMP-1 secretion was comparable between primary and immortalized TAFs (2 ADC, 1 SCC) (**Figure 19**), underscoring that TIMP-1 secretion is not affected by hTERT immortalization.

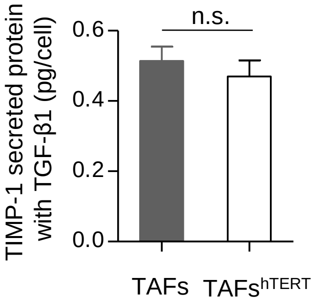

Figure 19. TIMP-1 secretion in immortalized lung TAFs. ELISA quantification of TIMP-1 protein (pg of TIMP-1/number of cells) secreted by primary and immortalized lung TAFs (2 ADC, 1 SCC) cultured as in Figure 12C. Error bars indicate mean ± s.e.m. n.s.: non-significant. All comparisons were done using Student *t*-test.

2.2. TGF-β1 promotes the expression and secretion of TIMP-1 in lung TAFs

To dissect the mechanism underlying the overexpression and secretion of TIMP-1 selectively found in ADC-TAFs, the expression and secretion of TIMP-1 in ADC and SCC-TAFs in response to TGF-β1 was determined. TGF-β1 induced TIMP-1 expression and secretion in both ADC and SCC-TAFs (**Figure 20A-B**). However, a significantly greater induction of secreted TIMP-1 was observed in ADC-TAFs compared to SCC-TAFs (**Figure 20B**).

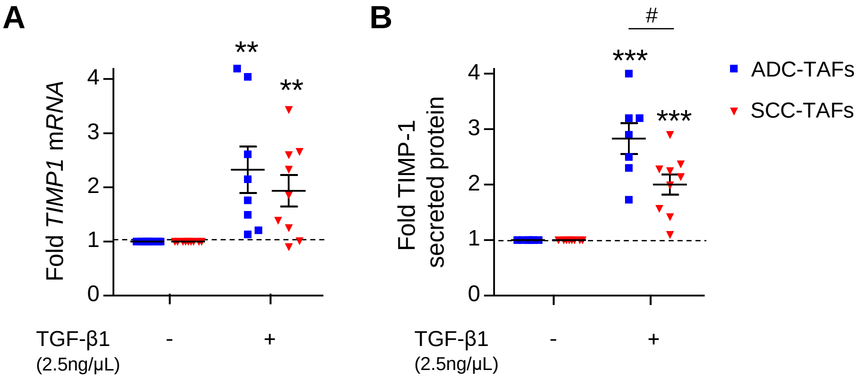

Figure 20. TGF-β1 induction of TIMP-1 expression and secretion in lung TAFs. A, Fold *TIMP1* mRNA expression of TAFs (8 ADC, 9 SCC) cultured as in Figure 12B. **B**, Fold TIMP-1 protein secretion of TAFs (7 ADC, 9 SCC) cultured as in Figure 12C. Error bars indicate mean ± s.e.m. **, $p < 0.01$; ***, $p < 0.005$ comparing TAFs with their respective untreated condition. #, $p < 0.05$; comparing ADC with SCC. All comparisons were done using Student *t*-test.

Once determined that ADC-TAFs are hyperresponsive to TGF-β1 in terms of TIMP-1 secretion, we wondered whether the autocrine production of TGF-β may be amplifying the overproduction of TIMP-1 in these TAFs. Therefore, the bioactivity of TGF-β secreted by lung TAFs was assessed using a luciferase assay encoding the TGF-β responsive sequence (p(CAGA)$_{12}$ luciferase-reporter). In brief, HEK 293T cells were transfected with the p(CAGA)$_{12}$ luciferase-reporter and incubated for 6 hours with the conditioned medium derived from lung TAFs (**Figure 21A**), and the observed luciferase activity of HEK 293T cells was indicative of TGF-β activity within the secretome of primary TAFs. Interestingly, ADC-TAFs showed a significantly greater autocrine production of TGF-β than SCC-TAFs, as illustrated by the larger luciferase activity (**Figure 21B**).

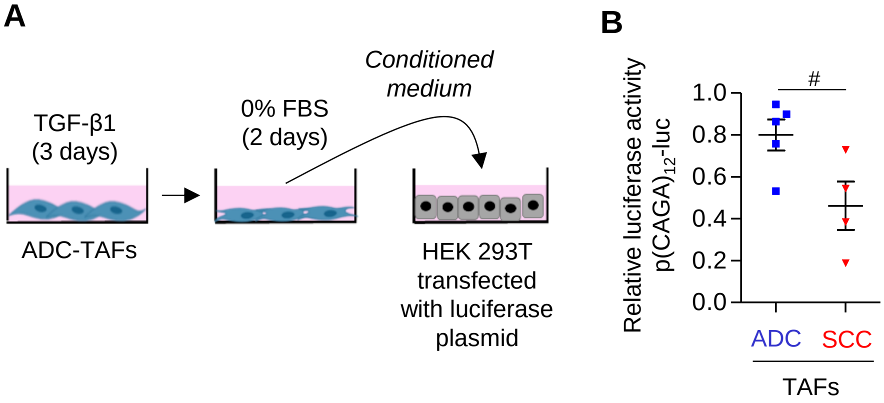

Figure 21. Assessment of the production of TGF-β by lung TAFs. A, Outline of the experimental design used to assess TGF-β activity using HEK 293T cells. **B,** Bioactivity of the TGF-β secreted into the conditioned medium by TAFs (5 ADC, 4 SCC) cultured as in Figure 12C and kept in culture medium without exogenous TGF-β for 48 hours. Error bars indicate mean ± s.e.m. #, $p < 0.05$; comparing ADC with SCC. All comparisons were done using Student *t*-test.

2.3. *SMAD3* expression is necessary for the induction of TIMP-1 expression and secretion with TGF-β1

Since the selective hyperactivation of the canonical TGF-β1/SMAD3 pathway is a key mechanism driving the aberrant phenotype of ADC-TAFs, we wondered whether SMAD3 was underlying the excessive expression and/or secretion of TIMP-1 in response to TGF-β1 in this histologic subtype. To this aim, both pharmacologic and genetic SMAD3 loss-of-function approaches were used.

First, CF^{hTERT} (#5) was stimulated with the potent SMAD3 inhibitor SB431542 (SB) (**Figure 22A**), which elicited a marked downregulation in *TIMP1* mRNA (**Figure 22B**) and secreted levels (**Figure 22C**). In contrast, the reduction in TIMP-1 expression and secretion caused by the weak SMAD3 inhibitor galunisertib (GNB) (**Figure 22A**) was less pronounced with respect to SB (**Figure 22B-C**).

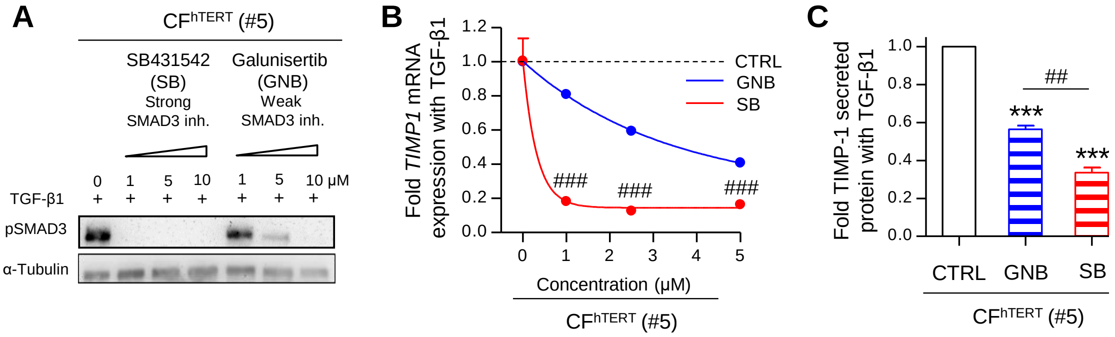

Figure 22. TIMP-1 expression and secretion after pharmacologic downregulation of SMAD3 in lung fibroblast. A, Representative Western Blot for pSMAD3 and α-tubulin of CF^{hTERT} (#5) stimulated with 2.5 ng/mL TGF-β1 for 60 minutes in the presence of increasing doses of SB or GNB (0-10 µM). **B**, Fold *TIMP1* mRNA expression of CF^{hTERT} (#5) stimulated with 2.5 ng/mL TGF-β1 for 3 days alone or in the presence of increasing concentrations of SB or GNB (0-5 µM). **C** Fold TIMP-1 secretion of CF^{hTERT} (#5) stimulated with 2.5 ng/mL TGF-β1 for 3 days alone or in the presence of 2.5µM SB or 2.5µM GNB and subsequently maintained in serum-free medium for 2 days. Error bars indicate mean ± s.e.m. ***, $p < 0.005$ comparing SB and GNB treatment with untreated conditions. ##, $p < 0.01$; ### $p < 0.005$ comparing SB with GNB treatment. All comparisons were done using Student *t*-test.

Consistently, knocking-down *SMAD3* in 2 CFs (#5 and #15) by shRNA (**Figure 23A-B**) was sufficient to downregulate TIMP-1 at mRNA and protein level upon TGF-β1 stimulation in comparison to shRNA control (shCTRL) (**Figure 23C-F**).

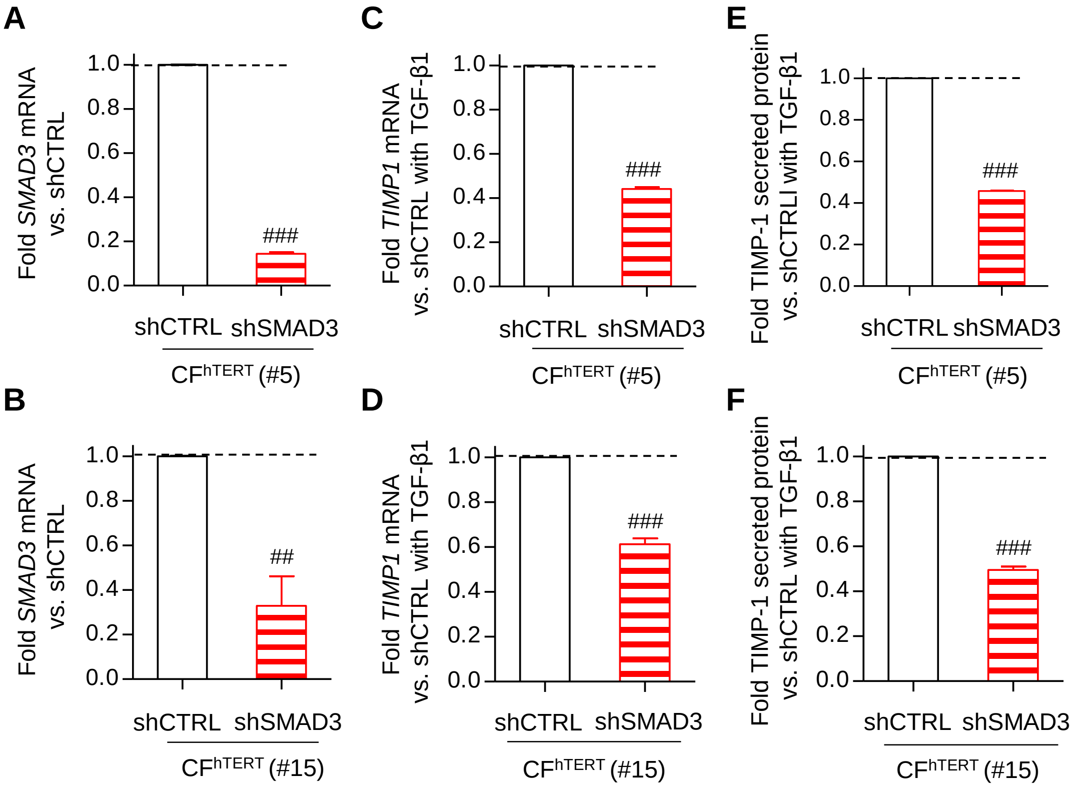

Figure 23. TIMP-1 expression and secretion after genetic downregulation of SMAD3 in control fibroblasts. A-B, Fold *SMAD3* expression of shSMAD3 CF^{hTERT} (#5) (A) and (#15) (B) with respect to control shRNA maintained in fibroblast culture medium supplemented with 10% FBS. **C-D**, Fold *TIMP1* mRNA of shSMAD3 CF^{hTERT} (#5) (C) and (#15) (D) with respect to control shRNA fibroblasts cultured as in Figure 12B. **E-F**, Fold TIMP-1 secretion of shSMAD3 CF ^{hTERT} (#5) (E) and (#15) (F) with respect to control shRNA fibroblasts cultured as in Figure 12C. Error bars indicate mean ± s.e.m. ##, $p < 0.01$; ###, $p < 0.005$ comparing shCTRL with shSMAD3 fibroblasts. All comparisons were done using Student *t*-test.

Finally, SMAD3 was also knocked-down in hTERT-immortalized ADC-TAF from a randomly selected patient (ADC-TAF^{hTERT} (#37)) (**Figure 24A**). In agreement with our previous results, a downregulation of *TIMP1* mRNA (**Figure 24B**) and protein secretion (**Figure 24C**) was found in shSMAD3 fibroblasts upon TGF-β1 stimulation.

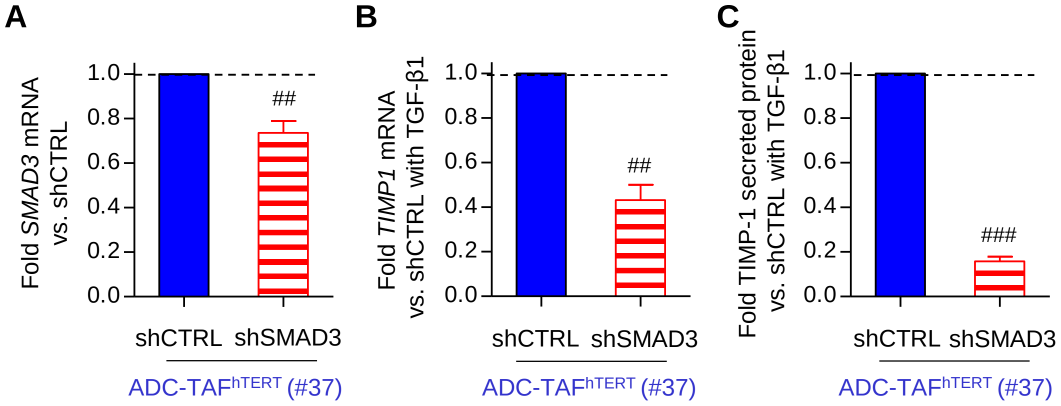

Figure 24. TIMP-1 expression and secretion after genetic downregulation of SMAD3 in lung TAF. A, Fold *SMAD3* expression of shSMAD3 ADC-TAF^{hTERT} (#37) with respect to control shRNA maintained as in Figure 23A. **B**, Fold *TIMP1* mRNA of shSMAD3 ADC-TAF^{hTERT} (#37) with respect to shCTRL fibroblasts cultured as in Figure 12B. **C**, Fold TIMP-1 secretion of ADC-TAF^{hTERT} (#37) with respect to shCTRL fibroblasts cultured as in Figure 12C. Error bars indicate mean ± s.e.m. ##, $p < 0.01$; ###, $p < 0.005$ comparing shCTRL with shSMAD3 fibroblasts. All comparisons were done using Student *t*-test.

2.4. *SMAD3* overexpression is sufficient to promote the expression and secretion of TIMP-1 with TGF-β1

To further implicate SMAD3 in TIMP-1 regulation, we studied TIMP-1 induction in fibroblasts overexpressing *SMAD3*. To this aim *SMAD3* overexpressing CF^{hTERT} (#5) was generated with retroviral transduction (rv-SMAD3) (**Figure 25A**). Of note, rv-SMAD3 alone (in the absence of TGF-β1) markedly upregulated *TIMP1* expression (**Figure 25B**). Moreover, TGF-β1 slightly increased *TIMP1* expression, which may indicate that it had reached saturation, and markedly promoted its secretion in rv-SMAD3 fibroblast with respect to rv-GFP used as a control (**Figure 25C-D**).

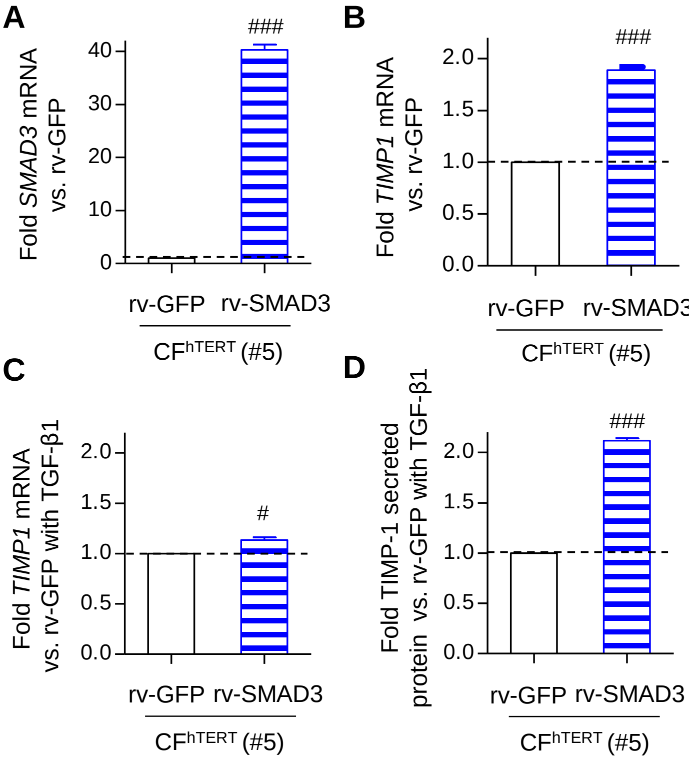

Figure 25. TIMP-1 expression and secretion after SMAD3 overexpression in control fibroblast. A-B, Fold *SMAD3* (A) and *TIMP1* (B) expression of rv-SMAD3 CF^{hTERT} (#5) with respect to control rv-GFP fibroblast maintained as in Figure 23A. **C**, Fold *TIMP1* mRNA of rv-SMAD3 CF^{hTERT} (#5) with respect to control rv-GFP fibroblasts cultured as in Figure 12B. **D**, Fold TIMP-1 secretion of rv-SMAD3 CF ^{hTERT} (#5) with respect to control rv-GFP fibroblasts cultured as in Figure 12C. Error bars indicate mean ± s.e.m. #, $p < 0.05$; ###, $p < 0.005$ comparing rv-GFP with rv-SMAD3 fibroblasts. All comparisons were done using Student *t*-test.

3. PRO-TUMORIGENIC CROSSTALK BETWEEN TIMP-1 FROM TAFs AND CD63 IN CANCER CELLS IN LUNG ADC

To study the potential pro-tumoral traits of TIMP-1 within the TAFs secretome, we developed an *in vitro* functional assay based on the stimulation of cancer cells with the conditioned medium (CM) of activated TAFs [37], in which we assessed cell density as a growth metric (top right) and migration across basement membrane (Matrigel) in Transwells as an invasion metric (bottom right) (**Figure 26**). To clarify the function of TIMP-1 and CD63 overexpression in ADC-TAFs and ADC cancer cells, respectively, this functional assay was done after knocking-down either *TIMP1* in TAFs or *CD63* in cancer cells (**Figure 26**).

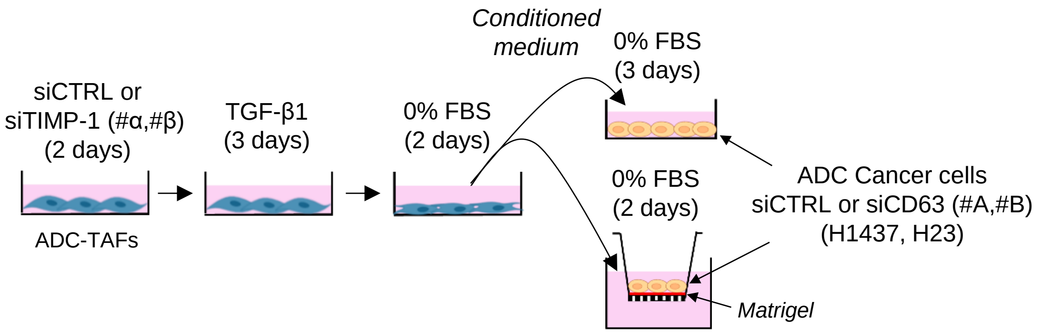
siCTRL or
siTIMP-1 (#α,#β)
(2 days)
ADC-TAFs
TGF-β1
(3 days)
0% FBS
(2 days)
Conditioned
medium
0% FBS
(3 days)
0% FBS
(2 days)
ADC Cancer cells
siCTRL or siCD63 (#A,#B)
(H1437, H23)
Matrigel

Figure 26. Crosstalk model. Outline of the experimental design used to assess growth (top right) and invasion (bottom right) of ADC cancer cell lines (siCTRL or siCD63) stimulated with basal medium or CM from activated ADC-TAFs (siCTRL or siTIMP-1).

To this aim, two ADC cell lines (H1437 and H23) exhibiting high surface expression of CD63 to mimic ADC patients were used. CD63 expression was determined by flow cytometry revealing that ~70% of H1437 and ~90% of H23 cells were positive for CD63 (**Figure 27**), which were referred to as CD63^{high} ADC cells.

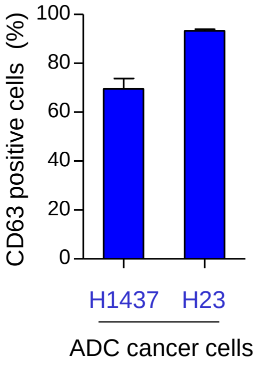

Figure 27. CD63 levels in lung ADC cell lines. Percentage of CD63 positive H1437 and H23 assessed by flow cytometry (n=4).

3.1. Inhibition of TIMP-1 in ADC-TAFs diminishes the pro-tumoral activity of their secretome

To conduct the TIMP-1 loss-of-function experiments, *TIMP1* was knocked-down in ADC-TAFs from 4 randomly selected patients (#7, #12, #13, and #37) using two siRNA constructs (#α and #β) that consistently elicited a >90% reduction of secreted TIMP-1 (**Figure 28A**).

As a control, it was first examined whether siTIMP-1 may alter TAF response to TGF-β1, but we found virtually no difference in the expression of fibrosis activation markers in comparison to siCTRL fibroblasts (**Figure 28B-F**), supporting that silencing *TIMP1* did not alter the content of other factors secreted in the CM of those TAFs.

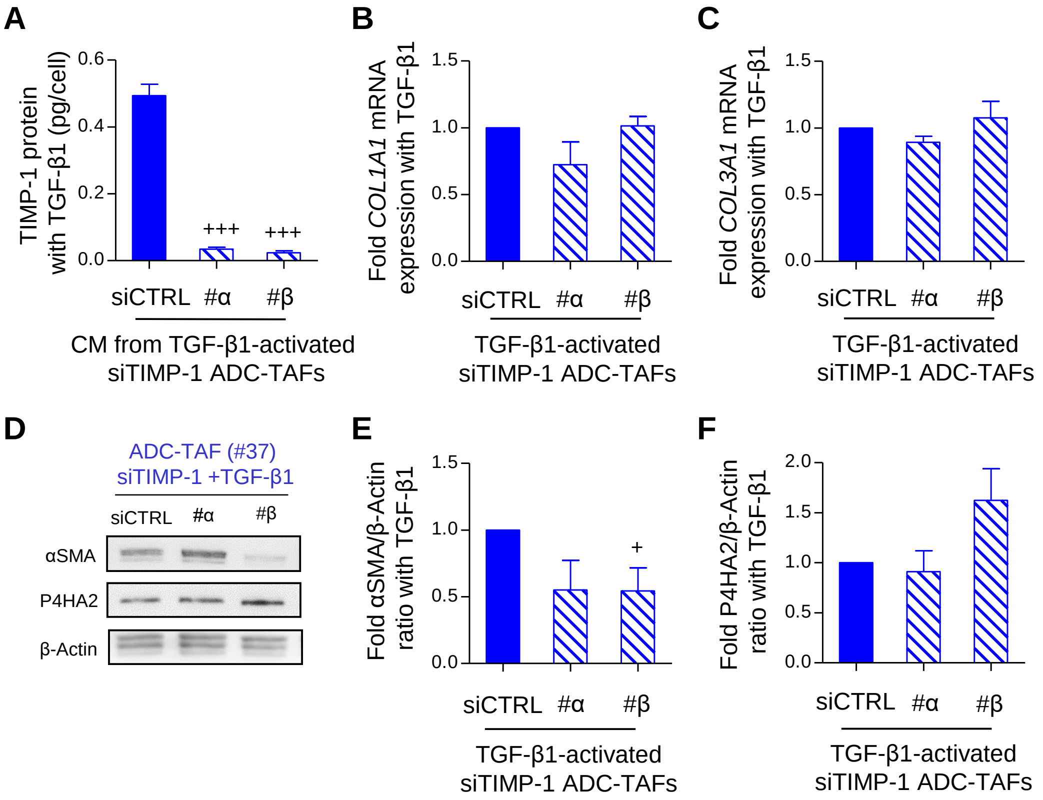

Figure 28. Fibrosis markers on siTIMP-1 fibroblasts. A, ELISA quantification of TIMP-1 protein (pg of TIMP-1/number of cells) secreted by siTIMP-1 ADC-TAFs cultured as in Figure 12C (n = 4). **B-C**, Fold *COL1A1* and *COL3A1* mRNA (siTIMP-1/siCTRL) of fibroblasts cultured as in Figure 12B. **D**, Representative Western Blot for αSMA, Prolyl 4-hydroxylase subunit α-2 (P4HA2) and β-Actin of siTIMP-1 ADC-TAFs cultured as in (B). **E-F**, Densitometry analysis expressed as fold (siTIMP-1/siCTRL) of αSMA/β-Actin (E) and P4HA2/ β-Actin (F) of fibroblasts (n=3) cultured as in (B). Error bars indicate mean ± s.e.m. +, $p < 0.05$; +++, $p < 0.005$ comparing siTIMP-1 with siCTRL fibroblasts. All comparisons were done using Student *t*-test.

Next, H1437 and H23 WT cells were stimulated with siCTRL-CM or siTIMP-1-CM from ADC-TAFs and we found that silencing TIMP-1 secretion in ADC-TAFs significantly attenuated the proliferation (**Figure 29A-B**) and invasion (**Figure 29C-D**) of CD63^{high} ADC cells elicited with the secretome of parental ADC-TAFs, indicating that TIMP-1 is necessary for the tumor promoting effects of the CM of ADC-TAFs.

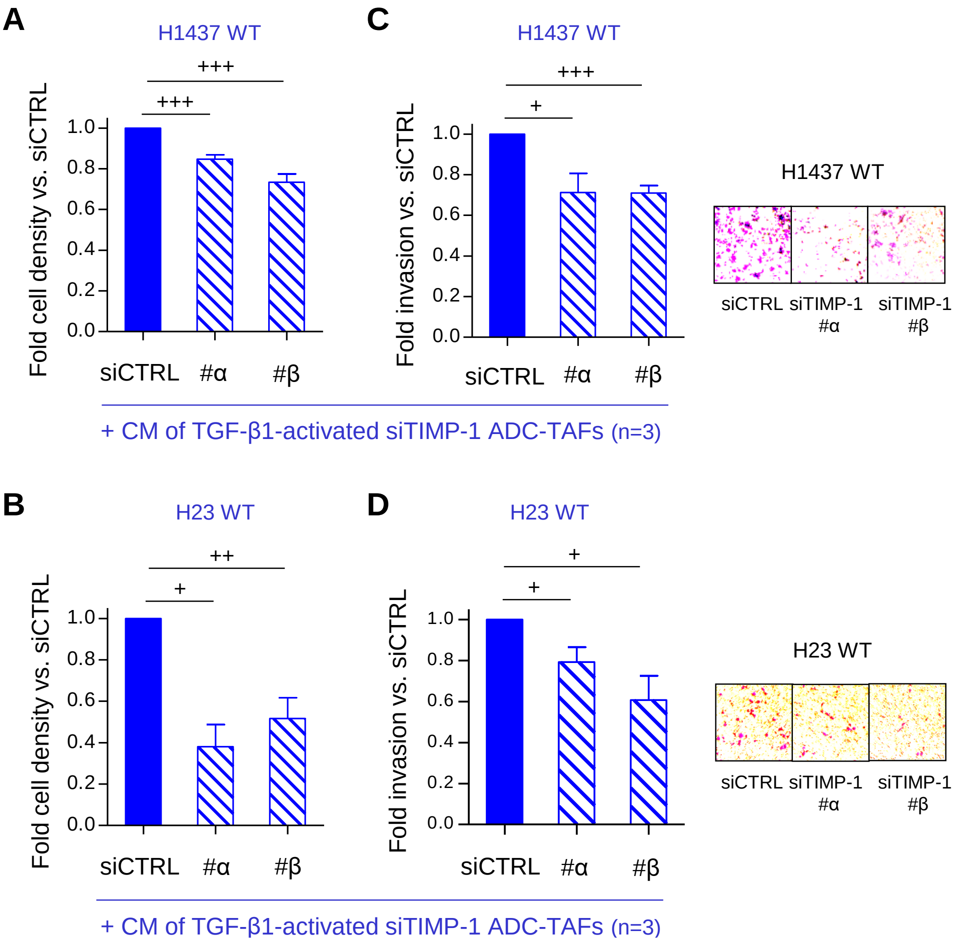

Figure 29. Cancer cell growth and invasion induction after silencing TIMP-1 on ADC-TAFs. A-D, Fold cancer cell number density and invasion of H1437 WT (A and C, respectively) and H23 WT (B and D) cells stimulated with the CM of siCTRL or siTIMP-1 fibroblasts cultured as in Figure 26. Representative images of invading cancer cells are shown right invasion plots. Error bars indicate mean ± s.e.m. +, $p < 0.05$; ++, $p < 0.01$; +++, $p < 0.005$ comparing with siCTRL condition. All comparisons were done using Student *t*-test.

It is worth noting that the concentration of soluble TIMP-1 was significantly lower in the CM of H1437 and H23 than in the CM of activated ADC-TAFs (**Figure 30**). Therefore, our model is consistent with the overproduction of stromal TIMP-1 found in ADC tissue (**Figure 11-12**).

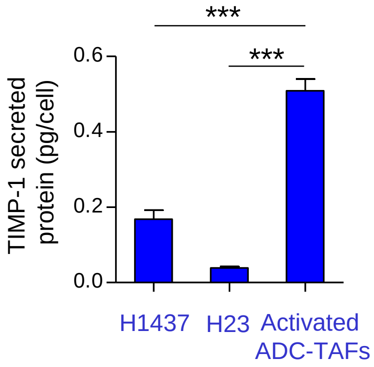

Figure 30. ELISA quantification of TIMP-1 protein (pg of TIMP-1/number of cells) secreted by H1437, H23 and TGF-β1-activated ADC-TAFs cultured as in Figure 12C. Error bars indicate mean ± s.e.m. ***, $p < 0.005$ comparing ADC-TAFs with either H1437 or H23 cells. All comparisons were done using Student *t*-test.

3.2. CD63 in ADC cells is necessary for a tumor-promoting crosstalk with the stromal secretome

To conduct CD63 loss-of-function experiments, transient transfection of ADC cells with two siRNA constructs against CD63 (#A and #B) was used, which elicited a significant downregulation of their *CD63* expression (**Figure 31A-B**) and surface membrane content (~90% reduction in the percentage of CD63 positive cells) in comparison to cells transfected with the siCTRL construct (**Figure 31C-D**). Accordingly, the mean fluorescence intensity (MFI) of siCD63 H1437 and H23 (dashed blue line) was similar to the MFI of cells without CD63-antibody bound (solid grey line) (**Figure 31E-F**).

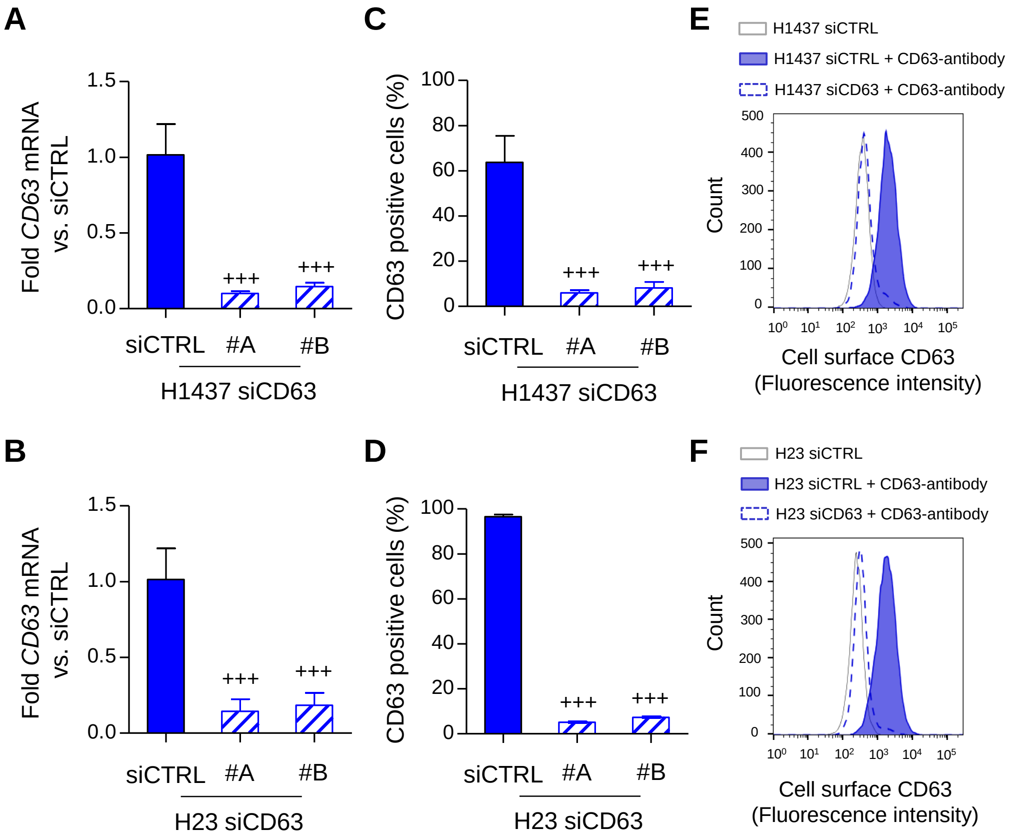

Figure 31. Assessment of CD63 expression on siCD63 cancer cells. A-B, Fold *CD63* mRNA expression of H1437 (A) and H23 (B) siCD63 cells (#A, #B) with respect to siCTRL cells. **C-D**, Percentage of CD63 positive H1437 (C) and H23 (D) cells after transfection with siCD63 (#A, #B) and siCTRL. **E-F**, Representative histogram of fluorescence intensity of H1437 (E) and H23 (F) siCD63 (#A, #B) and siCTRL. Grey solid line indicates cells stained with secondary antibody alone; blue indicates CD63 staining followed by fluorescence-labeled secondary antibody, blue solid line is used for siCTRL cells and blue dashed line is used for siCD63 cells. Error bars represent mean ± s.e.m. +++, $p < 0.005$ comparing with siCTRL cells. All comparisons were done using Student *t*-test.

Next, the effect of knocking-down *CD63* on cancer cell growth and invasion was assessed in basal conditions. CD63 attenuation barely increased cancer cell growth (**Figure 32A-**

B) and invasion (**Figure 32C-D**) in comparison to siCTRL cells, although it did not reach significance in most cases.

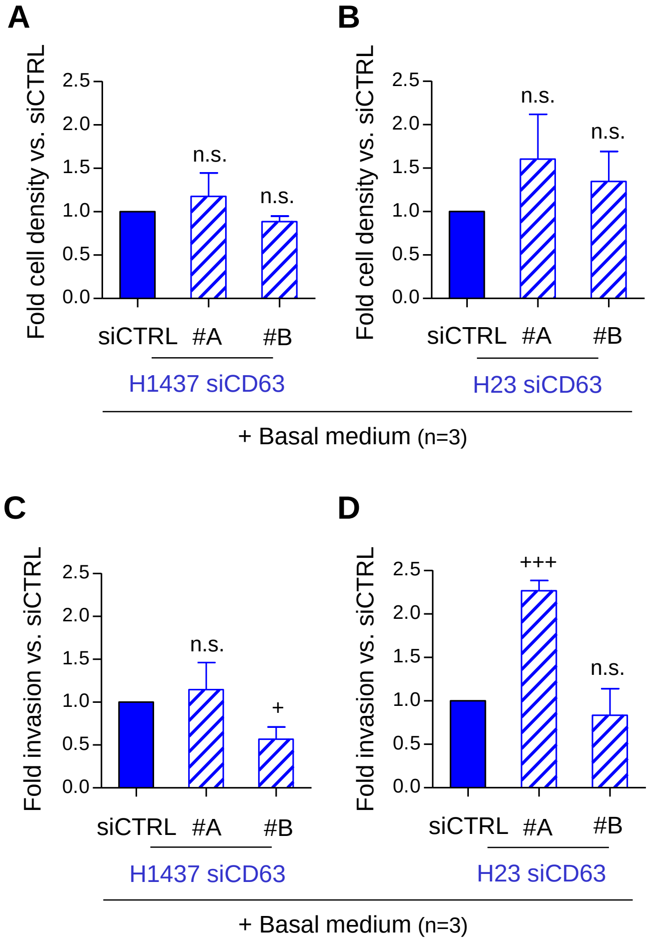

Figure 32. Growth and invasion of siCD63 cells in basal conditions. A-D, Fold cell density and invasion induction of siCD63 H1437 (A and C, respectively) and siCD63 H23 (B and D) stimulated with the basal medium. Error bars represent mean ± s.e.m. +, $p < 0.05$; +++, $p < 0.005$ comparing with siCTRL cells. n.s.: non-significant. All comparisons were done using Student *t*-test.

Then, we examined the role of CD63 in the response to the CM from activated ADC-TAFs. In agreement with previous results of our group [37], the CM of ADC-TAFs induced cancer cell growth and invasion of siCTRL H1437 and siCTRL H23 in comparison to the corresponding basal medium (**Figure 33A-D**). In contrast, the increase in growth and invasion elicited with the stromal CM was decreased when CD63 was silenced in both cell lines (**Figure 33A-D**). Of note, cell density of siCD63 cells stimulated with the CM was similar to that obtained with basal medium (**Figure 33A, C**), indicating that growth induction with the CM of TAFs requires elevated expression of CD63. Likewise, knocking-down *CD63* reduced the invasion elicited with the CM, although the level of downregulation was cell-type dependent (**Figure 33B, D**).

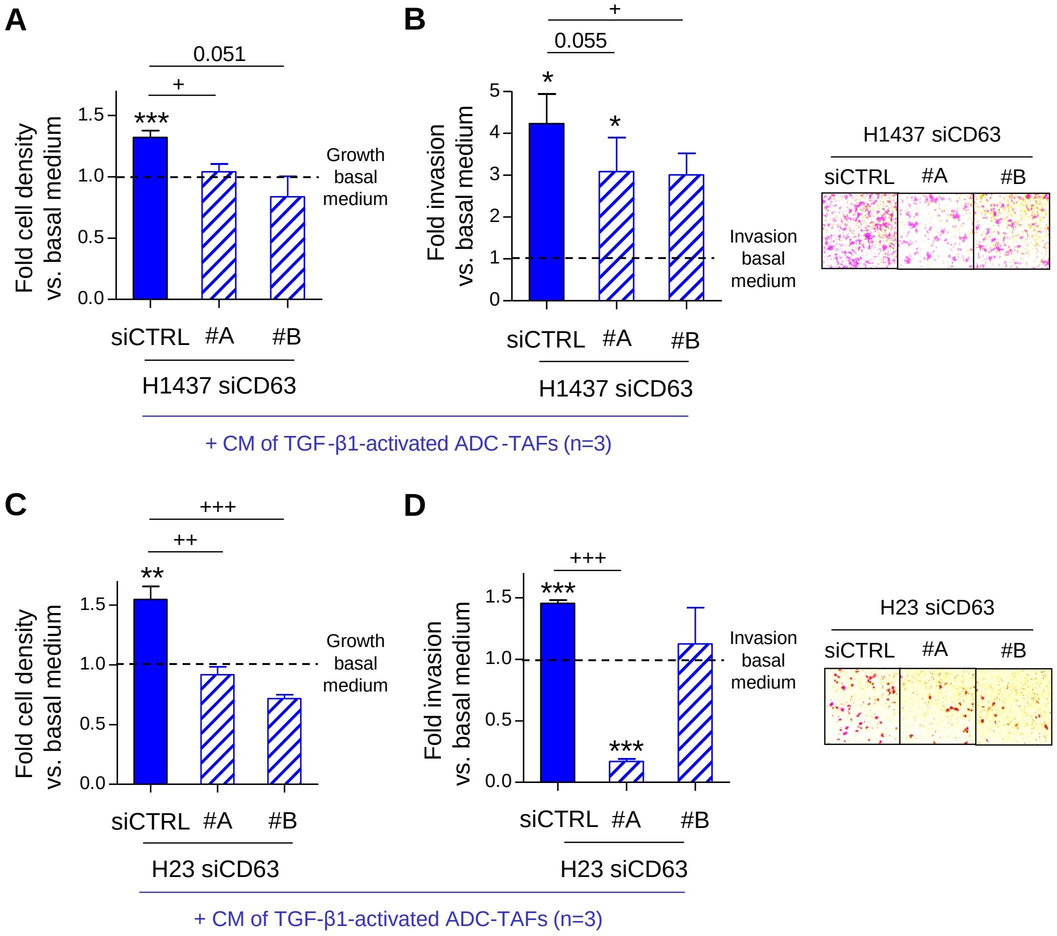

Figure 33. Effect of silencing CD63 on cancer cells in the response to TAFs secretome. A and **C**, Fold cell density induction of siCD63 H1437 (A) and siCD63 H23 cells (C) stimulated with the CM of fibroblasts cultured as in Figure 26 with respect to basal medium. **B** and **D**, Fold cell invasion of siCD63 H1437 (B) and siCD63 H23 cells (D) stimulated with the CM of fibroblasts cultured as in (A) with respect to basal medium. Representative images of invading cancer cells are shown right invasion plots. Error bars represent mean ± s.e.m. *, $p < 0.05$; **, $p < 0.01$; ***, $p < 0.005$ comparing with basal medium. +, $p < 0.05$; ++, $p < 0.01$; +++, $p < 0.005$ comparing with corresponding siCTRL cells. All comparisons were done using Student *t*-test.

3.3. TIMP-1 in TAFs and CD63 in cancer cells are both necessary effector proteins of a tumor-promoting paracrine interaction in lung ADC

To further establish a link between the function of TAF-derived TIMP-1 and CD63, functional assays were performed upon simultaneous downregulation of both proteins. In agreement with our previous results (**Figure 33**), siCD63 H1437 and siCD63 H23 cells were less responsive to the secretome of siCTRL-TAFs than siCTRL ADC cells in terms of growth and invasion (**Figure 34A-D**, comparing solid bars). Likewise, silencing TIMP-1 secretion in ADC-TAFs significantly reduced the growth and invasion induction of ADC cells expressing CD63 (siCTRL) (**Figure 34A-D**, comparing solid bars with hatched bars on the left). However, stimulating siCD63 H1437 and siCD63 H23 cells with siTIMP-1-CM had a similar effect on growth and invasion (**Figure 34A-D**, comparing solid bars with hatched bars on the right) promotion than the stimulation with the siCTRL-CM, further underscoring that inhibiting CD63 is sufficient to abrogate the tumor-promoting activity of TAF-derived TIMP-1.

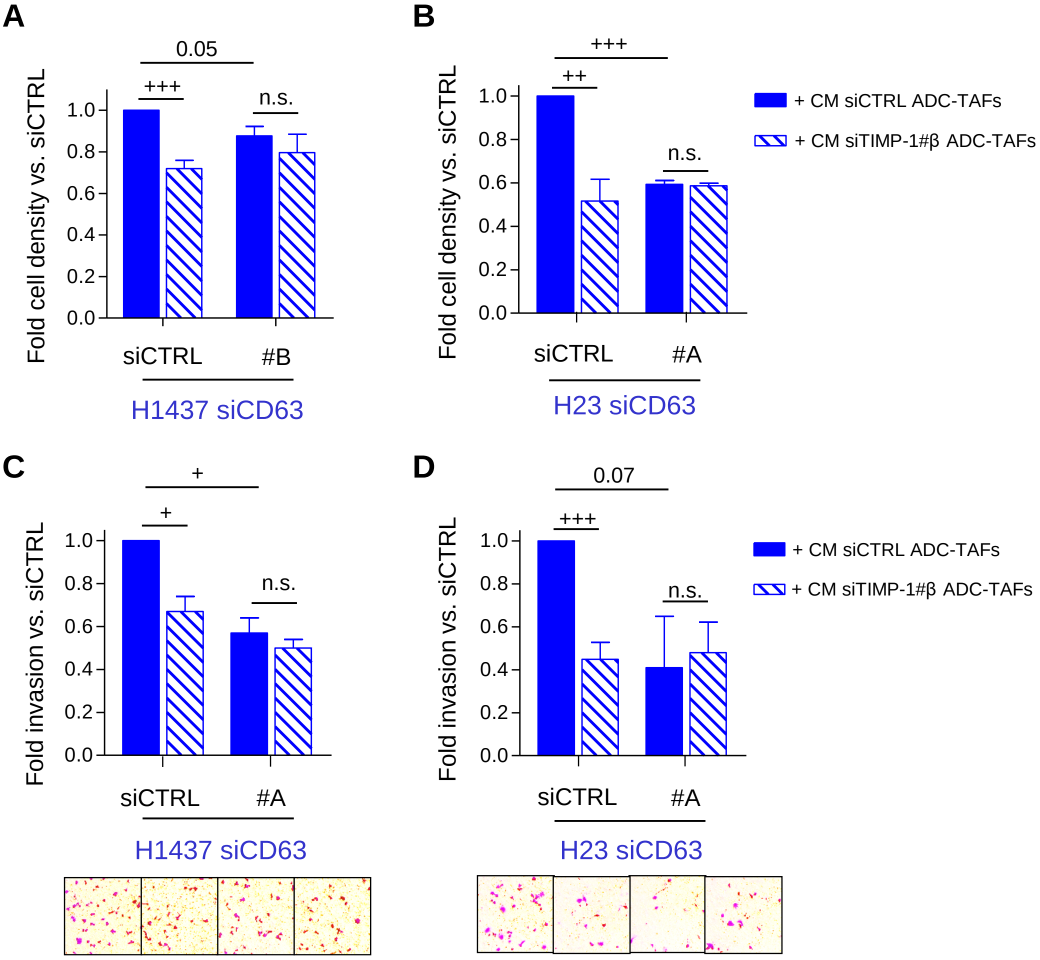

Figure 34. Effect of simultaneus knock-down of TIMP-1 in TAFs and CD63 in cancer cells. A-B, Fold cancer cell density of H1437 (A) and H23 (B) transfected with siCTRL (left bars) or siCD63#A (right bars) and stimulated as in Figure26. **C-D**, Fold cancer cell invasion of H1437 (C) and H23 (D) transfected with siCTRL (left bars) or siCD63#A (right bars) and stimulated as in (A). Representative images of invading cells are shown below invasion plots. Error bars indicate mean ± s.e.m. +, *p* < 0.05; ++, *p* < 0.01; +++, *p* < 0.005 comparing with corresponding siCTRL condition. n.s.: non-significant. All comparisons were done using Student *t*-test.

3.4. Recombinant TIMP-1 is sufficient to promote growth and invasion of ADC cells in a CD63-dependent manner

Once established that TIMP-1 is necessary for the tumor-promoting effects of ADC-TAFs, we assessed whether recombinant human TIMP-1 (rhTIMP-1) was sufficient to increase growth and invasion independently of other components within the TAFs' secretome. Since the MMP-inhibitory or cytokine-like activity of TIMP-1 appears to be determined by its concentration [87], stimulation with a suitable concentration was critical. To identify that suitable concentration, the fold in growth and invasion was plotted as a function of TIMP-1 present in the CM, and it was found that cancer cell growth and invasion increased linearly with the amount of secreted (unnormalized) TIMP-1 present within the CM of ADC-TAFs used in each experiment (**Figure 35A-D**).

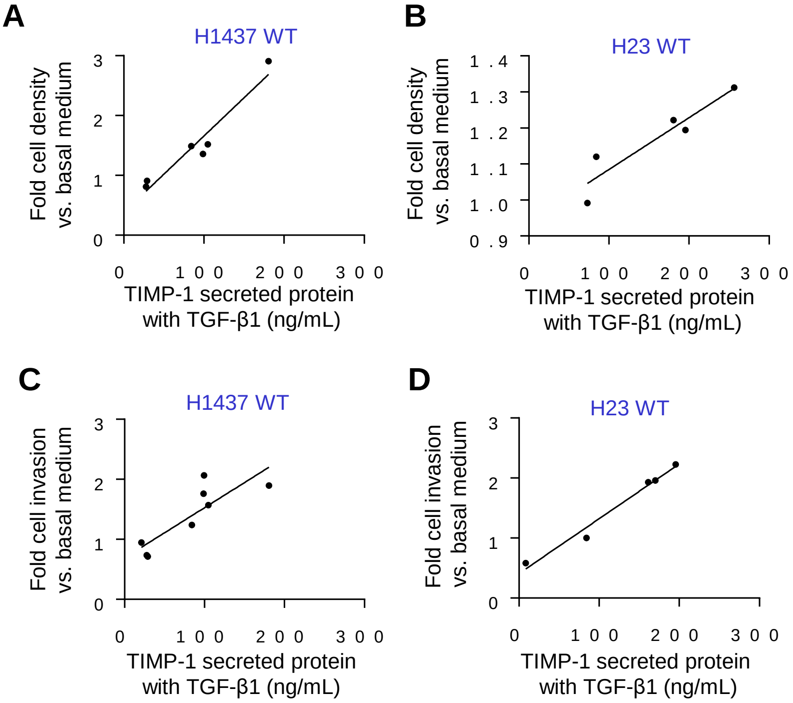

Figure 35. Correlation between TIMP-1 content in the CM and the induction of growth and invasion. A-D, Correlation betwen TIMP-1 secreted protein (ng/mL) and fold cell density and invasion of H1437 (A and C, respectively) and H23 (B and D) stimulated with CM from ADC-TAFs (n=5-7).

Accordingly, CD63^{high} ADC cells were treated with 160 ng/mL of rhTIMP-1 (**Figure 36A**), which covered the average amount of secreted (unnormalized) TIMP-1 by activated ADC-TAFs (**Figure 36B**) and is comparable with doses used elsewhere [77]. Reaching induction values similar to those obtained with the CM of ADC-TAFs, rhTIMP-1 stimulation enhanced the growth of both ADC cell lines up to ~12% on average (**Figure 36C-D**). Likewise, rhTIMP-1 elicited an even higher average increase in invasion by ~60%, although this effect was smaller than that elicited with the CM of activated ADC-TAFs (**Figure 36E-F**). These data reveals that TAF-derived TIMP-1 is a key factor promoting the growth of cancer cells, whereas other factors within the secretome may contribute to invasion enchancement.

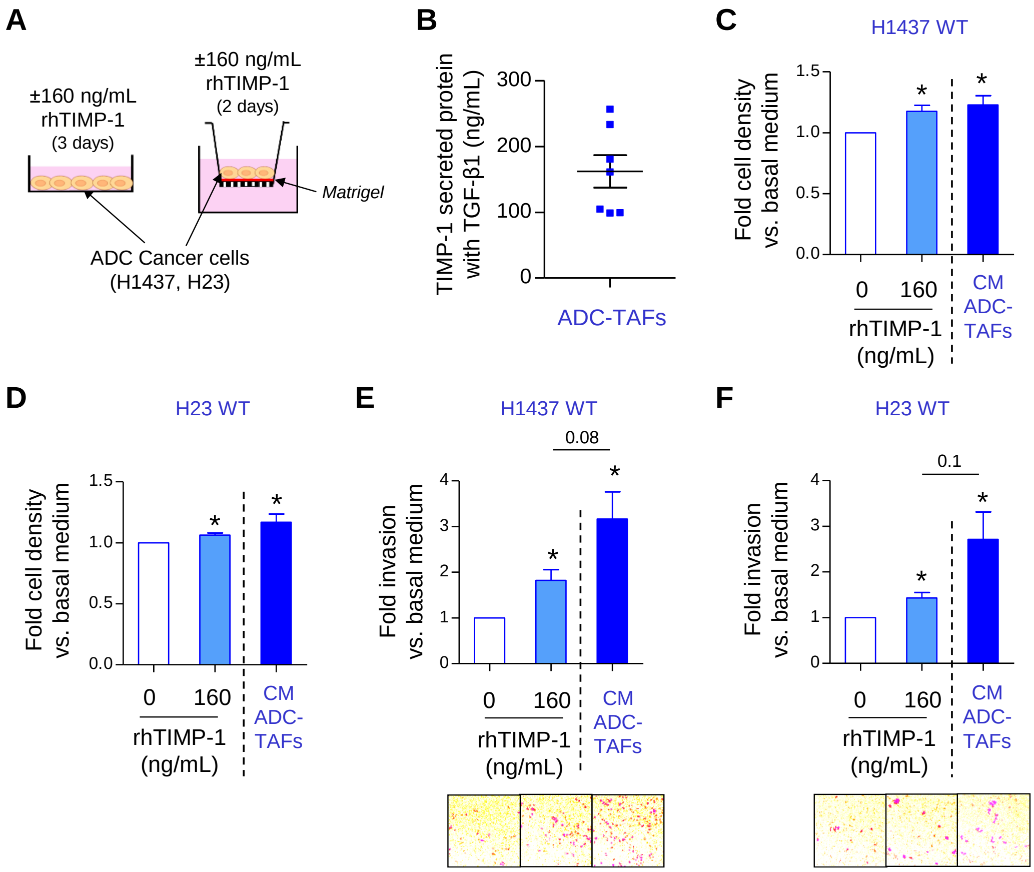

Figure 36. Effect of rhTIMP-1 treatment on cancer cell growth and invasion. A, Outline of the experimental design used to assess growth (left) and invasion (right) of ADC cancer cell lines stimulated with basal medium or 160ng/mL of rhTIMP-1. **B**, TIMP-1 secreted protein (ng/mL) of ADC-TAFs (n = 7) cultured as in Figure 12C. **C** and **E**, Fold cancer cell density (C) and invasion (E) of H1437 stimulated with 160ng/mL of rhTIMP-1 or the CM of ADC-TAFs (n=4) cultured as in (B). **D** and **F**, Fold cancer cell density (D) and invasion (F) of H23 stimulated with 160ng/mL of rhTIMP-1 or the CM of ADC-TAFs (n=4) cultured as in (B). Representative images of invading cells are shown below invasion plots. Error bars indicate mean ± s.e.m. *, $p < 0.05$; comparing either rhTIMP-1 or CM with basal medium. All comparisons were done using Student *t*-test.

Once determined that CD63 is required to promote growth and invasiveness of CD63^{high} ADC cell lines with stromal TIMP-1, we validated the TIMP-1/CD63 axis using rhTIMP-1 with siCD63 cells. rhTIMP-1 failed to enhance the proliferation of siCD63 cells in comparison to siCTRL cells (**Figure 37A-B**). Likewise, knocking-down *CD63* significantly attenuated the invasion increase elicited by rhTIMP-1 in both ADC lines with one siCD63 construct (#A) (**Figure 37C-D**).

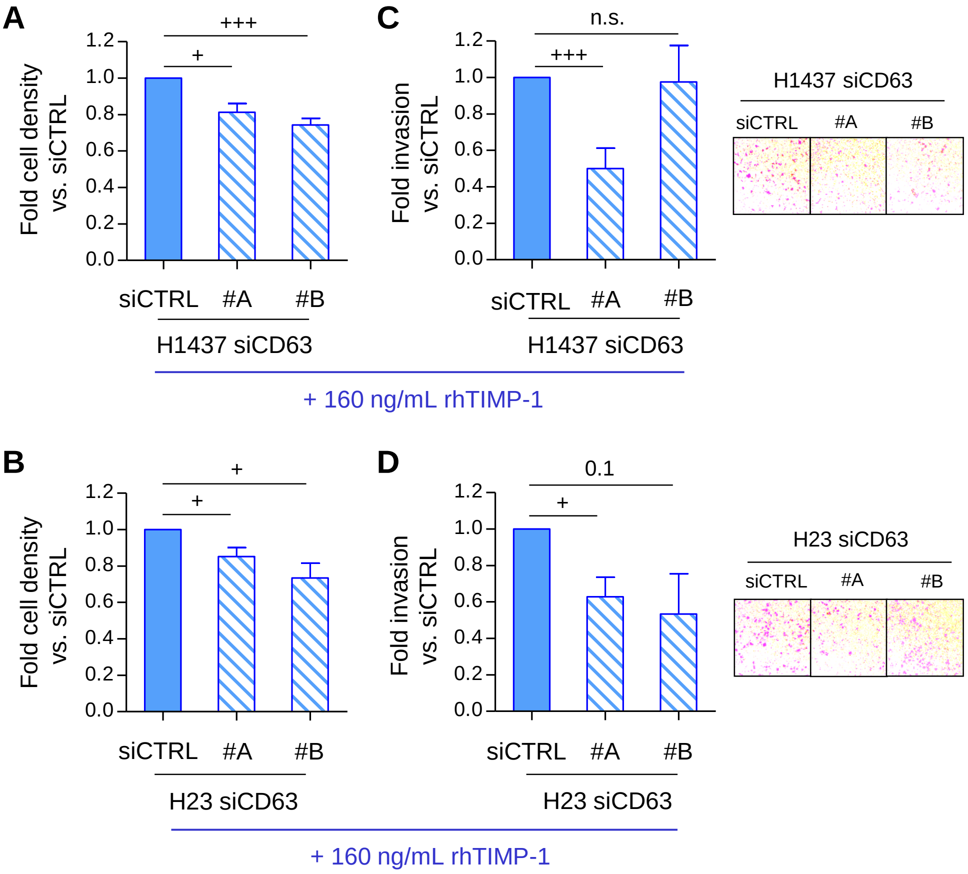

Figure 37. Effect of rhTIMP-1 treatment on cancer cell growth and invasion upon knocking-down CD63 in ADC cells. A and **C**, Fold cancer cell density (A) and invasion (C) of siCD63 H1437 with respect to siCTRL cells stimulated with 160ng/mL of rhTIMP-1. **B-D**, Fold cancer cell density (B) and invasion (D) of siCD63 H23 with respect to siCTRL cells stimulated with 160ng/mL of rhTIMP-1. Representative images of invading cells are shown right invasion plots. Error bars indicate mean ± s.e.m. +, $p < 0.05$; +++, $p < 0.005$ comparing with corresponding siCTRL cells. n.s.: non-significant. All comparisons were done using Student *t*-test.

3.5. TIMP-1/CD63/pAkt axis in lung ADC

Next we started to investigate which proteins may be involved in the signal transduction downstream of TIMP-1 and CD63 interaction to promote growth and invasion of cancer cells. Cui and colleagues described that the interaction of TIMP-1 with CD63 led to enhanced tumorigenesis through Akt activation in a model of lung ADC [99]. Accordingly, it was observed that stimulating H1437 with CM from activated ADC-TAFs for 24h (**Figure 38A**) significantly induced Akt phosphorylation (Akt^{pS473}) (**Figure 38B-C**), supporting that the paracrine signaling between ADC-TAFs and ADC cells may induce growth and invasion of ADC cells through Akt activation.

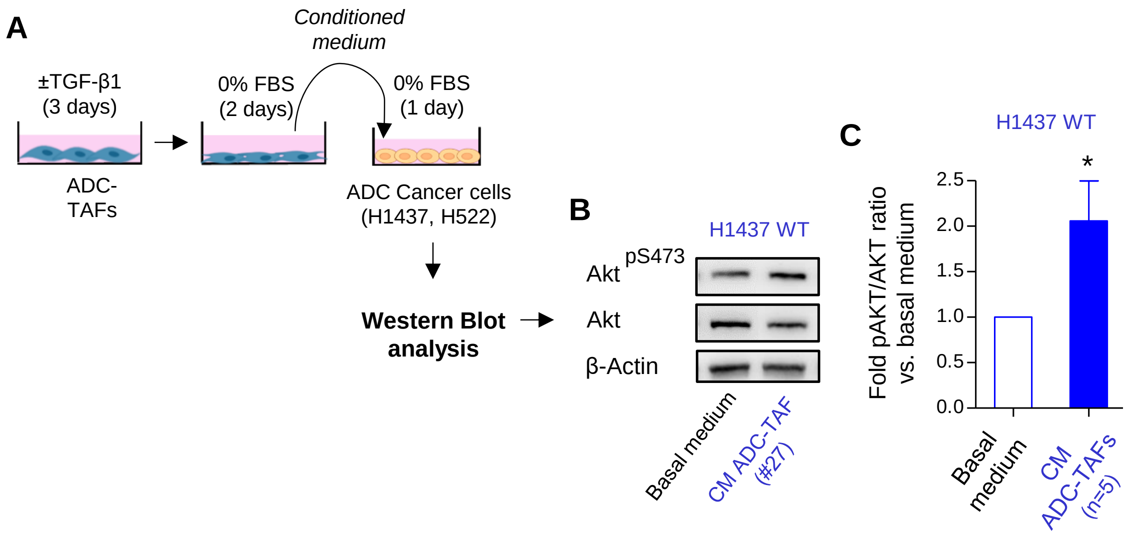

Figure 38. Effect of CM on Akt activation of ADC cells. A, Outline of the experimental design used to assessed Akt phosphorylation of ADC cell lines stimulated with CM from activated ADC-TAFs for 24 hours. **B**, Representative Western blot for pAKT (pS473), Akt and β-Actin of H1437 WT cultured as in (A). **C**, Densitometry analysis expressed as fold (conditioned medium/basal medium) of pAkt/Akt of H1437 WT cultured as in (A) (n=5). Error bars indicate mean ± s.e.m. *, $p < 0.05$ comparing with basal medium. All comparisons were done using Student *t*-test.

To further implicate pAkt in the TIMP-1/CD63 axis signaling, we stimulated the CD63^{low} ADC cell line H522 with CM and evaluated the activation of Akt. H522 showed a significantly lower CD63 content than H1437, with only ~15% of H522 cells positive for CD63 (**Figure 39A**). The H552 cell line was used as a model of low CD63 expression instead of siCD63 H1437 for these experiments due to the variability found in pAkt activity after siRNA transfection in basal conditions (**Figure 39B**). Remarkably, the secretome of activated ADC-TAFs not only did not promote Akt phosphorylation in H522 cells but downregulated its activation (**Figure 39C-D**).

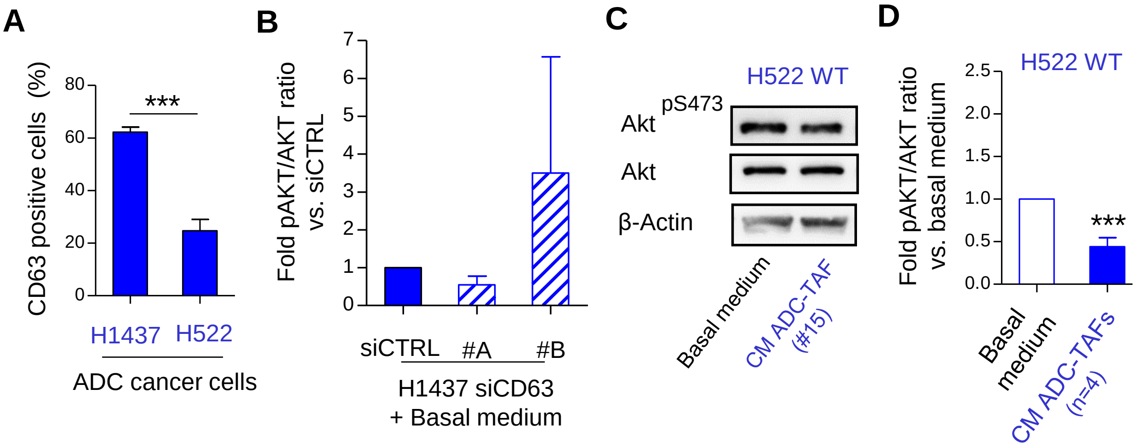

Figure 39. Akt activation in ADC cells depening on CD63 levels. A, Percentage of CD63 positive H1437 and H522 assessed by flow cytometry. **B**, Densitometry analysis expressed as fold (siCD63/siCTRL) of pAkt/Akt of siCD63 H1437 stimulated with basal medium (n=2). **C**, Representative Western blot for pAkt (pS473), Akt and β-Actin of H522 WT cultured as in Figure 38A. **D**, Densitometry analysis expressed as fold (conditioned medium/basal medium) of pAkt/Akt of H522 WT cultured as in (C) (n=4). Error bars indicate mean ± s.e.m. ***, $p < 0.005$ comparing with basal medium. All comparisons were done using Student *t*-test.

Next, Akt phosphorylation was evaluated in H1437 upon stimulation with CM of activated siTIMP-1 ADC-TAFs. Knocking-down stromal *TIMP1* consistently diminished pAkt expression in H1437 cells by both siRNA constructs, although this downregulation attained marginal significance in siTIMP-1#α (**Figure 40A-B**). These results underscore that the crosstalk between TIMP-1 and CD63 is potentially driving tumor progression through activation of the Akt signalling pathway in ADC cells.

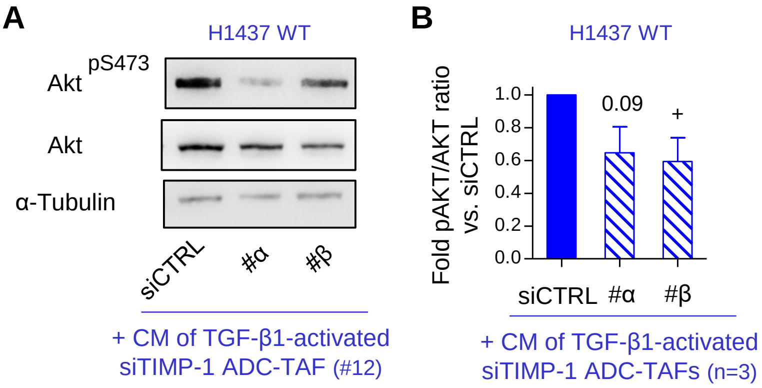

Figure 40. Effect of silencing TIMP-1 in TAFs on Akt activation of ADC cells A, Representative Western blot for pAkt (pS473), Akt and α-Tubulin of H1437 WT cultured as in Figure 38A. **D**, Densitometry analysis expressed as fold (conditioned medium/basal medium) of pAkt/Akt of H1437 WT cultured as in (A) (n=3). Error bars indicate mean ± s.e.m. +, $p < 0.05$ comparing siCTRL with siTIMP-1. All comparisons were done using Student *t*-test.

4. TIMP-1 SECRETED FROM LUNG ADC-TAFS ENHANCES INVASIVE GROWTH *IN VIVO*

Next, the tumor-promoting activity of stromal TIMP-1 was tested *in vivo*. To this aim, H1437 cells were co-injected subcutaneously with either activated siCTRL or siTIMP-1 ADC-TAF^{hTERT} (#37) into NOD/SCID mice, and tumor growth was monitored for 3 weeks (**Figure 41A**). This relatively short time window was used to minimize the expected contribution of host stromal cells at longer times [119]. We did not use shTIMP-1 ADC-TAF^{hTERT} owing to technical difficulties in expanding this cell population. Nonetheless, siTIMP-1 ADC-TAF^{hTERT} (#37) maintained a strong downregulation (>90%) of secreted TIMP-1 in culture throughout the experimental time window (**Figure 41B**). TAFs were pre-activated with TGF-β1 for 3 days before co-injection to mimic the profibrotic phenotype of TAFs found in patients. In agreement with cell culture observations, tumor growth was consistently lower in tumors co-injected with siTIMP-1 ADC-TAFs (**Figure 41C**) throughout the experimental time window and up to ~25% at the end of the observation period.

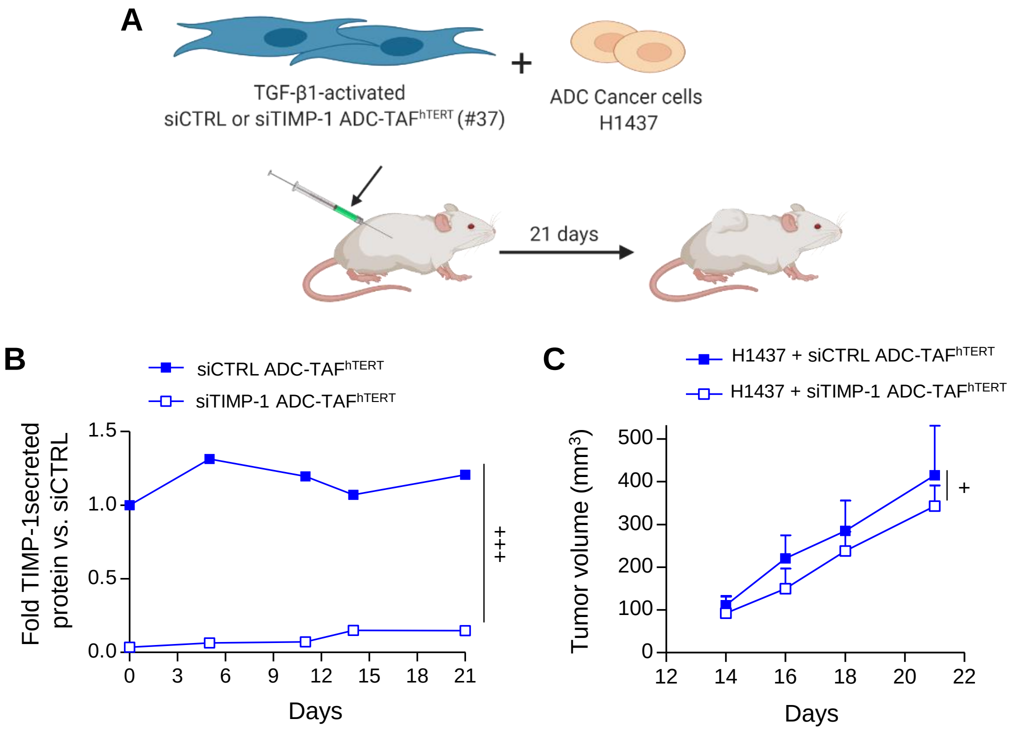

Figure 41. Tumor growth assessment in tumor xenografts bearing TIMP-1-less fibroblast. A, Outline of the experimental design used to assess tumor growth of H1437 cells subcutaneously co-injected with siCTRL or siTIMP-1#α ADC-TAF^{hTERT} (#37) (1:1 ratio) into immunodeficient NOD/SCID mice (n = 4 mice/condition). Fibroblasts were pre-activated with 2.5 ng/mL with TGF-β1 for 3 days before co-injection (drawings from Biorender). **B**, Fold TIMP-1 secretion of activated siTIMP-1#α ADC-TAF^{hTERT} (#37) with respect to siCTRL maintained for 21 days in serum-free medium. **C**, Average tumor growth for each experimental condition. Error bars indicate mean ± s.e.m. + < p 0.05; +++, $p < 0.005$ comparing siCTRL with siTIMP-1. Two-group comparisons within time-dependent TIMP-1 secretion or tumor volume data were performed with two-way ANOVA.

To further evaluate the role of stromal TIMP-1 in tumor aggressiveness, tumor budding in the histologic samples of tumor xenografts was examined as an histologic marker of invasion by analazing pan-cytokeratin staining (**Figure 42**). Tumor budding is defined as the presence of cancer cells, either as single cells or clusters of cells (pointed by black arrowheads in **Figure 42**), in the invasive front. We scored the invasion of tumor xenografts into their adjacent host tissue into 3 categories: 0 (negative), 1 (< 7 tumor nests, with a clear pseudocapsule), and 2 (≥ 7 tumor nests, usually without a clear pseudocapsule). The pseudocapsule corresponds to the reactive stromal host tissue that tends to encapsulate the tumor. Aggressive tumors lose this pseudocapsule, which enables finding tumor nests within the reactive adjacent connective tissue (pointed by yellow arrowheads in **Figure 42**) or even in contact or enclosing the muscle (pointed by green arrowheads in **Figure 42**).

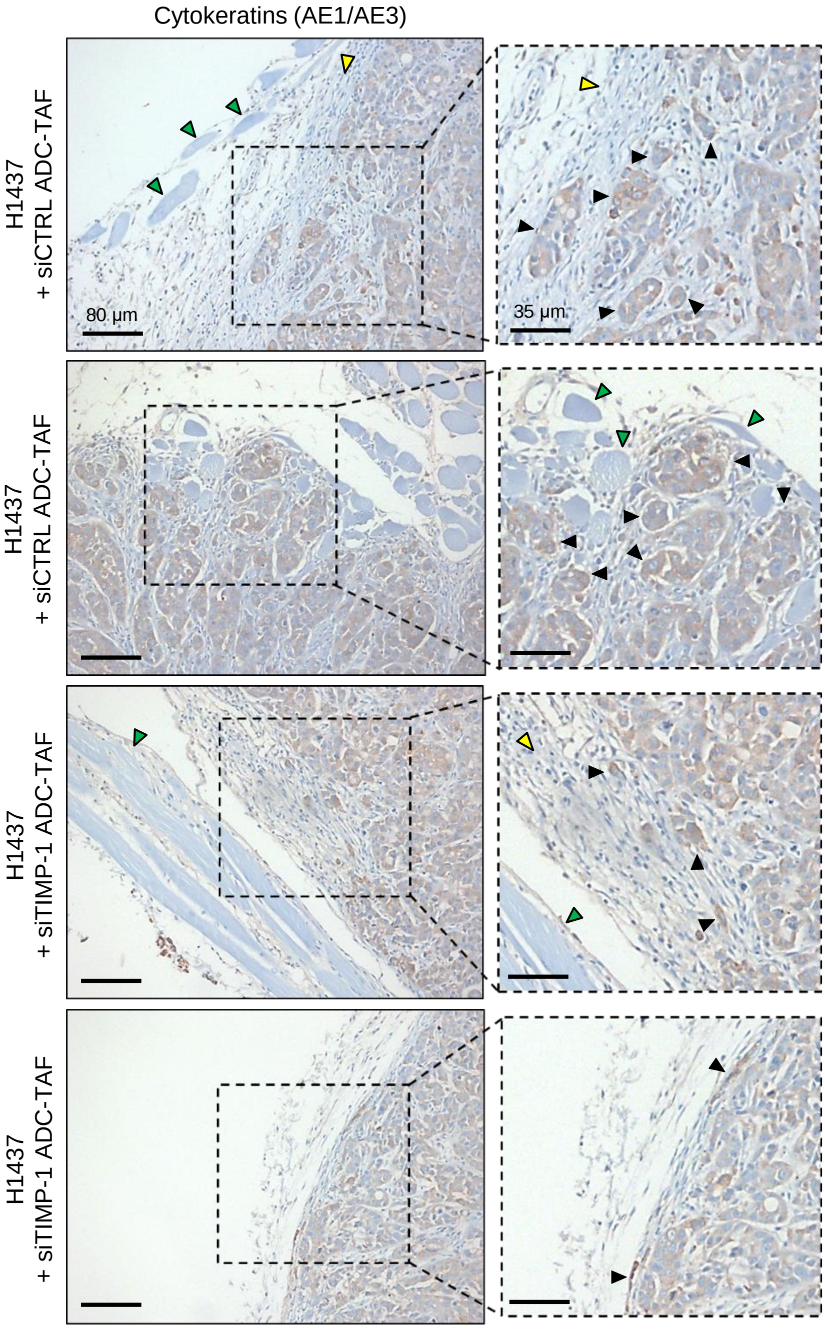
Cytokeratins (AE1/AE3)
H1437 + siCTRL ADC-TAF
H1437 + siCTRL ADC-TAF
H1437 + siTIMP-1 ADC-TAF
H1437 + siTIMP-1 ADC-TAF
80 µm
35 µm

Figure 42. Tumor budding into the adjacent host tissue. Representative images of the tumor edge of pan-cytokeratin staining with AE1/AE3. Black arrowheads indicate invasive tumor nests. Yellow arrowheads indicate the reactive connective tissue. Green arrowheads indicate the muscular tissue.

In agreement with the pro-invasive effects of stromal TIMP-1 elicited in culture, the frequency of tumor nests invading the adjacent host tissue (grade 2) was significantly reduced in tumors bearing siTIMP-1 ADC-TAFs compared to parental fibroblasts (**Figure 43A-B**).

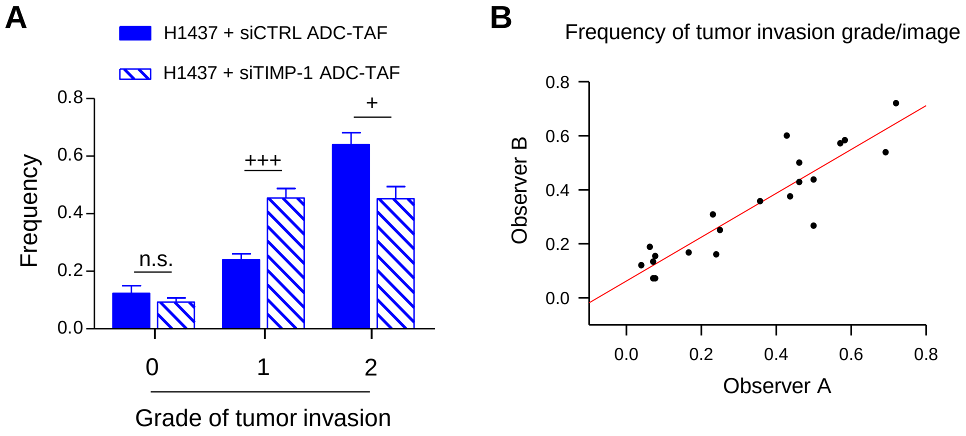

Figure 43. Grade of tumor invasion into the adjacent host tissue A, Frequencies of tumor invasion scores assessed from each AE1/AE3 staining image (10 images/tumor in average). **B**, Correlation between frequencies assessed from two observers shown. Error bars indicate mean ± s.e.m. +, $p < 0.05$; +++, $p < 0.005$ comparing siCTRL with siTIMP-1. n.s.: non-significant. All comparisons were conducted using Student *t*-test.

5. LACK OF TIMP-1 MEDIATES RESISTANCE TO NINTEDANIB *IN VITRO* AND *IN VIVO*

Nintedanib is an antifibrotic drug that has been clinically approved only for patients with advanced lung ADC due to the selective benefits observed in the LUME Lung-1 clinical trial in ADC but not SCC patients [19]. Remarkably, our group has recently reported that ADC-TAFs are more responsive to nintedanib than SCC-TAFs *in vitro*, owing to the large epigenetic repression of *SMAD3* in SCC-TAFs (**Figure 6**) [56]. Moreover, we also found that the selective effect of nintedanib in ADC involves both a secreted factor by TAFs and intrinsic features of ADC cells [37]. To assess whether the selective TIMP-1/CD63 crosstalk of ADC could underly the selective effect of nintedanib, *in vitro* and *in vivo* experiments were conducted as described below.

5.1. Nintedanib abrogates the pro-tumorigenic crosstalk between TIMP-1 from TAFs and CD63^{high} cells

First, the anti-tumor effects of nintedanib *in vitro* were assessed using the paracrine crosstalk model with the CM of activated ADC-TAFs treated with nintedanib on the CD63^{high} ADC cells (**Figure 44A**). ADC-TAFs treated with nintedanib failed to enhance the growth and invasion of both H1437 (**Figure 44B-C**) and H23 cells (**Figure 44D-E**) in comparison to the CM from non-treated ADC-TAFs, indicating that nintedanib treatment alters the composition of ADC-TAFs secretome, hindering its pro-tumoral activity. Moreover, the levels of CD63 on the H1437 membrane surface were checked after stimulation with CM of ADC-TAFs treated or not with nintedanib, and no difference was found (**Figure 44F**), thereby indicating that the anti-tumoral activity of nintedanib is not due to an alteration of CD63 levels on cancer cells.

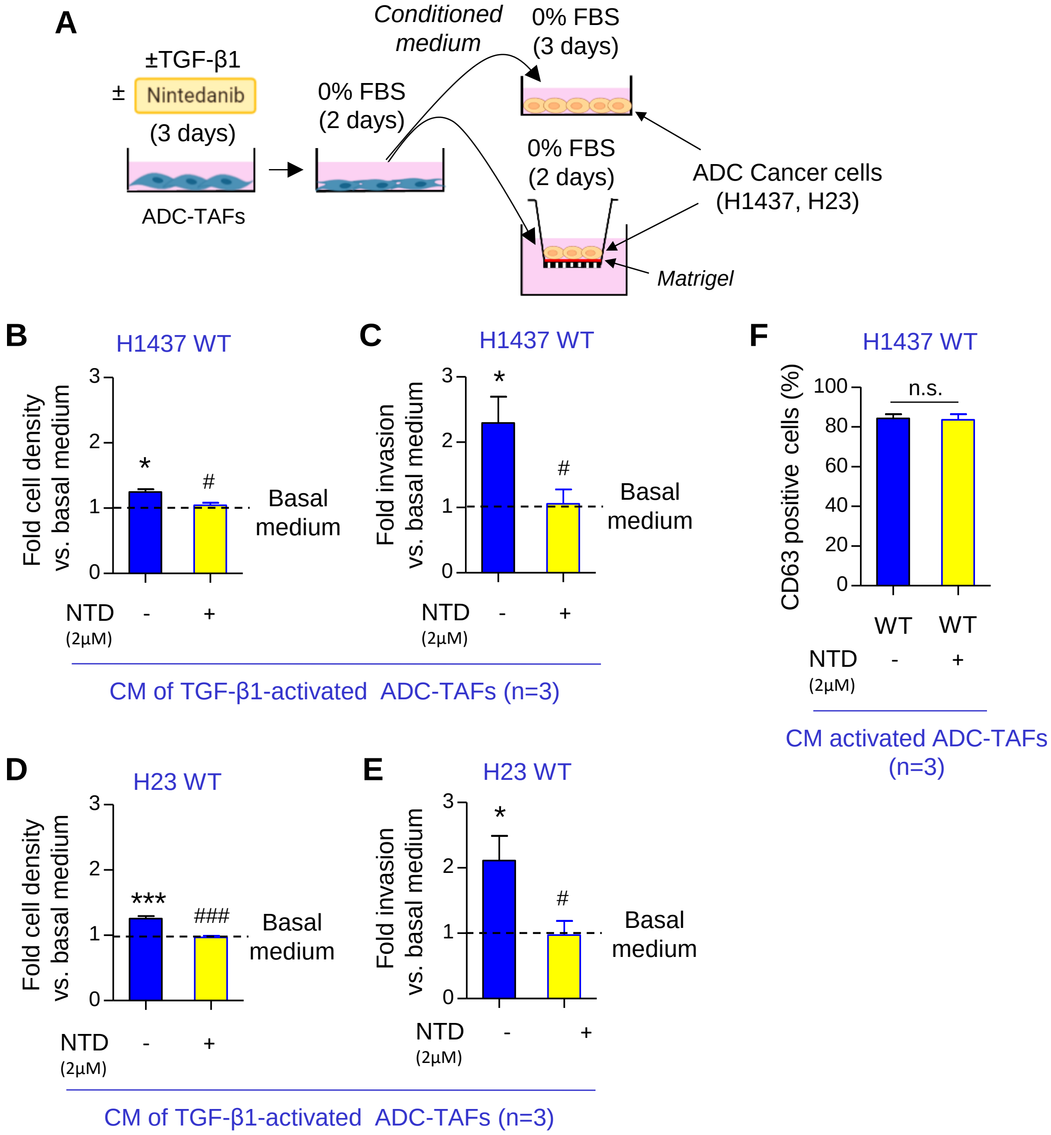

Figure 44. Anti-tumor effects of nintedanib *in vitro*. A, Outline of the experimental design used to assess growth (upper right) and invasion (bottom right) of ADC cancer cell lines stimulated with CM of ADC-TAFs activated with 2.5ng/mL TGF-β1 in the presence or absence of 2μM nintedanib (NTD) for 3 days and subsequently maintained in serum-free medium for 2 days. **B-C**, Fold cancer cell density (B) and invasion (C) of H1437 stimulated with the CM of ADC-TAFs cultured as in (A). **D-E**, Fold cancer cell density (D) and invasion (E) of H23 stimulated with the CM of ADC-TAFs cultured as in (A). **F**, Percentage of CD63 positive H1437 stimulated with the CM of ADC-TAFs cultured as in (A). Error bars indicate mean ± s.e.m. *, $p < 0.05$; ***, $p < 0.005$ comparing with the basal medium. #, $p < 0.05$; ###, $p < 0.005$; comparing nintedanib treatment with untreated condition. n.s.: non-significant. All comparisons were done using Student *t*-test.

5.2. Nintedanib markedly reduces TIMP-1 secretion in ADC-TAFs but not in SCC-TAFS

Based on the findings found in the previous chapter, we wondered whether the selective anti-tumoral effects of nintedanib in ADC are mediated by the inhibition of TIMP-1 secretion in TAFs. To evaluate the relationship between the antifibrotic drug and stromal TIMP-1, activated ADC and SCC-TAFs were treated with 2µM nintedanib, and we evaluated the impact on TIMP-1 expression and secretion. Nintedanib treatment significantly reduced *TIMP1* mRNA levels of both ADC and SCC-TAFs (**Figure 45A**). Nonetheless, nintedanib significantly inhibited TIMP-1 secretion specifically in ADC-TAFs (**Figure 45B**), supporting that TIMP-1 is one of the factors targeted by nintedanib that may underly the selective anti-tumoral effect of nintedanib in lung ADC.

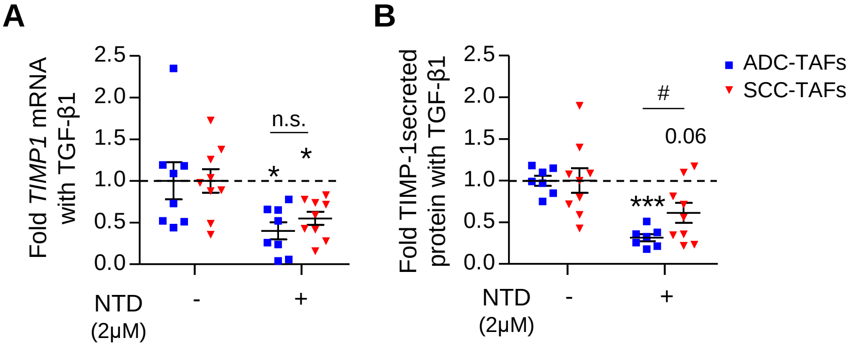

Figure 45. TIMP-1 expression and secretion in lung TAFs treated with nintedanib. A, Fold *TIMP1* mRNA expression of TAFs (8 ADC, 9 SCC) activated with 2.5ng/mL TGF-β1 in the presence or absence of 2µM nintedanib for 3 days. **B**, Fold TIMP-1 protein secretion of TAFs (7 ADC, 9 SCC) activated with 2.5ng/mL TGF-β1 in the presence or absence of 2µM nintedanib for 3 days and subsequently maintained in serum-free medium for 2 days. Error bars indicate mean ± s.e.m. *, $p < 0.05$; ***, $p < 0.005$ comparing with their respective untreated condition. #, $p < 0.05$; comparing ADC with SCC. n.s.: non-significant. All comparisons were done using Student *t*-test.

Remarkably, nintedanib reduced TIMP-1 secretion up to ~70% (**Figure 46A**) in ADC-TAFs without modifying their viability (**Figure 46B**), as assessed by determining the number of cells/mL at the end of the experiment.

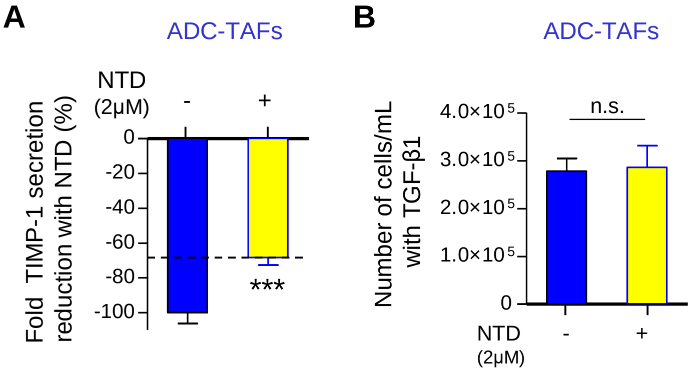

Figure 46. Reduction of TIMP-1 secretion with nintedanib in ADC-TAFs. A, Fold relative reduction in TIMP-1 secretion of ADC-TAFs (n=7) cultured as in Figure 45B. Fold relative reduction was computed as $100(E_{nintedanib} - E)/E$, where $E_{nintedanib}$ and E are the average secretion of TIMP-1 with or without the nintedanib, respectively. **B**, Number of cells/mL assessed with the Neubauer chamber after the collection of the CM. Error bars indicate mean ± s.e.m. ***, $p < 0.005$ comparing their respective untreated condition. n.s.: non-significant. All comparisons were done using Student *t*-test.

5.3. Nintedanib treatment inhibits pAkt stimulation with TAFs secretome only in CD63^{high} ADC cells

Next, the activation of Akt on either CD63^{high} or CD63^{low} ADC cells was checked using the CM from nintedanib treated ADC-TAFs. While pAkt activity significantly decreased by ~40% in H1437 stimulated with the secretome of activated ADC-TAFs pre-treated with nintedanib (**Figure 47A-B**), pAKT remained unchanged in CD63^{low} H522 ADC cells (**Figure 47C-D**). These results underscore that nintedanib treatment abrogates the pro-tumoral activation of the Akt pathway elicited by ADC-TAFs secretome in a CD63 dependent manner.

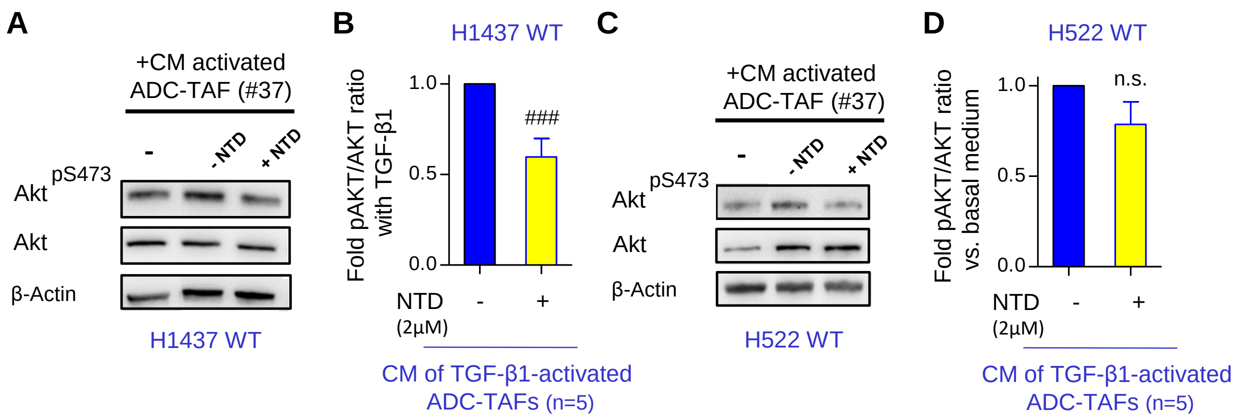

Figure 47. Effect of nintedanib treatment on Akt activation. A and **C**, Representative Western blots for pAkt (pS473), Akt and β-Actin of H1437 WT (A) and H522 WT (C) cultured as in Figure 38A. **B** and **D**, Densitometry analysis expressed as fold (conditioned medium/basal medium) of H1437 WT (B) and H522 WT (D) cultured as in (A) (n=4). Error bars indicate mean ± s.e.m. ###, $p < 0.005$; comparing nintedanib treatment with untreated condition. n.s.: non-significant. All comparisons were done using Student *t*-test.

5.4. SCC models show resistance to nintedanib *in vivo*

To further validate that the response to nintedanib in NSCLC is influenced by the specific TME of each histologic subtype, the anti-tumor effect of nintedanib was tested on 2 tumor xenograft models mimicking either ADC or SCC microenvironments using CD63^{high} (H1437) and CD63^{low} cells (H520) (**Figure 48**), respectively.

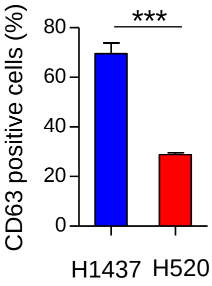

Figure 48. Percentage of CD63 positive H1437 and H520 assessed by flow cytometry. Error bars indicate mean ± s.e.m. ***, $p < 0.005$; comparing H1437 with H520. All comparisons were done using Student *t*-test.

For the ADC model, CD63^{high} H1437 cells were subcutaneously co-injected with activated ADC-TAF^{hTERT} (#37) into NOD/SCID mice and corresponding tumor growth was monitored for 3 weeks (**Figure 49A**). Alternatively, CD63^{low} SCC cell line, H520, was subcutaneously co-injected with activated SCC-TAF^{hTERT} (#20) into NOD/SCID mice and monitored tumor growth during the same time window (**Figure 49B**). TAFs were pre-activated with TGF-β1 for 3 days before co-injection to mimic the profibrotic phenotype of TAFs found in patients. 10 days after injection, tumor-bearing mice (size ≥ 50 mm^3) were treated with nintedanib or PBS for 11 days. Of note, nintedanib significantly reduced the tumor volume of H1437 co-injected with ADC-TAFs (**Figure 49C**) while it did not alter the tumor growth rate of H520 co-injected with SCC-TAFs (**Figure 49D**), in agreement with the resistance of SCC patients to nintedanib observed in the LUME Lung-1 clinical trial.

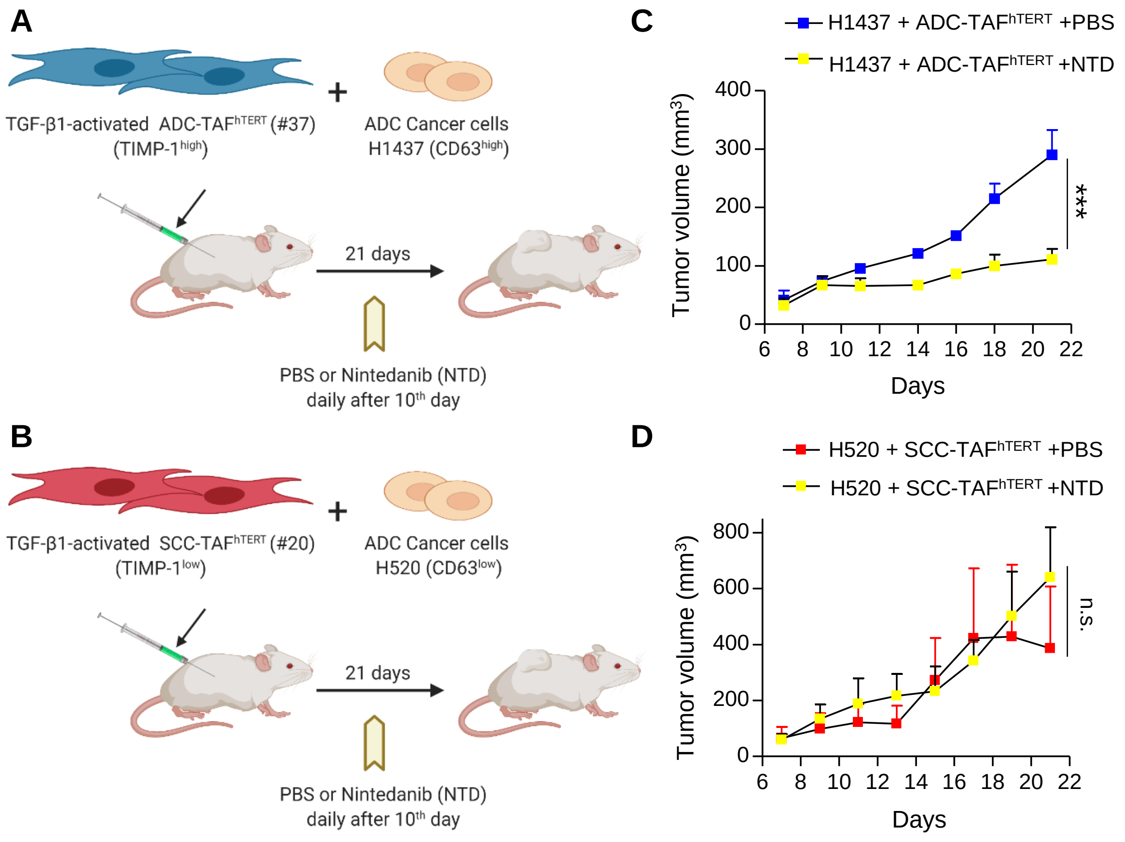

Figure 49. Specific anti-tumor effect of nintedanib in ADC *in vivo* models. **A**, Outline of the experimental design used to assess tumor growth of H1437 cells subcutaneously co-injected with ADC-TAF^{hTERT} (#37) (1:1 ratio) into immunodeficient NOD/SCID mice (n = 4 mice/condition). 10 days postinjection, mice were treated daily with nintedanib or PBS by oral gavage during 11 days. **B**, Outline of the experimental design used to assess tumor growth of H520 cells subcutaneously co-injected with SCC-TAF^{hTERT} (#20) (1:1 ratio) into immunodeficient NOD/SCID mice (n = 4 mice/condition). 10 days postinjection, mice were treated daily with nintedanib or PBS by oral gavage during 11 days. In both experiments, fibroblasts were pre-activated with 2.5 ng/mL with TGF-β1 for 3 days before co-injection (drawings from Biorender). **C** and **D**, Average tumor growth for each experimental condition in ADC model (C) and SCC model (D). Error bars indicate mean ± s.e.m. ***, $p < 0.005$ comparing PBS with nintedanib treatment. n.s.: non-significant. Two-group comparisons within time-dependent tumor volume data was performed with two-way ANOVA.

5.5. Knocking-down TIMP-1 secretion in ADC-TAFs abrogates the anti-tumor function of nintedanib *in vitro* and *in vivo*

Once determined that nintedanib selectively abrogates tumor growth of ADC-TAFs co-injected with ADC cells and TIMP-1 secretion in ADC-TAFs, the CM of siTIMP-1 ADC-TAFs treated with nintedanib was used in our crosstalk model (**Figure 50A**). The inhibition of growth and invasion in CD63^{high} ADC cells elicited by the CM from nintedanib treated ADC-TAFs was markedly reduced when stromal TIMP-1 secretion was knocked-down by siRNA (**Figure 50B-E**).

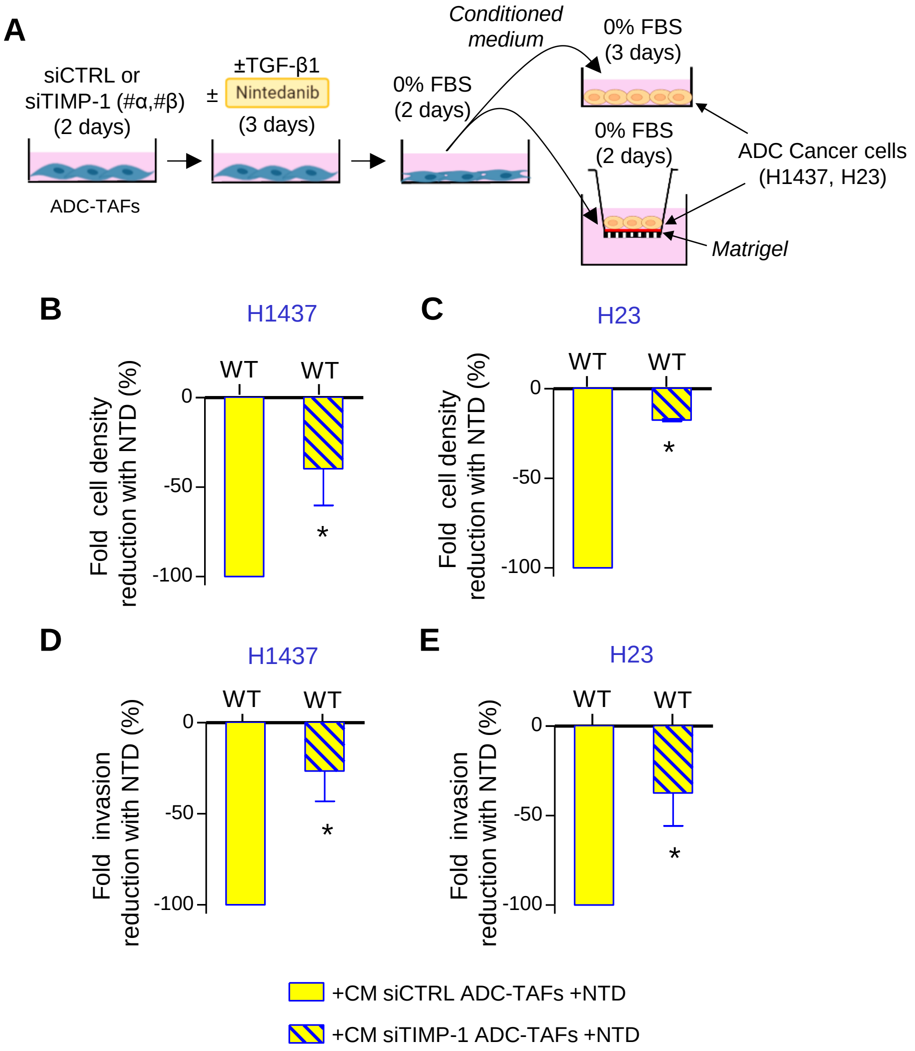

Figure 50. Role of TIMP-1 in the anticancer effects of nintedanib in ADC-TAFs *in vitro*. A, Outline of the experimental design used to assess growth (upper right) and invasion (bottom right) of ADC cancer cell lines stimulated with CM of siCTRL or siTIMP-1 ADC-TAFs activated with 2.5ng/mL TGF-β1 in the presence or absence of 2µM nintedanib (NTD) for 3 days and subsequently maintained in serum-free medium for 2 days. **B-E**, Fold relative reduction in growth and invasion of H1437 (B and D) and H23 (C and E) cultured as in (A). Fold relative reduction was computed as 100($E_{nintedanib}$ –E)/E, where $E_{nintedanib}$ and E are the average cell density or invasion with or without the nintedanib, respectively. Error bars indicate mean ± s.e.m. *, $p < 0.05$; comparing siCTRL with siTIMP-1. All comparisons were done using Student *t*-test.

To validate our observations *in vivo*, H1437 cells were subcutaneously co-injected with either activated siCTRL or siTIMP-1 ADC-TAF^{hTERT} (#37) into NOD/SCID mice, and tumor growth was monitored for 3 weeks (**Figure 51A**). TAFs were pre-activated with TGF-β1 for 3 days before co-injection to mimic the profibrotic phenotype of TAFs found in patients. 10 days after injection, tumor-bearing mice (size ≥ 50 mm^3) were treated with nintedanib or PBS daily for 11 days. In agreement with *in vitro* findings, nintedanib elicited a lower reduction of tumor growth in tumors bearing siTIMP-1 ADC-TAFs in comparison to siCTRL with marginal significance (**Figure 51B**). Altogether, these results show that fibroblasts deficient in TIMP-1 exhibit resistance *in vitro* and *in vivo* to the anti-tumor activity elicited by nintedanib treatment.

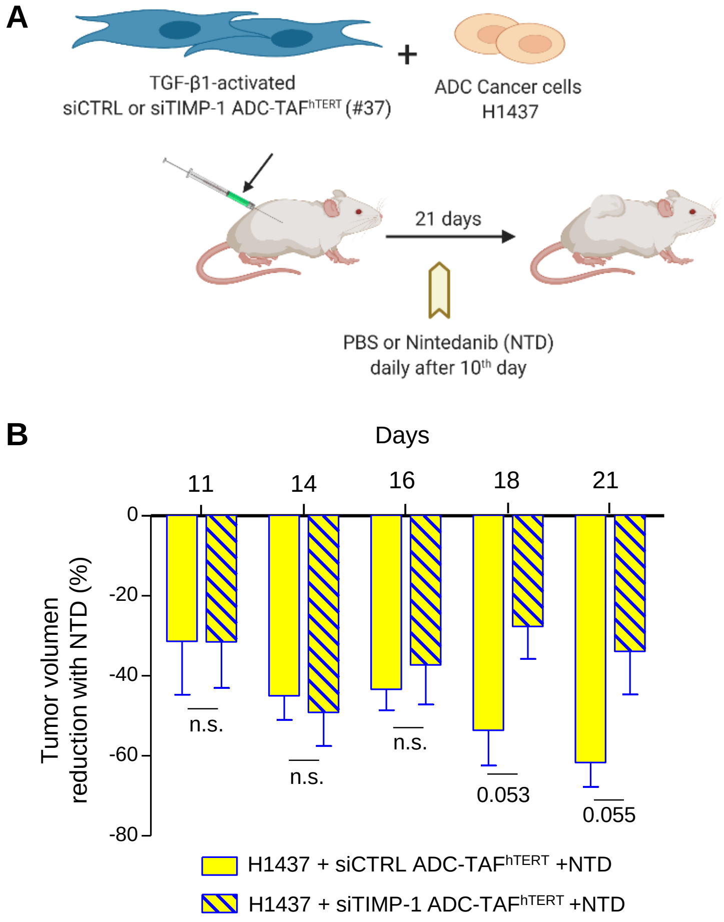

Figure 51. Role of TIMP-1 in the anticancer effects of nintedanib in ADC-TAFs *in vivo*. A, Outline of the experimental design used to assess tumor growth of H1437 cells subcutaneously co-injected with ADC-TAF^{hTERT} (#37) (1:1 ratio) into immunodeficient NOD/SCID mice (n = 4 mice/condition). 10 days postinjection, mice were treated daily with nintedanib or PBS by oral gavage during 11 days. Fibroblasts were pre-activated with 2.5 ng/mL with TGF-β1 for 3 days before co-injection (drawings from Biorender). **B**, Percentatge of the tumor volume reduction with nintedanib. Percentatge of reduction was computed as $100(E_{nintedanib} - E)/E$, where $E_{nintedanib}$ and E are the average tumor volume with or without the nintedanib, respectively. Error bars indicate mean ± s.e.m. All comparisons were done using Student *t*-test.

DISCUSSION

1. HISTOLOGIC SUBTYPE DEPENDENT EXPRESSION OF STROMAL TIMP-1 AND TUMORAL CD63 IN NSCLC

In the TME research field, it is widely recognized that tumoral and stromal composition varies considerably between lung cancer patients (intertumor heterogeneity) [15]. In addition to intertumor heterogeneity, the intratumor heterogeneity within the TME is becoming increasingly apparent. Of note, Lambrechts and colleagues identified 52 subtypes of stromal cells within lung tumors [17], including five distinct populations of fibroblasts, although the functional role of each population was not defined. Additionally, previous investigations of our group indicated that in each major NSCLC histologic subtype, ADC and SCC, there is a prevailing TAF phenotype [20, 37, 56]. Therefore, we hypothesized that the pro-tumoral secretome of lung TAFs might be different between ADC and SCC.

Aiming to identify specific heterotypic crosstalks between TAFs and cancer cells depending on the specific microenvironment of each histologic subtype, we studied the distribution of TIMP-1 and CD63 among ADC and SCC patients. In agreement with previous results reporting increased levels of TIMP-1 in ADC than in SCC [86, 99, 136], we found that *TIMP1* mRNA levels are larger in ADC compared to either SCC or control lungs.

The cellular source of TIMP-1 in NSCLC had remained unclear, with some studies favoring stromal while others tumoral expression [93, 94]. In our analyses, while *TIMP1* expression was similar between ADC and SCC cells, TIMP-1 secretion was significantly higher in ADC-TAFs compared to either ADC cells or SCC-TAFs. Therefore, our results indicate that TIMP-1 is expressed by both stromal and cancer cells but is overexpressed selectively in ADC-TAFs compared to SCC-TAFs.

Since the tumor stroma has an aberrant phenotype compared to the physiologic counterpart, comparing TAFs to paired CFs is relevant to determine the pathologic factors secreted within tumors. Of note, ADC-TAFs showed an aberrant secretion of TIMP-1 with respect to their matched CFs. Furthermore, the TGF-β transcription factor SMAD3, which is also upregulated in ADC-TAFs in comparison to paired CFs [56], has emerged as a relevant factor regulating TIMP-1 expression and secretion in lung fibroblasts and TAFs. Mechanistically, our results strongly support that the aberrant TIMP-1 overexpression in ADC-TAFs is driven by their hyperactive TGF-β1/SMAD3 profibrotic pathway recently reported by our group [56]. In contrast, the epigenetic repression of *SMAD3* caused by an excessive exposure to cigarette smoke particles, which leads to marked attenuation of the TGF-β/SMAD3 signaling pathway in SCC-TAFs, may potentially explain the unaltered secretion of TIMP-1 found in SCC-TAFs. Although testing this hypothesis was beyond the scope of this thesis, we could envision two complementary experiments to address this question. First, treating SCC-TAFs with a global DNA demethylating agent like 5-AZA, which inhibits the maintenance of DNA methyltransferase enzyme [137], should elicit an increased secretion of TIMP-1. Alternatively, it would be interesting to treat lung ADC-TAFs with cigarette smoke condensate, which has been reported to increase SMAD3 promoter methylation in lung fibroblasts *in vitro* [56] and assess TIMP-1 secretion. If the hypermethylation of the *SMAD3* promoter by cigarette smoke particles underlies the reduced secretion of TIMP-1 in SCC-TAFs, we should find a decrease in TIMP-1 secretion by ADC-TAFs after cigarette smoke condensate treatment.

Regarding CD63, the transmembrane protein that initiates signaling cascades after interacting with TIMP-1, our TCGA analysis revealed that *CD63* mRNA is upregulated in ADC compared to SCC. Intriguingly, SCC tissue had a reduced expression of *CD63* than paired control lungs, whereas its levels were similar between ADC and control tissue. Although the downregulation of CD63 in SCC remains poorly understood, it has been speculated to be related to the cellular origin. Since CD63 is found in alveolar type II cells under physiologic conditions [138, 139], it is conceivable that CD63 is maintained in ADC cells, which generally arise from alveolar type II cells. In contrast, SCC tumors typically arise from basal cells that are negative for CD63 [3, 140]. Nonetheless, the potential effects of low CD63 in SCC remain undefined.

In agreement with our data obtained by analyzing CD63 staining in lung tumors, Kwon and colleagues found that SCC patients showed a consistent low expression of CD63, whereas ADC showed a diverse range of CD63 positivity [140]. Furthermore, it is worth mentioning that this work observed that CD63 negativity in ADC was associated with low survival only in early stages (stages I and II), suggesting that CD63 can perform different functions along with tumor progression. However, this study did not evaluate the underlying mechanism of CD63 loss in some ADC patients nor the role of CD63 in cancer progression [140]. The role of CD63 in cancer cell-autonomous processes is addressed in the next section of the discussion.

Overall, the results of this thesis unveil a differential expression pattern for TIMP-1 and its cell surface partner, CD63, in the two main NSCLC subtypes. ADC-TAFs show an aberrant secretion of TIMP-1, whereas CD63 positive cells are mainly found in ADC. We propose that stromal TIMP-1 drives a specific crosstalk in lung ADC by interacting with CD63. In further support to this hypothesis, the mRNA levels of the natural competitor of CD63, *MMP9* [103], were strongly downregulated in ADC compared to SCC tumors, revealing that ADC tumors are potentially more primed to exhibit free TIMP-1 that can interact with CD63 expressing cancer cells (**Figure 9**). However, the availability of free TIMP-1 (unbound to proMMP-9) depends on other multiple factors [89] that have not been addressed in this thesis.

2. TIMP-1 IS AN ESSENTIAL SECRETED FACTOR IN THE ABERRANT CROSSTALK BETWEEN TAFs AND CD63^{high} CANCER CELLS IN LUNG ADC

Defining TIMP-1 function in cancer has been a subject of intense research. Although emerging evidence indicates cell-context-dependent roles for TIMP-1 in different tumors [89], the vast majority of studies have evaluated the role of endogenous TIMP-1 on cancer cells behavior [79, 99]. Since TIMP-1 is overproduced by ADC-TAFs and ADC patients are positive for CD63, it is reasonable to expect stromal TIMP-1 interacting with CD63 in cancer cells in the TME of lung ADC patients. Therefore, here we assessed the role of such crosstalk in lung ADC progression.

As we had previously established that the secretome of ADC-TAFs promoted the proliferation and invasion of ADC cells, we studied the response of CD63^{high} ADC cells to the CM after silencing TIMP-1 in ADC-TAFs. Altogether our *in vitro* data revealed that TIMP-1 secreted by ADC-TAFs promotes cancer cell growth and invasion concomitantly with Akt activation in ADC cells. In addition, we found that CD63 expression in ADC cells is required to convey the tumor-promoting effects of TIMP-1. However, whether the interaction between stromal TIMP-1 and CD63 in cancer cells is direct or indirect needs to be further determined; considering the large interactome of TIMP-1 (**Figure 8**), we cannot rule out the presence of other factors influencing this crosstalk. In addition, CD63 generally forms tetraspanin-enriched microdomains with multiple membrane proteins such as integrins and other receptors, which may indirectly mediate the activation of signaling pathways following TIMP-1 and CD63 interaction [79, 141].

In agreement with our *in vitro* data, stromal TIMP-1 emerged as a crucial factor promoting an invasive growth of ADC-based tumor xenografts. Of note, the characteristic pattern of invasive growth is associated with more aggressive tumors in the clinic; therefore, our data is consistent with the association between high TIMP-1 and poor outcome, and supports a causal relationship. To further investigate the role of ADC-TAFs in boosting an invasive growth of lung ADC, it would be interesting to assess the tumor budding in tumor xenografts of ADC cells injected alone or co-injected either with CFs or ADC-TAFs.

It is relevant that we obtained equivalent results *in vitro* and *in vivo* because several investigations observed an opposite activity of TIMP-1 *in vivo* to that found using cell-free *in vitro* systems, illustrating the complexity of studying TIMP-1 and further underscoring that TIMP-1 functions are highly context-dependent [89]. Considering that the tumor xenograft model developed during this thesis is a representative model of the holistic functions of stromal TIMP-1 within the TME of ADC, additional histochemical analyses of this model can generate relevant information regarding the influence of stromal TIMP-1 in the TME. Since TIMP-1 harbors anti-apoptotic activity [78, 79, 102] and can influence cells of the TME in addition to cancer cells [80], including endothelial cells [142], it would be interesting to compare apoptosis and angiogenesis levels between those tumors bearing parental ADC-TAFs and ADC-TAFs silenced for TIMP-1.

Notably, TIMP-1 was initially considered to be detrimental for cancer cell invasion because it is a natural inhibitor of several MMPs. Hence, our results showing that TIMP-1 from TAFs is necessary to promote cancer cell invasion *in vitro* and *in vivo* point that stromal TIMP-1 is primed for acting through its cytokine-like functions rather than MMP-inhibitory functions, particularly in ADC. In addition to the elevated concentration of TIMP-1 within the secretome of ADC-TAFs, its molecular composition may be another key aspect favoring such cytokine-like signaling activity. In this scenario, different possibilities are conceivable to explain our observations. First, since TIMP-1 bound to proMMP-9 is unable to promote cell signaling through CD63 binding, and *MMP9* is downregulated in ADC compared to SCC, our results support that there is more free TIMP-1 (proMMP9-unbound) in ADC. However, it is worth mentioning that some cell types secrete TIMP-1 already bound to proMMP-9 [143]. Thus, it would be interesting to study the differential content of the TIMP-1-proMMP-9 complex in the CM of ADC and SCC-TAFs. Second, the glycosylation status can also alter the function of TIMP-1 since aberrant glycosylated TIMP-1 has a weaker affinity for some metalloproteinases [144, 145]. Although under physiologic conditions, TIMP-1 harbors two glycosylation sites in the N-terminal domain [102, 146], little is known about the glycosylation status of TIMP-1 in pathologic conditions [147]. Moreover, it remains to be established whether the glycosylation status of TIMP-1 in TAFs may be characteristic of each histologic subtype.

Overall our results support that, at least in lung ADC, TIMP-1 overexpression identifies a population of TAFs with pro-tumoral functions. In contrast, the effects of stromal TIMP-

1 in SCC remain ill defined. If we compare *CD63*, *MMP9*, and *TIMP1* mRNA levels between ADC and SCC, we can hypothesize that in the TME of SCC, the availability of free TIMP-1 may be lower in comparison to ADC. In this context, TIMP-1 secreted from SCC-TAFs is likely to mainly inhibit the proteolytic degradation of the ECM (**Figure 9**) [89]. However, it is becoming apparent that the antiproteolytic functions of TIMP-1 cannot be intrinsically considered tumor-suppressive. Indeed, the role of MMPs in cancer progression is more complicated than simply degrading the ECM since MMPs can interfere with tumoral signaling by cleaving cytokines [148, 149]. Alternatively, a previous study on TIMPless fibroblasts reported a tumor-promoting phenotype through the aberrant secretion of exosomes and the enhanced induction of epithelial-mesenchymal transition [150], which could apply to the low TIMP-1 conditions of SCC reported here.

On the other hand, the role of CD63 in tumor progression independently of TIMP-1 interaction has not been fully elucidated but seems to be protective rather than promoting [151]. In agreement with our observation that TIMP-1 signaling through CD63 is crucial for cancer cell invasion, genetic manipulation of CD63 in cancer cells altered the invasion capacity of cancer cells. However, CD63 itself appears to be inhibitory for the invasion of melanoma cells [152]. This effect correlates with our observation that in basal conditions silencing CD63 increased the invasive capacity of H23 with one of the siRNA constructs (**Figure 32D**). Moreover, the above-mentioned association of low CD63 expression with bad prognosis in NSCLC could be explained by a potential protective role of CD63 [140]. Although we have underscored that CD63 and downstream Akt signaling elicits the pro-tumoral activity of TIMP-1, it remains to be established what cues are involved in CD63 signaling in the absence of TIMP-1. Therefore we propose that CD63 needs to be studied taking into consideration its potential interaction with TIMP-1, depending on the expression pattern of both proteins in each cancer type.

Finally, since the elevated expression of TIMP-1 is associated with a bad prognosis in several cancers, it is tempting to speculate that similar aberrant crosstalk may drive tumor progression in other tumors, particularly in those with CD63^{high} cells.

3. LIMITED TIMP-1 IN SCC-TAFs ELICITS RESISTANCE TO NINTEDANIB

The implication of the stroma, particularly TAFs, in the patient response to anti-cancer therapies is increasingly recognized. Some of the TAF-dependent resistance mechanisms that have been described are limiting drug access, interfering with chemotherapy and radiotherapy by providing pro-survival factors, and hindering immunotherapy by secreting immunomodulatory factors [71]. Alternatively, the TME heterogeneity of lung tumors [17] may underlie the different efficacy observed with drugs targeting the TME in lung cancer as immunotherapy, bevacizumab, and nintedanib. Because it is unlikely that these treatments would be effective for all patients with lung cancer, we need to find accurate biomarkers of the response of patients to improve their outcomes [15].

In the case of nintedanib, we hypothesize that the diverse TAF phenotypes may underlie the different responses found in NSCLC. Hence, our data provide new mechanistic insights on the selective efficacy of nintedanib in lung ADC [19]. Silencing ADC-TAF-derived TIMP-1 consistently reduced the response to nintedanib both in our *in vitro* and *in vivo* models, illustrating that this antifibrotic drug inhibits TIMP-1 secretion in ADC-TAFs, thereby abrogating their TIMP-1-dependent pro-tumoral paracrine signaling with cancer cells. In this scenario, the resistance mechanism to nintedanib specifically observed in SCC-TAFs [37] can be explained, at least in part, by their reduced secretion of TIMP-1. Moreover, these results underscore that SCC-TAFs are less responsive to antifibrotic treatments like nintedanib due to the epigenetic repression of SMAD3 in SCC-TAFs since SMAD3 is a crucial regulator of TIMP-1 expression and secretion.

However, the lack of stromal TIMP-1 did not fully abrogate the anti-tumor effects of nintedanib, indicating that other pro-tumoral factors are targeted by this drug. In TAFs from intrahepatic cholangiocarcinoma nintedanib hindered interleukin-6 and interleukin-8 [69]. Nonetheless, in lung TAFs, the identity of other TAF-derived pro-tumoral factors that may be inhibited by nintedanib remains unknown.

Although the role of CD63 in the response to nintedanib has not been fully elucidated, it is remarkable that nintedanib treatment abrogated the activation of Akt elicited by the secretome of TAFs exclusively in ADC cells with elevated levels of CD63. Therefore, we propose that both TIMP-1 and CD63 should be evaluated as candidate predictive biomarkers for the positive response to nintedanib. As a proof-of-concept, TIMP-1 and CD63 levels could be retrospectively analyzed in patients treated with nintedanib to evaluate whether high TIMP-1 and high CD63 correlate with better outcomes.

Another translationally-relevant aspect of our data is the identification of a subset of lung ADC patients, those expressing high levels of TIMP-1 and CD63, as clinically important. In support of this interpretation, it has been observed that upregulated TIMP-1 mediates resistance to tyrosine kinase inhibitors in PDAC [153]. Therefore, the TIMP-1/CD63 pro-tumoral axis here described might be implicated in the resistance mechanism to targeted therapies in lung and other cancer types. If lung ADC patients with elevated TIMP-1 and CD63 levels show increased resistance to targeted therapies, it would be interesting to evaluate the possibility of using targeted therapies together with nintedanib as a tumor-stroma-targeting strategy in this subset of patients.

Alternatively, the crosstalk between TIMP-1 from TAFs and CD63 in cancer cells might be targeted using other approaches rather than nintedanib. Since TIMP-1 is a multifunctional protein, we propose that antibodies neutralizing specifically its C-terminal domain, the one harboring cytokine-like functions, would disrupt the interaction with CD63 interfering thus the pro-tumoral paracrine signaling. However, to our knowledge, such neutralizing antibodies are not available yet.

Moreover, our data support that drugs targeting the pro-tumoral crosstalk between TAFs and cancer cells rather than eliminating TAFs may be a suitable approach limiting the tumor supportive microenvironment.

4. IMPLICATION OF THE TIMP-1/CD63 AXIS IN OTHER PULMONARY DISEASES

Idiopathic pulmonary fibrosis (IPF) and lung ADC are two pulmonary diseases sharing some key biological characteristics. In IPF patients, fibrotic lesions commonly appear in the distal lung, similar to the usual location of ADC [3, 154]. Moreover, nintedanib treatment is approved for both diseases [19, 65]. To initially examine whether a similar mechanism of action of nintedanib could be occurring both in IPF and in lung ADC, we assessed the mRNA expression of *TIMP1* and *CD63* in IPF patients using publicly available databases. Interestingly, the expression of both *TIMP1* and *CD63* is significantly higher in IPF lungs compared to healthy lungs (**Figure 52**).

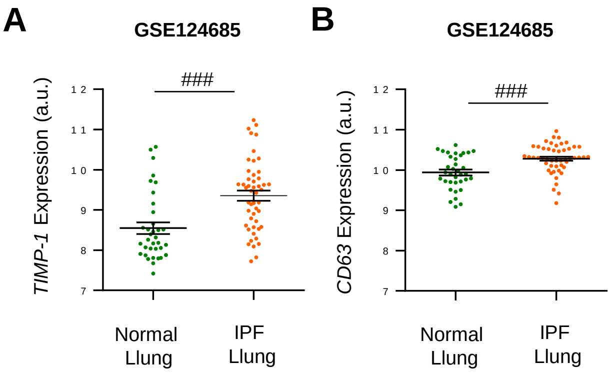

Figure 52. Expression of *TIMP1* and *CD63* in IPF. A-B, RNA-seq data of *TIMP1* (A) and *CD63* (B) mRNA in normal and IPF lung (35 normal, 49 IPF). Error bars represent mean ± s.e.m. ###, $p < 0.005$ comparing normal with IPF. Statistical comparisons were done using Mann Whitney test.

Based on these results, it is tempting to speculate that TIMP-1 and CD63 are potentially involved in the beneficial effect of nintedanib in IPF patients. Moreover, these results underscore our hypothesis that TIMP-1 and CD63 could be predictive biomarkers of positive response to nintedanib.

5. EMERGING MODEL: TGF-β1/SMAD3 pathway drives a tumor-promoting TAF-carcinoma crosstalk in ADC through TIMP-1/CD63 that is inhibited by nintedanib

A major challenge addressed in this work has been to define how a complex and controversial protein like TIMP-1 acts in the specific TME of lung ADC patients where there is an aberrant secretion of TAF-derived TIMP-1 and abundant ADC cells positive for CD63. Moreover, our results underscore that the crosstalk between TIMP-1 from TAFs and CD63 in cancer cells is a novel potential therapeutic target. The model emerging from this work shows that nintedanib inhibits the secretion of TIMP-1 in hyperactivated ADC-TAFs (through high TGF-β1/SMAD3), hindering the TIMP-1/CD63 pro-tumoral axis in lung ADC (**Figure 53**).

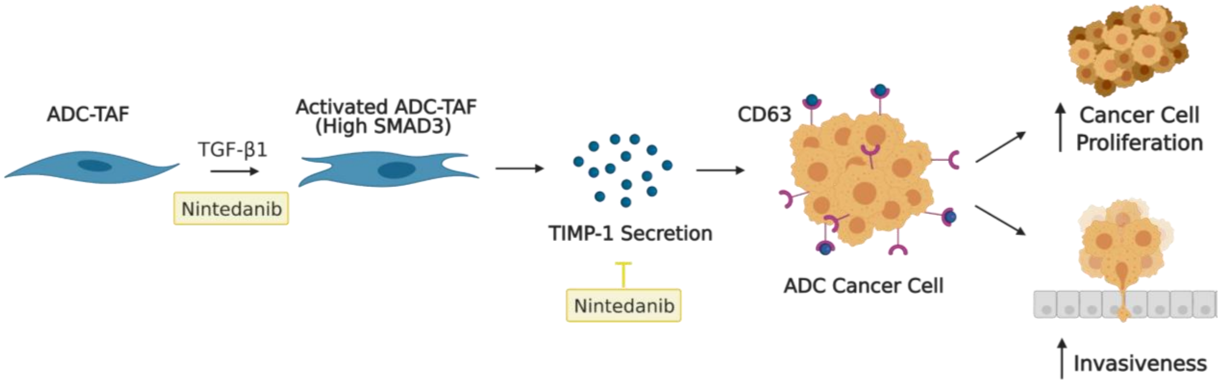
ADC-TAF
TGF-β1
Nintedanib
Activated ADC-TAF (High SMAD3)
TIMP-1 Secretion
Nintedanib
CD63
ADC Cancer Cell
↑ Cancer Cell Proliferation
↑ Invasiveness

Figure 53. Emerging model of the tumor-promoting role of the aberrant SMAD3/TIMP-1 expression of ADC-TAFs with CD63 expressing ADC cells that is inhibited by nintedanib. Drawings from Biorender.

CONCLUSIONS

1. There is a higher expression of TIMP-1 and CD63 in patients with lung ADC than in patients with lung SCC. This expression pattern is the consequence of excessive expression and secretion of TIMP-1 in ADC-TAFs and the loss of CD63 expression in the cancer cells of SCC patients.

2. TGF-β1 promotes TIMP-1 expression and secretion through the transcription factor SMAD3 in lung fibroblasts and TAFs. Moreover, the aberrant hyperactivation of the TGF-β1/SMAD3 fibrotic pathway underlies the excessive secretion of TIMP-1 in lung ADC-TAFs.

3. We unveil for the first time a pro-tumoral paracrine signaling between TAFs and cancers cells occurring specifically in lung ADC patients. In this crosstalk, the interaction between TIMP-1 from ADC-TAFs and CD63 in cancer cells promotes proliferation and invasion of lung ADC cells concomitantly with Akt activation.

4. TIMP-1 secreted by ADC-TAFs is necessary to promote invasive tumoral growth of an ADC cell line *in vivo*.

5. Our results provide compelling evidence that the low levels of TIMP-1 and CD63 characteristic of patients with lung SCC are major contributors to the selective resistance of SCC patients to nintedanib.

SCIENTIFIC ACTIVITY

PUBLICATIONS

P. Duch, N. Díaz-Valdivia, R. Ikemori, M. Gabasa, E.S. Radisky, M. Arshakyan, S. Gea-Sorlí, A. Mateu-Bosch, P. Bragado, H. Mori, J. Ramírez, C. Teixidó, N. Reguart, C.Fillat, D. Radisky, J. Alcaraz. Aberrant TIMP-1 overexpression in tumor-associated fibroblasts drives tumor progression through CD63 in lung adenocarcinoma. (Under revision in Matrix Biology)

M. Gabasa, E.S. Radisky, R. Ikemori, G. Bertolini, M. Arshakyan, A. Hockla, **P. Duch**, O. Rondinone, A. Llorente, M. Maqueda, A. Davalos, E. Gavilán, A. Perera, J. Ramírez, P. Gascón, N. Reguart, L. Roz, D.C. Radisky, J. Alcaraz. MMP1 drives tumor progression in large cell carcinoma of the lung through fibroblast senescence. Cancer Letters, **2021**, 507:1-12. [IF: 8.679, Q1].

R. Ikemori, M. Gabasa, **P. Duch**, M. Vizoso, P. Bragado, M. Arshakyan, I.C. Luis, A. Marín, S. Morán, M. Castro, G. Fuster, S. Gea-Sorli, T. Jauset, L. Soucek, L.M. Montuenga, M. Esteller, E. Monso, V.I. Peinado, P. Gascon, C. Fillat, F. Hilberg, N. Reguart, J. Alcaraz. Epigenetic SMAD3 repression in tumor-associated fibroblasts impairs fibrosis and response to the antifibrotic drug nintedanib in lung squamous cell carcinoma. *Cancer Res.* **2020**, 80(2):276-290 [IF: 12.701, Q1].

L. Sala, H. Franco-Valls, J. Stanisavljevic, J. Curto, J. Vergés, R. Peña, **P. Duch**, J. Alcaraz, A. García de Herreros, J. Baulida. Abrogation of myofibroblast activities in metastasis and fibrosis by methyltrasnferase inhibition. *Int J Cancer*. **2019**, 145(11): 3064-3077 [IF: 4.982, Q1].

I. Almendros, H. Alsafadi, D. Bolukbas, J. Collins, **P. Duch**, E. Garrido-Martin, N. Kahn, T. Karampitsakos, I. Persson, A. Tzouvelekis, F. Uhl, S. Bartel. Early Career Members at the LSC: Cell-matrix interactions in lung disease and regeneration. Breathe, **2018**, 14(2), e78-e83 [IF: 0.7].

A. Giménez, **P. Duch**, M. Puig, M. Gabasa, A. Xaubet, J. Alcaraz. Dysregulated Collagen Homeostasis by Matrix Stiffening and TGF-β1 in Fibroblasts from Idiopathic Pulmonary Fibrosis Patients: Role of FAK/Akt. *Int J Mol Sci.* **2017**, 18(11), 2431 [IF: 3.226, Q2]

M. Gabasa, **P. Duch**, I. Jorba, A. Giménez, R. Lugo, I. Pavelescu, F. Rodríguez-Pascual, M. Molina-Molina, A. Xaubet, J. Pereda, J. Alcaraz. Epithelial contribution to the profibrotic stiff microenvironment and myofibroblast population in lung fibrosis. *Mol Biol Cell*. **2017**, 28(26):3741-3755 [IF: 3.685, Q2].

ANNEX

A1. Viral transduction of immortalized fibroblasts

1. Introduction

This is the optimized protocol for stably SMAD3 knockdown and knockin of immortalized fibroblasts. For the knockdown, we worked with lentiviral shRNA mission plasmids (Sigma); for the knockin, we used retroviral plasmids from Addgene.

This protocol includes 3 parts: bacteria growing (bacteria containing plasmids needed to be expanded before use), viral production, and fibroblasts transduction. For technical reasons, the bacteria growing and viral production are done in the lab of Cristina Fillat (CEK).

2. Material and reagents

MATERIAL	COMPANY AND Cat#	LOCATION
shSMAD3 – TRCN 0000330128	Sigma (shRNA Mission)	-80°C Freezer
SCH002 – shRNA control (mammalian control)	Sigma (shRNA Mission)	-80°C Freezer
rv-SMAD3 (#12638)	Addgene	-80°C Freezer
rv-GFP (#65436)	Addgene	-80°C Freezer
Erlenmeyer shakers		Fillat's lab
Autoclaved Erlenmeyer		Fillat's lab
Autoclaved LB medium		Fillat's lab
Alcohol burner		Fillat's lab
Maxiprep kit	QIAGEN, #12162	Fillat's lab
CalPhos mammalian Transfection Kit	TakaraBio	Fillat's lab
Puromycin	Gibco, #A11138-03	-20°C Freezer
Polybrene	Sigma	-20°C Freezer
Fibroblast culture medium (DMEM based)	Gibco	Fridge

3. Procedure

1. Prepare the bacteria growing medium in Erlenmeyers doing everything in around a fire source (including pipette tips): 250 ml of Maxiprep (1 ml ampicilin 100 mg/ml for 1000 ml of LB medium – final concentration of 100 ug/ml – antibiotics should be added after sterilization and in a temperature lower than 50oC).
2. Fire heat the tweezers and get a small amount of bacteria and drop it in the LB medium (900 ml water, 10 g Bacto tryptome, 5 g yeast extract, 10 g NaCl) and keep it in Erlenmeyer shakers overnight 37oC.
3. The next day, freeze bacteria after growth to have a stock (800ul bacteria + 200ul glycerol) and use the Maxiprep QIAGEN kit as described by the manufacturer to extract the plasmid.
4. Measure the final DNA concentration of the extracted plasmid in the nanodrop.

5. Use HEK293T for lentivirus production and Phoenix 293T for retrovirus production. Maintain 293T cells in DMEM high glucose medium with L-glutamine in 10 cm tissue culture dishes. Do not use 293T cells that are in culture for more than 30 passages.
6. Seed the cells for transfection. Ideally cells should be ~80% confluent on the day of transfection.
7. Two hours before transfection, replace the medium with 10 ml of fresh DMEM medium preheated at 37°C.

Plasmids cotransfection procedure for viral production

In this step we cotransfect 293T cells with our plasmid of interest together with the plasmids encoding vector components (kindly provided by Cristina Fillat) using the CalPhos mammalian Transfection Kit.

For ONE (1) 10 cm plate to be transfected, prepare the following transfection mix in a sterile 15 ml conical tube.

Lentiviral production	**Retroviral production**
9.8 µg transfer vector plasmid (the shSMAD3 or control plasmids)	10 µg transfer vector plasmid (the rv-SMAD3 or rv-GFP plasmids)
3.4 µg pMD2G (VSVG)	
6.3 µg p8.91 (gag/rev/pol)	
87 µL CalPhos	87 µL CalPhos
Adjust with sterile water to obtain a final volume of **700 µL**	Adjust with sterile water to obtain a final volume of **700 µL**

1. Add to the tube 700 ul of HBSS 2X concentrated VERY SLOWLY UNDER AGITATION USING A VORTEX (this is done to increase air entry in solution while CalPhos and plasmids make a complex)
2. Leave the precipitate at room temperature for at least 15 min but do not exceed 30 min (DO NOT TOUCH IT OR MOVE IT, IT HAS TO STAND STILL)
3. Add to the cell little by little 1500 ul/dish of precipitate from step 1. Mix by gentle swirling until the medium has recovered a uniform red color. Incubate overnight.
4. Medium needs to be changed within approximately 16h of addition of the DNA, then aspirate the medium and slowly add 10 ml of fresh DMEM, prewarmed to 37°C. From that moment transfected 293T cells will produce virus with our plasmid of interest. To obtain the virus we will harvest the culture medium of the virus producer cells.
5. If fluorescent reporter is encoded in the vector plasmid, we can check for transfection efficiency under microscope. As a transfection control, we recommend always testing the reagents with a test transfection of a GFP encoding lentiviral vector.
6. After 24 h of media change, harvest the culture medium from each plate to a 50 ml centrifuge tube and keep it at 4ºC. Add another 10 ml to the plates for more 24 h.

7. The next day, harvest again the culture medium from each plate and add it to the 50 ml centrifuge tubes from step 6 kept at 4ºC. Centrifuge 5 min at 2000 rpm at 4°C to pellet detached cells and debris.
8. Filter the pooled supernatant using a 0.45 µm filter unit.
9. Aliquot virus in 2 ml tubes and keep them at -80oC. Virus lose effectiveness in each freeze-thaw cycle, so avoid it.

NOTE: Cautious medium replacement is necessary because 293T cells have a high tendency to detach and detached cells do not produce virus. Use a pipette that pours the medium very slowly and do not pour medium directly in 293T cells because they will detach.

Fibroblast transduction procedure

Lung fibroblasts are easily transduced by lentiviral vectors for knockdown, but not for knockin. Virus handling tips: always keep virus on ice. Do not heat or vortex them.

1. Seed fibroblasts in a $1.6x10^4$ cells / cm^2 in the morning. Ideal experiment should have a plate/flask with cells that are going to be expanded or used in the experiment and a 6-well plate seeded with cells for mRNA extraction and knockdown evaluation. Also, a non-transduced well in the 6-well plate should be done to test puromycin effectiveness.
2. In the evening, prepare a medium containing complete medium and viral supernatant with polibrene to 8 ug/ml (4 ul in 1 ml of medium from a 2 mg/ml stock solution). Leave cells transducing overnight. For **knockdown**, add 1.5-3% of viral supernatant (higher viral concentrations can decrease fibroblast proliferation and are not recommended). For **knockin**, mix 50% complete medium and 50% viral supernatant.
3. Next morning, change medium and start cell selection with puromycin 2 ug/ml for 4 days (human fibroblasts).
4. Maintain transduced cells with complete medium containing puromycin 1 ug/ml.

A2. Transient transfection of fibroblasts and cancer cells using siRNA

1. Introduction

Setting up the suitable siRNA concentration and transfection timing: depending on your final read-out, the cells, and the protein you are targeting, you should try three different concentrations (low - recommended datasheet - high) and at least two time points (24h-48h-72h).

2. Material and reagents

MATERIAL	COMPANY AND Cat#	LOCATION
OPTI-MEM (1X)	Gibco, #31985-062	Fridge
Lipofectamine RNAiMAX	Invtrogen, #13778-030	Fridge
Select Negative Control No. 1 siRNA	Thermofisher, #4390843	-80ºC Freezer
2 Silencer Select pre-designed siRNA constructs targeting your protein of interest	Thermofisher	
Epithelial culture medium (RPMI based)	Gibco	Fridge
Fibroblast culture medium (DMEM based)	Gibco	Fridge

3. Procedure

Day 0: resuspend the silencer pre-designed siRNA and the negative control silencer with nuclease-free water (provided with the siRNA constructs) to achieve a concentration of **100uM** and make aliquots.

Day 1: Seed the cells in complete medium to achieve a 50% confluence for the next day.

PLATE FORMAT	CELL LINE	num of cells/well	TIME FOR TRANSFECTION
6-well plates	H1437	200.000	24h
	H23*	375.000	24h
	Fibroblasts	40.000	48h

* H23 are sensible to transfection and need to be at 80% confluence

NOTE: If you need another plate format, scale the number of cells.

Day 2: Change the complete medium to RPMI or DMEM not supplemented. Add 1ml of RPMI or DMEM per well and prepare the Lipofectamine and siRNAs dilutions. Since Lipofectamine and the siRNAs **CAN'T** be diluted together, we need to prepare different dilution mediums for each one.

Dilutions procedure

1. Calculate the total of wells you need and prepare a pre-dilution of each siRNA at 10µM with OPTI-MEM (dilution 1:10 of the stock 100uM) according to the final volume.

2. Prepare Dilution medium A: to achieve a final siRNA concentration of **30nM/well**, you need to mix 100ul of OPTI-MEM + 3.6ul of siRNA 10uM per well. Prepare enough for your total of experimental conditions.
3. Prepare Dilution medium B: for each volume of siRNA, add half of lipofectamine (for each **3.6ul of siRNA**, you need **1.8ul of lipofectamine**). Mix 100ul of OPTI-MEM + 1.8ul of Lipofectamine per well.

Plate format	**Final siRNA concentration**	**Total volume/well**	**siRNA 10uM**	**Dilution medium A**	**Lipofectamine**	**Dilution medium B**
6-well plates	30nM	1.2 ml	3.6 ul	100ul OPTI-MEM +3.6ul siRNA	1.8 ul	100ul OPTI-MEM +1.8ul Lipo
	30nM	1.2 ml	3.6 ul		1.8 ul	
	30nM	1.2 ml	3.6 ul		1.8 ul	

NOTE: If you need another plate format, scale the volumes.

4. Mix dilution medium A + dilution medium B 1:1 and incubate at RT for 5-15min. Add 200ul of the transfection medium per well.
5. Change the medium for complete RPMI or DMEM after 4-6 hours.

Day 3 or 4**:** The cells are ready for gene knockdown assessment and to do the loss-of-function assay.

A3. Flow cytometry of CD63 (membrane protein)

1. Introduction

For each cell type and protein, the suitable dilution of the primary and secondary antibodies needs to be set up. To be sure that with the flow cytometry, you quantify the actual protein present in the cell, each molecule of your protein of interest has to be bound to an antibody molecule. Keep in mind that an excess of unbound antibodies in the sample enhances the background noise.

2. Material and reagents

MATERIAL	COMPANY AND Cat#	LOCATION
Cytometry tubes	Corning, #352008	Lab
Anti-CD63	Abcam, #ab8219	-20ºC Freezer
Anti-mouse AF 488	Invitrogen, #A-11029	Fridge
FBS	Gibco	Fridge
PBS		Lab
Ice		
FACS Canto II cytometer	BD Biosciences	Cytometry platform at IDIBAPS

3. Procedure

For each cell type, you will have a minimum of 5 experimental conditions: 2 controls and 3 technical replicates.

Cytometry control 1: cells without any antibody bound are necessary to determine the autofluorescence settings.

Cytometry control 2: cells stained only with the secondary antibody are used to ensure the specificity of the primary antibody.

1. The day before prepare the PBS 2% FBS and keep it at 4ºC until use.
2. Prepare the cytometry tubes. Each condition will be stained in one cytometry tube and you will have as many tubes as experimental conditions.
3. Trispinize and count the cells. Add 200.000 of cells to each cytometry tube.
4. Centrifuge at 300g for 8 min at 4ºC.
5. Resuspend the cells as a single cell suspension with 2 mL of cold PBS 2% FBS.
6. Centrifuge at 300 g 8 min 4ºC.
7. Add 50 µL of primary antibody staining cocktail to each tube. Dilute **1:50** the anti-CD63 primary antibody in cold PBS 2% FBS.
8. Shake the tubes and incubate for 30 min at 4ºC in dark.
9. Add 4mL of cold PBS 2% FBS.
10. Centrifuge at 300 g 8 min 4ºC.
11. Resuspend the cells as a single cell suspension with 2 mL of cold PBS 2% FBS.
12. Centrifuge at 300 g 8 min 4ºC.
13. Add 50 µL of primary antibody staining cocktail to each tube. Dilute **1:100** the anti-mouse AF488 secondary antibody in cold PBS 2% FBS.
14. Shake the tubes and incubate for 30 min at 4ºC in dark.
15. Add 4mL of cold PBS 2% FBS.

16. Centrifuge at 300 g 8 min 4ºC.
17. Resuspend the cells as a single cell suspension with 2 mL of PBS (without 2% FBS).
18. Centrifuge at 300 g 8 min 4ºC.
19. Add 0,5mL PFA 2% (in PBS) and incubate for 15 min at RT in dark.
20. Add 4mL of cold PBS 2% FBS.
21. Centrifuge at 300 g 8 min 4ºC.
22. Resuspend the cells with 2 mL of cold PBS 2% FBS.
23. Centrifuge at 300 g 8 min 4ºC.
24. Add 0.5 mL of PBS 2% FBS, cover with parafilm each tube and maintain in dark at 4ºC until you go to the cytometer.
25. Analyze the cells the same day (FACS Canto II cytometer (BD Biosciences) in the IDIBAPS facility).

A4. TGF-β activity assay

1. Introduction

This is a cell-based system using HEK293T cells.

2. Material and reagents

MATERIAL	COMPANY AND Cat#	LOCATION
HEK293T	ATCC, #CRL-3216	
OPTI-MEM (1X)	Gibco, #31985-062	Fridge
Lipofectamine 3000	Invitrogen, #L3000-008	Fridge
pCAGA-Luc12X	Provided by Elena Sancho at IRB	-20ºC Freezer
pRL-TK Renilla Luciferase Control Reporter Vector	Promega, #E2241	-20ºC Freezer
Dual-Luciferase®Reporter Assay	Promega, #E1910	-20ºC Freezer
96 well white flat-bottom plates	Corning®, #3912	Lab
SPARK® 10M Multimode reader	TECAN	Common services at the Medicine School (UB)

3. Procedure

For each experimental condition, you will need 1 well of transfected HEK293T. Seed enough wells to assess your experimental conditions in duplicate and 3 extra wells for the controls.
Negative Control: HEK293T cells not transfected are necessary to ensure the specificity of the luciferases activity and to measure the luciferase background.
Basal Control: transfected HEK293T cells without treatment are necessary to determine the basal TFGβ activity of these cells.
Positive Control: transfected HEK293T cells stimulated with 2.5 ng/mL of TGFβ.

Day 1: Seed HEK293T cells at 100.000 cells/well in complete medium in 24-well plates (approx. 16h before transfection) to achieve a 50% confluence for the next day.

Day 2: Change the complete medium to DMEM no supplemented (200 µL/well) and prepare the Lipofectamine and siRNAs dilutions for the transfection. Prepare the dilution mediums to achieve the final amount (ng/well) of each reporter plasmid indicated below:

pCAGA-Luc12X (TGFβ reporter with firefly luciferase activity)	pRL-TK (Control reporter with *Renilla* luciferase activity)
100ng/well	20ng/well

Dilutions procedure

1. Prepare Dilution medium A(25µL/well): CAGA plasmid + Renilla plasmid + P3000 reagent (1ul/well) + Optimem. Prepare enough for your total of experimental conditions.
2. Prepare Dilution medium B(25µL/well): Lipo 3000 (0.75ul/well) + Optimem.
3. Mix dilution medium A + dilution medium B 1:1 and incubate at RT for 5-15min. Add 50ul of the transfection medium per well.
4. 6h after transfection change medium. Add starvation medium (DMEM 0.2%FBS).

Day 3: Treat transfected cells with your experimental conditions for 6h (200ul/well) and use the Dual-Luciferase®Reporter Assay following the manufacturer's instructions. In brief, lyse the cells in 200ul 1x PLB for 15min at RT with shaking. Transfer 50µl of each homogenized lysate into a well (96 well white flat-bottom plates). In the room you have the luminometer, add 20µl of LARII and measure luminescence at 560 nm (firefly luciferase activity). Next, add 20µl of Stop & Glo Reagent and measure luminescence at 480nm (*Renilla* luciferase activity). To obtain the TGFβ activity, calculate the Firefly/Renilla activities ratio for each well before averaging replicates.

A5. Tumor xenograft model of lung fibroblasts co-injected with cancer cells

1. Introduction

This protocol is for the co-injection of fibroblasts transfected with siRNA. If you don't need to transfect the cells before co-injection, start the protocol at Day 5, seeding fibroblasts with DMEM ITS 1% in 0.1% collagen-coated plates. This protocol includes the treatment with nintedanib.

2. Material and reagents

MATERIAL	COMPANY AND Cat#	LOCATION
OPTI-MEM (1X)	Gibco, # 31985-062	Fridge
Lipofectamine RNAiMAX	Invtrogen, # 13778-030	Fridge
Select Negative Control No. 1 siRNA	Thermofisher, # 4390843	-80°C Freezer
2 Silencer Select pre-designed siRNA constructs targeting your protein of interest	Thermofisher	
DMEM 10%FBS	Gibco	Fridge
DMEM 1%ITS	Gibco	Fridge
RPMI 10%FBS	Gibco	Fridge
RPMI 1%ITS	Gibco	Fridge
Recombinant human TGF-β1	R&D systems, #240-B	-80°C Freezer
Trypsin	Gibco	Fridge
Sterile 1000 µL and 200 µL tips		-20°C Freezer
Matrigel	Corning®, #356234	Fridge
Bovine dermis collagen	Koken, # I AC-50	Fridge
DMEM 10X concentrated	Gibco	-20°C Freezer
pH strips	METRIA, #CSPH-006-001	Lab
HCl 0.05 N diluted in sterile water	Sigma, #H9892	
NaOH 0.05 N diluted in sterile water	Sigma, #S770	
30G syringes	BD Medical, #320927	-20°C Freezer
Ice		
Nintedanib in powder	Boehringer Ingelheim	Lab
Reusable feeding needles	Fine Science Tools	Lab

3. Procedure

Day 1: Seed fibroblasts at 800.000 cells/P150 or 1.000.000 cells/T175 in the morning in complete DMEM medium.

Day 2: Transfect fibroblasts with a mixture of siRNA + Lipofectamine RNAiMAX for 6 h in DMEM without serum and antibiotics. 6 hours later change to complete medium.

Day 5: Change medium to DMEM ITS 1%. 4 hours later stimulate fibroblasts with 2.5 ng/mL of TGFβ-1.

Day 7: Prepare DMEM 10X concentrated to neutralize Koken collagen and store it at -20°C. Put at -20°C the syringes (if injecting 4 mice, prepare 6 syringes) and pipette tips (1000µL and 200µL) needed.

Day 8: the inoculation requires two people working together and can be divided in three parts: cells recovery, collagen-matrigel matrix and cells mixing, and animal inoculation.

CELLS RECOVERY

1. Recover fibroblasts (collect the CM for future ELISA) and cancer cells.
2. Centrifugate the cells and resuspend the pellet in DMEM 1%ITS or RPMI 1%ITS. Count the cells in Neubauer chambers
3. Calculate the number of cells necessary to mix fibroblasts and cancer cells in a 1:1 ratio ($1x10^6$ fibroblasts to $1x10^6$ cancer cells). In this step, prepare enough cells for **1.5 times of the needed cells**.
4. Centrifuge the mixture of cells (1800 rpm x 5 minutes) per condition.
5. Discard medium and resuspend the mixture in DMEM 1%ITS (**50ul for each 3 $x10^6$ mixture of cells**).

COLLAGEN-MATRIGEL MATRIX AND CELLS MIXING (estimated time ~ 1 h)

- Collagen must be prepared fresh for every experiment. Once prepared, it must be used within **the next 2-3 h**.
- Perform all steps on ice
- Prepare extra syringes in case you have problems with the inoculation

1. Every 450 ul Koken collagen are mixed with 50 ul of DMEM 10X. Add ~470 µL of Collagen to the bottom of a 50mL tube (you need to pipette more volume because part of the solution will stick on the tip walls). Add 50 ul of DMEM 10X. Shake vigorously by hand and avoid bubbles. Wait few seconds.
2. Check that pH falls within physiologic range with a pH strip. Adjust pH if needed with HCl 0.05N or NaOH 0.05N.
3. Collagen final concentration should be around 2 mg/ml.
4. Add the same volume of matrigel to generate the collagen-matrigel matrix (1:1).
5. Every $2x10^6$ mixture of cells is diluted with 100 µL of the collagen-matrigel matrix. Add the total volume of the collagen-matrigel matrix to the tube containing the suspension of cells (fibroblasts and cancer cells together).
6. Take out the syringe plunger in sterile conditions and place the syringes upside down in ice. Using 200 µL cold tips, pipette 110-120 µL of cells in the back of the syringe. It's important not to change the tip in between syringes to not to lose the cells sticking in the wall.
7. After all syringes are filled, put back again the syringe plunger.
8. Shake vigorously the syringe to have the mixture of cells stacked on the plunger.
9. Push cells without moving them out of the syringe.

ANIMAL INOCULATION

- All animals should be handled in sterile conditions in the specific pathogen free are of the animal facility.
- All syringes should be kept on ice until animal inoculation

1. Inoculate the cells subcutaneously in the flank of 4-8 weeks old NOD/SCID mice (Janvier).

Day 10: check the animals and palpate them in the inoculation area. From that point you have to look over the mice every 2 days. Depending on the characteristics of the cells inoculated, the tumor growth rate will be different.

Next days: at the beginning, the tumors will be palpable but not measurable (PNM). Once the tumors are measurable, measure them three times/week using calipers. Calculate tumor volume using the following formula: tumor volume = (smallest diameter^2 x largest diameter)/2. To plot tumor volume against time, the day of inoculation is considered to be day = 0.

NINTEDANIB TREATMENT

Start treating animals with nintedanib (50 mg of nintedanib/kg of animal) when the tumors reach a volume of ±50-100 mm^3. Treat them for 14 days.

Dilute nintedanib at 5 mg/ml and for every 10 g of animal, treat them with 100 ul of nintedanib solution. Avoid treating the mice with more than 250 ul (depending on the weight of the animals, dilute nintedanib to the suitable concentration). Treat control animals with the same volume of sterile PBS.

Oral gavage tips should be washed overnight in ethanol 70%, cleaned in ultrapure water, and then autoclaved.

Be careful, animals treated with oral gavage lose weight.

- Nintedanib dilution: at least 24h before treatment, dilute 50 mg of nintedanib in 10 ml of sterile PBS to reach a final concentration of 5 mg/ml. ***DO NOT FILTER THE SOLUTION AND PROTECT IT FROM LIGHT***. Diluted nintedanib can be kept at room temperature for up to 1 week and needs to be shaken vigorously before oral gavage due to drug decantation.

After 14 days, animals should be euthanized with 4 mg/kg ketamine (Richterpharma) and 0.4 mg/ml xylazine (Bayer) followed by cervical dislocation. Excise tumors and weigh and measure them. Fix tumors in PFA 4% for 24h at RT. Then exchange PFA for ethanol 70% for at least 48h.

DMEM 10X concentrated to neutralize Koken collagen
DMEM 10X – 10 ml
1.338 g DMEM powder
0.37 g sodium bicarbonate
Add 7.6 ml Miliq water + 2.4 ml HCl 1N to the powder and filter it in 0.22 µm filters.

A6. List of ADC and SCC cell lines used in this study and expression values of key genes obtained in the Sanger database

HISTOLOGY	NAME	*TIMP1* (log2)
ADC	A549	10,9
ADC	ABC-1	8,3
ADC	Calu-3	9,7
ADC	COLO-699	10,0
ADC	COR-L105	11,1
ADC	DV-90	11,5
ADC	EKVX	11,8
ADC	HCC2279	10,0
ADC	HCC4006	10,1
ADC	HCC44	11,9
ADC	HCC78	10,9
ADC	HCC827	9,4
ADC	HOP-62	12,0
ADC	HS229T	12,8
ADC	HS618T	13,1
ADC	LXF-289	8,9
ADC	MOR-CPR	10,8
ADC	NCI-H1355	10,6
ADC	NCI-H1373	10,7
ADC	NCI-H1395	7,7
ADC	NCI-H1437	12,1
ADC	NCI-H1563	11,4
ADC	NCI-H1573	10,7
ADC	NCI-H1623	8,7
ADC	NCI-H1648	10,1
ADC	NCI-H1650	10,3
ADC	NCI-H1651	11,1
ADC	NCI-H1666	10,8
ADC	NCI-H1693	9,3
ADC	NCI-H1734	10,5
ADC	NCI-H1755	10,7
ADC	NCI-H1781	7,6
ADC	NCI-H1792	12,2
ADC	NCI-H1793	9,2
ADC	NCI-H1838	10,4
ADC	NCI-H1975	11,2
ADC	NCI-H1993	7,7
ADC	NCI-H2009	10,2
ADC	NCI-H2023	8,9
ADC	NCI-H2030	11,4
ADC	NCI-H2085	9,3
ADC	NCI-H2087	11,1
ADC	NCI-H2122	10,2
ADC	NCI-H2126	8,9
ADC	NCI-H2228	11,5
ADC	NCI-H2291	10,8
ADC	NCI-H23	12,9
ADC	NCI-H2342	5,3
ADC	NCI-H2347	10,8
ADC	NCI-H2405	12,2
ADC	NCI-H322	8,7
ADC	NCI-H322M	8,6
ADC	NCI-H358	9,9
ADC	NCI-H441	9,4
ADC	NCI-H522	9,4
ADC	NCI-H650	13,6
ADC	NCI-H727	12,2
ADC	NCI-H854	11,9
ADC	PC-14	9,4
ADC	RERF-LC-Ad1	10,1
ADC	RERF-LC-Ad2	10,1
ADC	RERF-LC-MS	13,5
ADC	SK-LU-1	11,7
ADC	SW1573	11,1
ADC	UMC-11	8,0
SCC	Calu-1	11,6
SCC	EBC-1	9,7
SCC	EPLC-272H	10,3
SCC	HARA	9,1
SCC	HCC15	11,7
SCC	HCC95	7,5
SCC	HLF-a	12,4
SCC	KNS-62	10,6
SCC	LC-1F	9,7
SCC	LC-1-sq-SF	7,8
SCC	LK-2	7,7
SCC	LOU-NH91	11,4
SCC	LUDLU-1	7,0
SCC	NCI-H1385	4,4
SCC	NCI-H157	11,9
SCC	NCI-H1703	9,9
SCC	NCI-H1869	8,4
SCC	NCI-H2170	9,1
SCC	NCI-H226	10,9
SCC	NCI-H520	4,9
SCC	RERF-LC-AI	11,2
SCC	RERF-LC-Sq1	9,8
SCC	SK-MES-1	11,2
SCC	Sq-1	9,6
SCC	SW900	11,9

BIBLIOGRAPHY

1. Sung, H., et al., *Global Cancer Statistics 2020: GLOBOCAN Estimates of Incidence and Mortality Worldwide for 36 Cancers in 185 Countries.* CA Cancer J Clin, 2021. **71**(3): p. 209-249.
2. Herbst, R.S., D. Morgensztern, and C. Boshoff, *The biology and management of non-small cell lung cancer.* Nature, 2018. **553**(7689): p. 446-454.
3. Chen, Z., et al., *Non-small-cell lung cancers: a heterogeneous set of diseases.* Nature Reviews Cancer, 2014. **14**(8): p. 535-546.
4. Goldstraw, P., et al., *The IASLC Lung Cancer Staging Project: Proposals for Revision of the TNM Stage Groupings in the Forthcoming (Eighth) Edition of the TNM Classification for Lung Cancer.* Journal of Thoracic Oncology, 2016. **11**(1): p. 39-51.
5. Majem, M., et al., *SEOM clinical guidelines for the treatment of non-small cell lung cancer (2018).* Clinical and Translational Oncology, 2019. **21**(1): p. 3-17.
6. Mittal, V., et al., *The Microenvironment of Lung Cancer and Therapeutic Implications*. 2016, Springer International Publishing. p. 75-110.
7. Rosa, R., et al., *In Vitro and In Vivo Models for Analysis of Resistance to Anticancer Molecular Therapies.* Current Medicinal Chemistry, 2014. **21**(14): p. 1595-1606.
8. Mayekar, M.K. and T.G. Bivona, *Current Landscape of Targeted Therapy in Lung Cancer.* Clinical Pharmacology & Therapeutics, 2017. **102**(5): p. 757-764.
9. Fennell, D.A., et al., *Cisplatin in the modern era: The backbone of first-line chemotherapy for non-small cell lung cancer.* Cancer Treat Rev, 2016. **44**: p. 42-50.
10. Reck, M., et al., *Pembrolizumab versus Chemotherapy for PD-L1–Positive Non–Small-Cell Lung Cancer.* New England Journal of Medicine, 2016. **375**(19): p. 1823-1833.
11. Hirsch, F.R., et al., *Lung cancer: current therapies and new targeted treatments.* The Lancet, 2017. **389**(10066): p. 299-311.
12. Bissell, M.J. and W.C. Hines, *Why don't we get more cancer? A proposed role of the microenvironment in restraining cancer progression.* Nat Med, 2011. **17**(3): p. 320-9.
13. Hanahan, D. and Robert, *Hallmarks of Cancer: The Next Generation.* Cell, 2011. **144**(5): p. 646-674.
14. Bremnes, R.M., et al., *The role of tumor stroma in cancer progression and prognosis: emphasis on carcinoma-associated fibroblasts and non-small cell lung cancer.* J Thorac Oncol, 2011. **6**(1): p. 209-17.
15. Altorki, N.K., et al., *The lung microenvironment: an important regulator of tumour growth and metastasis.* Nat Rev Cancer, 2019. **19**(1): p. 9-31.
16. Mueller, M.M. and N.E. Fusenig, *Friends or foes — bipolar effects of the tumour stroma in cancer.* Nature Reviews Cancer, 2004. **4**(11): p. 839-849.
17. Lambrechts, D., et al., *Phenotype molding of stromal cells in the lung tumor microenvironment.* Nat Med, 2018. **24**(8): p. 1277-1289.
18. Sandler, A., et al., *Paclitaxel–Carboplatin Alone or with Bevacizumab for Non–Small-Cell Lung Cancer.* New England Journal of Medicine, 2006. **355**(24): p. 2542-2550.
19. Reck, M., et al., *Docetaxel plus nintedanib versus docetaxel plus placebo in patients with previously treated non-small-cell lung cancer (LUME-Lung 1): a phase 3, double-blind, randomised controlled trial.* The Lancet Oncology, 2014. **15**(2): p. 143-155.
20. Puig, M., et al., *Matrix Stiffening and beta(1) Integrin Drive Subtype-Specific Fibroblast Accumulation in Lung Cancer.* Molecular Cancer Research, 2015. **13**(1): p. 161-173.
21. Soltermann, A., et al., *Prognostic significance of epithelial-mesenchymal and mesenchymal-epithelial transition protein expression in non-small cell lung cancer.* Clin Cancer Res, 2008. **14**(22): p. 7430-7.
22. Kalluri, R. and M. Zeisberg, *Fibroblasts in cancer.* Nature Reviews Cancer, 2006. **6**(5): p. 392-401.
23. Dvorak, H.F., *Tumors: Wounds That Do Not Heal.* New England Journal of Medicine, 1986. **315**(26): p. 1650-1659.

24. Hasegawa, Y., et al., *Transforming growth factor-beta1 level correlates with angiogenesis, tumor progression, and prognosis in patients with nonsmall cell lung carcinoma.* Cancer, 2001. **91**(5): p. 964-71.
25. Hinz, B., *Myofibroblasts.* Experimental Eye Research, 2016. **142**: p. 56-70.
26. Tomasek, J.J., et al., *Myofibroblasts and mechano-regulation of connective tissue remodelling.* Nature Reviews Molecular Cell Biology, 2002. **3**(5): p. 349-363.
27. Huang, F. and Y.-G. Chen, *Regulation of TGF-β receptor activity.* Cell & Bioscience, 2012. **2**(1): p. 9.
28. Schiller, M., D. Javelaud, and A. Mauviel, *TGF-β-induced SMAD signaling and gene regulation: consequences for extracellular matrix remodeling and wound healing.* Journal of Dermatological Science, 2004. **35**(2): p. 83-92.
29. Shi, Y. and J. Massagué, *Mechanisms of TGF-β Signaling from Cell Membrane to the Nucleus.* Cell, 2003. **113**(6): p. 685-700.
30. Paulsson, J. and P. Micke, *Prognostic relevance of cancer-associated fibroblasts in human cancer.* Semin Cancer Biol, 2014. **25**: p. 61-8.
31. Navab, R., et al., *Prognostic gene-expression signature of carcinoma-associated fibroblasts in non-small cell lung cancer.* Proceedings of the National Academy of Sciences, 2011. **108**(17): p. 7160-7165.
32. Surowiak, P., et al., *Occurence of stromal myofibroblasts in the invasive ductal breast cancer tissue is an unfavourable prognostic factor.* Anticancer Res, 2007. **27**(4c): p. 2917-24.
33. Calon, A., et al., *Stromal gene expression defines poor-prognosis subtypes in colorectal cancer.* Nat Genet, 2015. **47**(4): p. 320-9.
34. Olumi, A.F., et al., *Carcinoma-associated fibroblasts direct tumor progression of initiated human prostatic epithelium.* Cancer Res, 1999. **59**(19): p. 5002-11.
35. Fernández-Nogueira, P., et al., *Tumor-Associated Fibroblasts Promote HER2-Targeted Therapy Resistance through FGFR2 Activation.* Clin Cancer Res, 2020. **26**(6): p. 1432-1448.
36. Orozco, C.A., et al., *Targeting galectin-1 inhibits pancreatic cancer progression by modulating tumor–stroma crosstalk.* Proceedings of the National Academy of Sciences, 2018. **115**(16): p. E3769-E3778.
37. Gabasa, M., et al., *Nintedanib selectively inhibits the activation and tumour-promoting effects of fibroblasts from lung adenocarcinoma patients.* British Journal of Cancer, 2017. **117**(8): p. 1128-1138.
38. Gaggioli, C., et al., *Fibroblast-led collective invasion of carcinoma cells with differing roles for RhoGTPases in leading and following cells.* Nature Cell Biology, 2007. **9**(12): p. 1392-1400.
39. Karagiannis, G.S., et al., *Cancer-Associated Fibroblasts Drive the Progression of Metastasis through both Paracrine and Mechanical Pressure on Cancer Tissue.* Molecular Cancer Research, 2012. **10**(11): p. 1403.
40. Özdemir, B.C., et al., *Depletion of carcinoma-associated fibroblasts and fibrosis induces immunosuppression and accelerates pancreas cancer with reduced survival.* Cancer Cell, 2014. **25**(6): p. 719-34.
41. Rhim, A.D., et al., *Stromal elements act to restrain, rather than support, pancreatic ductal adenocarcinoma.* Cancer Cell, 2014. **25**(6): p. 735-47.
42. Santos, A.M., et al., *Targeting fibroblast activation protein inhibits tumor stromagenesis and growth in mice.* Journal of Clinical Investigation, 2009. **119**(12): p. 3613-3625.
43. Wang, L., et al., *Cancer-associated fibroblasts enhance metastatic potential of lung cancer cells through IL-6/STAT3 signaling pathway.* Oncotarget; Vol 8, No 44, 2017.

44. Zhou, Z., et al., *VCAM-1 secreted from cancer-associated fibroblasts enhances the growth and invasion of lung cancer cells through AKT and MAPK signaling.* Cancer Lett, 2020. **473**: p. 62-73.
45. Wang, W., et al., *Crosstalk to Stromal Fibroblasts Induces Resistance of Lung Cancer to Epidermal Growth Factor Receptor Tyrosine Kinase Inhibitors.* Clinical Cancer Research, 2009. **15**(21): p. 6630-6638.
46. Owusu, B.Y., et al., *Targeting the tumor-promoting microenvironment in MET-amplified NSCLC cells with a novel inhibitor of pro-HGF activation.* Oncotarget; Vol 8, No 38, 2017.
47. Sahai, E., et al., *A framework for advancing our understanding of cancer-associated fibroblasts.* Nat Rev Cancer, 2020. **20**(3): p. 174-186.
48. Vicent, S., et al., *Cross-Species Functional Analysis of Cancer-Associated Fibroblasts Identifies a Critical Role for CLCF1 and IL-6 in Non–Small Cell Lung Cancer In Vivo.* Cancer Research, 2012. **72**(22): p. 5744-5756.
49. Jiang, L., et al., *Global Hypomethylation of Genomic DNA in Cancer-Associated Myofibroblasts.* Cancer Research, 2008. **68**(23): p. 9900-9908.
50. Kalluri, R., *The biology and function of fibroblasts in cancer.* Nature Reviews Cancer, 2016. **16**(9): p. 582-598.
51. Hu, M., et al., *Distinct epigenetic changes in the stromal cells of breast cancers.* Nat Genet, 2005. **37**(8): p. 899-905.
52. Alcaraz, J., et al., *Epigenetic Reprogramming of Tumor-Associated Fibroblasts in Lung Cancer: Therapeutic Opportunities.* Cancers, 2021. **13**(15).
53. Feinberg, A.P. and B. Tycko, *The history of cancer epigenetics.* Nature Reviews Cancer, 2004. **4**(2): p. 143-153.
54. Vizoso, M., et al., *Aberrant DNA methylation in non-small cell lung cancer-associated fibroblasts.* 2015: p. bgv146.
55. Chang, H.Y., et al., *Diversity, topographic differentiation, and positional memory in human fibroblasts.* Proc Natl Acad Sci U S A, 2002. **99**(20): p. 12877-82.
56. Ikemori, R., et al., *Epigenetic SMAD3 Repression in Tumor-Associated Fibroblasts Impairs Fibrosis and Response to the Antifibrotic Drug Nintedanib in Lung Squamous Cell Carcinoma.* Cancer Research, 2020. **80**(2): p. 276-290.
57. Samanta, D., et al., *Smoking attenuates transforming growth factor-β-mediated tumor suppression function through downregulation of Smad3 in lung cancer.* Cancer Prev Res (Phila), 2012. **5**(3): p. 453-63.
58. Hilberg, F., et al., *BIBF 1120: triple angiokinase inhibitor with sustained receptor blockade and good antitumor efficacy.* Cancer Res, 2008. **68**(12): p. 4774-82.
59. Ferrara, N. and T. Davis-Smyth, *The Biology of Vascular Endothelial Growth Factor.* Endocrine Reviews, 1997. **18**(1): p. 4-25.
60. Kerbel, R.S., *Tumor Angiogenesis.* New England Journal of Medicine, 2008. **358**(19): p. 2039-2049.
61. Casanovas, O., et al., *Drug resistance by evasion of antiangiogenic targeting of VEGF signaling in late-stage pancreatic islet tumors.* Cancer Cell, 2005. **8**(4): p. 299-309.
62. Nissen, L.J., et al., *Angiogenic factors FGF2 and PDGF-BB synergistically promote murine tumor neovascularization and metastasis.* The Journal of Clinical Investigation, 2007. **117**(10): p. 2766-2777.
63. Coward, W.R., G. Saini, and G. Jenkins, *The pathogenesis of idiopathic pulmonary fibrosis.* Ther Adv Respir Dis, 2010. **4**(6): p. 367-88.
64. Raghu, G., et al., *An official ATS/ERS/JRS/ALAT statement: idiopathic pulmonary fibrosis: evidence-based guidelines for diagnosis and management.* Am J Respir Crit Care Med, 2011. **183**(6): p. 788-824.
65. Richeldi, L., et al., *Efficacy and Safety of Nintedanib in Idiopathic Pulmonary Fibrosis.* New England Journal of Medicine, 2014. **370**(22): p. 2071-2082.

66. Hostettler, K.E., et al., *Anti-fibrotic effects of nintedanib in lung fibroblasts derived from patients with idiopathic pulmonary fibrosis.* Respir Res, 2014. **15**(1): p. 157.
67. Rangarajan, S., et al., *Novel Mechanisms for the Antifibrotic Action of Nintedanib.* Am J Respir Cell Mol Biol, 2016. **54**(1): p. 51-9.
68. Epstein Shochet, G., et al., *Nintedanib (BIBF 1120) blocks the tumor promoting signals of lung fibroblast soluble microenvironment.* 2016. **96**: p. 7-14.
69. Yamanaka, T., et al., *Nintedanib inhibits intrahepatic cholangiocarcinoma aggressiveness via suppression of cytokines extracted from activated cancer-associated fibroblasts.* Br J Cancer, 2020. **122**(7): p. 986-994.
70. Yoshida, G.J., et al., *Activated Fibroblast Program Orchestrates Tumor Initiation and Progression; Molecular Mechanisms and the Associated Therapeutic Strategies.* Int J Mol Sci, 2019. **20**(9).
71. Valkenburg, K.C., A.E. de Groot, and K.J. Pienta, *Targeting the tumour stroma to improve cancer therapy.* Nature Reviews Clinical Oncology, 2018. **15**(6): p. 366-381.
72. Wollin, L., et al., *Antifibrotic and Anti-inflammatory Activity of the Tyrosine Kinase Inhibitor Nintedanib in Experimental Models of Lung Fibrosis.* Journal of Pharmacology and Experimental Therapeutics, 2014. **349**(2): p. 209-220.
73. Eckfeld, C., et al., *Functional disparities within the TIMP family in cancer: hints from molecular divergence.* Cancer and Metastasis Reviews, 2019. **38**(3): p. 469-481.
74. Shimoda, M., H.W. Jackson, and R. Khokha, *Tumor suppression by stromal TIMPs.* Mol Cell Oncol, 2016. **3**(3): p. e975082.
75. Caley, M.P., V.L. Martins, and E.A. O'Toole, *Metalloproteinases and Wound Healing.* Adv Wound Care (New Rochelle), 2015. **4**(4): p. 225-234.
76. Rigg, A.S. and N.R. Lemoine, *Adenoviral delivery of TIMP1 or TIMP2 can modify the invasive behavior of pancreatic cancer and can have a significant antitumor effect in vivo.* Cancer Gene Therapy, 2001. **8**(11): p. 869-878.
77. Hayakawa, T., et al., *Growth-promoting activity of tissue inhibitor of metalloproteinases-1 (TIMP-1) for a wide range of cells. A possible new growth factor in serum.* FEBS Lett, 1992. **298**(1): p. 29-32.
78. Guedez, L., et al., *In vitro suppression of programmed cell death of B cells by tissue inhibitor of metalloproteinases-1.* Journal of Clinical Investigation, 1998. **102**(11): p. 2002-2010.
79. Jung, K.-K., et al., *Identification of CD63 as a tissue inhibitor of metalloproteinase-1 interacting cell surface protein.* The EMBO Journal, 2006. **25**(17): p. 3934-3942.
80. Grünwald, B., et al., *Pancreatic Premalignant Lesions Secrete Tissue Inhibitor of Metalloproteinases-1, Which Activates Hepatic Stellate Cells Via CD63 Signaling to Create a Premetastatic Niche in the Liver.* Gastroenterology, 2016. **151**(5): p. 1011-1024.e7.
81. Grunnet, M., M. Mau-Sørensen, and N. Brünner, *Tissue inhibitor of metalloproteinase 1 (TIMP-1) as a biomarker in gastric cancer: a review.* Scandinavian Journal of Gastroenterology, 2013. **48**(8): p. 899-905.
82. Cheng, G., et al., *Higher levels of TIMP-1 expression are associated with a poor prognosis in triple-negative breast cancer.* Molecular Cancer, 2016. **15**(1).
83. Zeng, Z., et al., *Elevated tissue inhibitor of metalloproteinase 1 RNA in colorectal cancer stroma correlates with lymph node and distant metastases.* Clinical cancer research : an official journal of the American Association for Cancer Research, 1995. **1**: p. 899-906.
84. Pesta, M., et al., *Prognostic significance of TIMP-1 in non-small cell lung cancer.* Anticancer Res, 2011. **31**(11): p. 4031-8.
85. Selvaraj, G., et al., *Prognostic Impact of Tissue Inhibitor of Metalloproteinase-1 in Non-Small Cell Lung Cancer: Systematic Review and Meta-Analysis.* Curr Med Chem, 2019. **26**(42): p. 7694-7713.

86. Fong, K.M., et al., *TIMP1 and adverse prognosis in non-small cell lung cancer.* Clin Cancer Res, 1996. **2**(8): p. 1369-72.

87. Chesler, L., et al., *Metalloproteinase inhibition and erythroid potentiation are independent activities of tissue inhibitor of metalloproteinases-1.* Blood, 1995. **86**(12): p. 4506-15.

88. Guedez, L., et al., *Tissue inhibitor of metalloproteinase-1 alters the tumorigenicity of Burkitt's lymphoma via divergent effects on tumor growth and angiogenesis.* The American journal of pathology, 2001. **158**(4): p. 1207-1215.

89. Grunwald, B., B. Schoeps, and A. Kruger, *Recognizing the Molecular Multifunctionality and Interactome of TIMP-1.* Trends Cell Biol, 2019. **29**(1): p. 6-19.

90. Moore, C.S. and S.J. Crocker, *An Alternate Perspective on the Roles of TIMPs and MMPs in Pathology.* The American Journal of Pathology, 2012. **180**(1): p. 12-16.

91. Tjomsland, V., et al., *Profile of MMP and TIMP Expression in Human Pancreatic Stellate Cells: Regulation by IL-1α and TGFβ and Implications for Migration of Pancreatic Cancer Cells.* Neoplasia, 2016. **18**(7): p. 447-56.

92. Resovi, A., et al., *Soluble stroma-related biomarkers of pancreatic cancer.* EMBO Mol Med, 2018. **10**(8).

93. An, H.J., et al., *The prognostic role of tissue and serum MMP-1 and TIMP-1 expression in patients with non-small cell lung cancer.* Pathol Res Pract, 2016. **212**(5): p. 357-64.

94. Nawrocki, B., et al., *Expression of matrix metalloproteinases and their inhibitors in human bronchopulmonary carcinomas: Quantificative and morphological analyses.* International Journal of Cancer, 1997. **72**(4): p. 556-564.

95. Park, S.-A., et al., *TIMP-1 mediates TGF-β-dependent crosstalk between hepatic stellate and cancer cells via FAK signaling.* 2015. **5**: p. 16492.

96. Öztürk Akcora, B., et al., *Tyrosine kinase inhibitor BIBF1120 ameliorates inflammation, angiogenesis and fibrosis in CCl(4)-induced liver fibrogenesis mouse model.* Sci Rep, 2017. **7**: p. 44545.

97. Liu, X.W., et al., *Tissue inhibitor of metalloproteinase-1 protects human breast epithelial cells against intrinsic apoptotic cell death via the focal adhesion kinase/phosphatidylinositol 3-kinase and MAPK signaling pathway.* J Biol Chem, 2003. **278**(41): p. 40364-72.

98. Warner, R.B., et al., *Establishment of Structure-Function Relationship of Tissue Inhibitor of Metalloproteinase-1 for Its Interaction with CD63: Implication for Cancer Therapy.* Scientific Reports, 2020. **10**(1): p. 2099.

99. Cui, H., et al., *Tissue inhibitor of metalloproteinases-1 induces a pro-tumourigenic increase of miR-210 in lung adenocarcinoma cells and their exosomes.* Oncogene, 2015. **34**(28): p. 3640-50.

100. Xia, Y., et al., *Reduced cell proliferation by IKK2 depletion in a mouse lung-cancer model.* Nat Cell Biol, 2012. **14**(3): p. 257-65.

101. Forte, D., et al., *The tissue inhibitor of metalloproteinases-1 (TIMP-1) promotes survival and migration of acute myeloid leukemia cells through CD63/PI3K/Akt/p21 signaling.* Oncotarget, 2017. **8**(2): p. 2261-2274.

102. Ries, C., *Cytokine functions of TIMP-1.* Cell Mol Life Sci, 2014. **71**(4): p. 659-72.

103. Itoh, Y. and H. Nagase, *Preferential Inactivation of Tissue Inhibitor of Metalloproteinases-1 That Is Bound to the Precursor of Matrix Metalloproteinase 9 (Progelatinase B) by Human Neutrophil Elastase *.* Journal of Biological Chemistry, 1995. **270**(28): p. 16518-16521.

104. Simi, L., et al., *Simultaneous measurement of MMP9 and TIMP1 mRNA in human non small cell lung cancers by multiplex real time RT-PCR.* Lung Cancer, 2004. **45**(2): p. 171-9.

105. Gouyer, V., et al., *Tissue inhibitor of metalloproteinase 1 is an independent predictor of prognosis in patients with nonsmall cell lung carcinoma who undergo resection with curative intent.* Cancer, 2005. **103**(8): p. 1676-84.
106. Gabasa, M., et al., *Lung Myofibroblasts Are Characterized by Down-Regulated Cyclooxygenase-2 and Its Main Metabolite, Prostaglandin E2.* PLoS ONE, 2013. **8**(6): p. e65445.
107. Goldstraw, P., et al., *The IASLC Lung Cancer Staging Project: proposals for the revision of the TNM stage groupings in the forthcoming (seventh) edition of the TNM Classification of malignant tumours.* J Thorac Oncol, 2007. **2**(8): p. 706-14.
108. Chang, H.Y., et al., *Diversity, topographic differentiation, and positional memory in human fibroblasts.* Proceedings of the National Academy of Sciences, 2002. **99**(20): p. 12877-12882.
109. Alcaraz, J., et al., *Stromal markers of activated tumor associated fibroblasts predict poor survival and are associated with necrosis in non-small cell lung cancer.* Lung Cancer, 2019. **135**: p. 151-160.
110. Choy, L., J. Skillington, and R. Derynck, *Roles of autocrine TGF-beta receptor and Smad signaling in adipocyte differentiation.* J Cell Biol, 2000. **149**(3): p. 667-82.
111. Salat-Canela, C., et al., *Internal translation of the connexin 43 transcript.* Cell Commun Signal, 2014. **12**: p. 31.
112. Blanco, R., et al., *A gene-alteration profile of human lung cancer cell lines.* Human Mutation, 2009. **30**(8): p. 1199-1206.
113. Bronte, G., et al., *Nintedanib in NSCLC: evidence to date and place in therapy.* Therapeutic Advances in Medical Oncology, 2016. **8**(3): p. 188-197.
114. Gabasa, M., et al., *MMP1 drives tumor progression in large cell carcinoma of the lung through fibroblast senescence.* Cancer Lett, 2021. **507**: p. 1-12.
115. Crombez, L., et al., *High level production of secreted proteins: Example of the human tissue inhibitor of metalloproteinases 1.* 2005. **337**(3): p. 908-915.
116. Batra, J., et al., *Matrix Metalloproteinase-10 (MMP-10) Interaction with Tissue Inhibitors of Metalloproteinases TIMP-1 and TIMP-2: BINDING STUDIES AND CRYSTAL STRUCTURE.* 2012. **287**(19): p. 15935-15946.
117. Gabasa, M., et al., *Epithelial contribution to the profibrotic stiff microenvironment and myofibroblast population in lung fibrosis.* Mol Biol Cell, 2017. **28**(26): p. 3741-3755.
118. Abràmoff, M.D., P.J. Magalhães, and S.J. Ram, *Image processing with ImageJ.* Biophotonics international, 2004. **11**(7): p. 36-42.
119. Lugo, R., et al., *Heterotypic paracrine signaling drives fibroblast senescence and tumor progression of large cell carcinoma of the lung.* Oncotarget, 2016. **7**: p. 82324-82337.
120. Gibson, G.E., et al., *A reproducible procedure for primary culture and subsequent maintenance of multiple lines of human skin fibroblasts.* Age (Omaha), 1998. **21**(1): p. 7-14.
121. Campillo, N., et al., *Role of Cyclooxygenase-2 on Intermittent Hypoxia-Induced Lung Tumor Malignancy in a Mouse Model of Sleep Apnea.* Sci Rep, 2017. **7**: p. 44693.
122. Hosokawa, Y., et al., *The Polymethoxy Flavonoid Sudachitin Inhibits Interleukin-1<i>β</i>-Induced Inflammatory Mediator Production in Human Periodontal Ligament Cells.* BioMed Research International, 2021. **2021**: p. 8826586.
123. Dennler, S., et al., *Direct binding of Smad3 and Smad4 to critical TGF beta-inducible elements in the promoter of human plasminogen activator inhibitor-type 1 gene.* Embo j, 1998. **17**(11): p. 3091-100.
124. Livak, K.J. and T.D. Schmittgen, *Analysis of relative gene expression data using real-time quantitative PCR and the 2(-Delta Delta C(T)) Method.* Methods, 2001. **25**(4): p. 402-8.
125. Uhlén, M., et al., *A Human Protein Atlas for Normal and Cancer Tissues Based on Antibody Proteomics.* Molecular & Cellular Proteomics, 2005. **4**(12): p. 1920-1932.

126. Hartel, M., et al., *Desmoplastic Reaction Influences Pancreatic Cancer Growth Behavior.* World Journal of Surgery, 2004. **28**(8): p. 818-825.
127. Yamauchi, K., et al., *Quantitative expression study of four cytokeratins and p63 in squamous cell carcinoma of the tongue: suitability for sentinel node navigation surgery using one-step nucleic acid amplification.* J Clin Pathol, 2011. **64**(10): p. 875-9.
128. Ueno, H., et al., *Tumour 'budding' as an index to estimate the potential of aggressiveness in rectal cancer.* Histopathology, 2002. **40**(2): p. 127-32.
129. Grazioli, L., et al., *The pseudocapsule in hepatocellular carcinoma: correlation between dynamic MR imaging and pathology.* Eur Radiol, 1999. **9**(1): p. 62-7.
130. Ritchie, M.E., et al., *limma powers differential expression analyses for RNA-sequencing and microarray studies.* Nucleic Acids Research, 2015. **43**(7): p. e47-e47.
131. Lee, Y.-F., et al., *CellExpress: a comprehensive microarray-based cancer cell line and clinical sample gene expression analysis online system.* Database, 2018. **2018**.
132. Alcorta, D.A., et al., *Involvement of the cyclin-dependent kinase inhibitor p16 (INK4a) in replicative senescence of normal human fibroblasts.* Proc Natl Acad Sci U S A, 1996. **93**(24): p. 13742-7.
133. Harley, C.B., A.B. Futcher, and C.W. Greider, *Telomeres shorten during ageing of human fibroblasts.* Nature, 1990. **345**(6274): p. 458-460.
134. Bodnar, A.G., et al., *Extension of life-span by introduction of telomerase into normal human cells.* Science, 1998. **279**(5349): p. 349-52.
135. Rodier, F. and J. Campisi, *Four faces of cellular senescence.* J Cell Biol, 2011. **192**(4): p. 547-56.
136. Safranek, J., et al., *Expression of MMP-7, MMP-9, TIMP-1 and TIMP-2 mRNA in lung tissue of patients with non-small cell lung cancer (NSCLC) and benign pulmonary disease.* Anticancer Res, 2009. **29**(7): p. 2513-7.
137. Mann, J., et al., *Regulation of myofibroblast transdifferentiation by DNA methylation and MeCP2: implications for wound healing and fibrogenesis.* Cell Death Differ, 2007. **14**(2): p. 275-85.
138. Lindskog, C., et al., *The lung-specific proteome defined by integration of transcriptomics and antibody-based profiling.* Faseb j, 2014. **28**(12): p. 5184-96.
139. Sincock, P.M., G. Mayrhofer, and L.K. Ashman, *Localization of the transmembrane 4 superfamily (TM4SF) member PETA-3 (CD151) in normal human tissues: comparison with CD9, CD63, and alpha5beta1 integrin.* J Histochem Cytochem, 1997. **45**(4): p. 515-25.
140. Kwon, M.S., et al., *CD63 as a biomarker for predicting the clinical outcomes in adenocarcinoma of lung.* Lung Cancer, 2007. **57**(1): p. 46-53.
141. Termini, C.M. and J.M. Gillette, *Tetraspanins Function as Regulators of Cellular Signaling.* Frontiers in Cell and Developmental Biology, 2017. **5**: p. 34.
142. Boulday, G., et al., *Exogenous tissue inhibitor of metalloproteinase-1 promotes endothelial cell survival through activation of the phosphatidylinositol 3-kinase/Akt pathway.* Ann N Y Acad Sci, 2004. **1030**: p. 28-36.
143. Roderfeld, M., et al., *Latent MMP-9 is bound to TIMP-1 before secretion.* Biol Chem, 2007. **388**(11): p. 1227-34.
144. Kim, Y.S., et al., *Functional proteomics study reveals that N-Acetylglucosaminyltransferase V reinforces the invasive/metastatic potential of colon cancer through aberrant glycosylation on tissue inhibitor of metalloproteinase-1.* Mol Cell Proteomics, 2008. **7**(1): p. 1-14.
145. Kim, Y.-S., et al., *Overexpression and β-1,6-N-Acetylglucosaminylation-initiated Aberrant Glycosylation of TIMP-1.* Journal of Biological Chemistry, 2012. **287**(39): p. 32467-32478.
146. Gasson, J.C., et al., *Molecular characterization and expression of the gene encoding human erythroid-potentiating activity.* Nature, 1985. **315**(6022): p. 768-71.

147. Jackson, H.W., et al., *TIMPs: versatile extracellular regulators in cancer.* Nat Rev Cancer, 2017. **17**(1): p. 38-53.
148. Schelter, F., et al., *Tumor cell-derived Timp-1 is necessary for maintaining metastasis-promoting Met-signaling via inhibition of Adam-10.* Clin Exp Metastasis, 2011. **28**(8): p. 793-802.
149. Balbín, M., et al., *Loss of collagenase-2 confers increased skin tumor susceptibility to male mice.* Nat Genet, 2003. **35**(3): p. 252-7.
150. Shimoda, M., et al., *Loss of the Timp gene family is sufficient for the acquisition of the CAF-like cell state.* Nat Cell Biol, 2014. **16**(9): p. 889-901.
151. Zöller, M., *Tetraspanins: push and pull in suppressing and promoting metastasis.* Nature Reviews Cancer, 2009. **9**(1): p. 40-55.
152. Jang, H.-I. and H. Lee, *A decrease in the expression of CD63 tetraspanin protein elevates invasive potential of human melanoma cells.* Experimental & Molecular Medicine, 2003. **35**(4): p. 317-323.
153. D'Costa, Z., et al., *Gemcitabine-Induced TIMP1 Attenuates Therapy Response and Promotes Tumor Growth and Liver Metastasis in Pancreatic Cancer.* Cancer Res, 2017. **77**(21): p. 5952-5962.
154. King, T.E., A. Pardo, and M. Selman, *Idiopathic pulmonary fibrosis.* The Lancet, 2011. **378**(9807): p. 1949-1961.